Doctoral Dissertation

A Study on Band Activity Ratio Control for Broadband Wireless Transmissions

Duong Quang Thang

August 2014

Graduate School of Engineering,
Osaka University

Preface

This dissertation is a summary of the study on band activity ratio (BAR) control for broadband wireless transmissions which is conducted by the author during his work toward the Ph.D. degree at the Department of Information and Communications Technology, Graduate School of Engineering, Osaka University, Japan. This dissertation is organized as follows.

Chapter 1 provides an introduction and outline of the dissertation.

Chapter 2 introduces a signal model for two broadband wireless transmission schemes: single carrier and orthogonal frequency division multiplexing (OFDM), which will be used throughout this dissertation. Then this chapter outlines the importance of BAR control in the enhancement of spectral efficiency for the broadband transmissions. After that, this chapter clarifies the impacts of BAR control and the issue of channel prediction in autonomous spectrum sharing with the aid of dynamic spectrum control (DSC). Finally, this chapter presents the effectiveness of wireless relaying in spectral efficiency enhancement and clarifies the spectral efficiency degradation issue of broadband amplify-and-forward (AF) relay. The issues of channel prediction in autonomous spectrum sharing and the spectral efficiency degradation issue of broadband AF relay clarify the contributions of this dissertation.

In Chapter 3, we formulate the issue of channel prediction for the entire system band when only a part of the system band is allocated to each user. This channel prediction is quite important for autonomous spectrum sharing with the aid of DSC in which a limited part of the system band with higher gain is dynamically selected for each link. Then we explain spectral efficiency degradation due to deterioration of channel state information (CSI) reliability when BAR is relatively small. Aiming at enhancing spectral efficiency, we propose CSI reliability guaranteeing subchannel selection scheme. Numerical analysis is given to show that BAR control based on the proposed subchannel selection scheme significantly enhances the spectral efficiency when BAR is controlled to be relatively small in networks with many links.

In Chapter 4, we explain challenges for broadband AF relay under frequency selective fading. We introduce subchannel pairing in order to enhance the spectral efficiency for the broadband AF relay. To further enhance the performance, we investigate the energy allocations for subchannels on the basis of convex optimizations. The effectiveness of subchannel pairing in spectral efficiency enhancement is verified via numerical analysis. After that, we proposes adaptive BAR control based on spectrum nulling as a low overhead alternative technique for subchannel pairing. Numerical analyses are given to confirm that the proposed adaptive BAR control achieves almost the same spectral efficiency with the subchannel pairing with a drastically re-

duced notification overhead.

Chapter 5 highlights the main results and contributions of this dissertation.

Acknowledgements

This dissertation is the outcome of my long and tiring but meaningful journey working toward the Ph.D. degree under the supervision of Prof. Seiichi Sampei at the Department of Information and Communications Technology, Graduate School of Engineering, Osaka University, Japan. While carrying my name as an author on the title page, this dissertation is in fact a collaborative effort of many individuals whom I wish to acknowledge for the rest of my life.

First and foremost I would like to express my deep sense of appreciation to my supervisor Prof. Seiichi Sampei for providing me with a wonderful opportunity to carry out this research. His constant encouragement, continuous support, inspiring guidance and critical suggestions have led me to the completion of this work.

I am greatly indebted to Prof. Noboru Babaguchi and Assoc. Prof. Shinichi Miyamoto for the careful review, constructive suggestions and helpful comments that make valuable contributions to this dissertation.

I would like to express my sincere gratitude to Prof. Tetsuya Takine, Prof. Kenichi Kitayama, Prof. Kyou Inoue and Prof. Emer. Zenichiro Kawasaki at the Graduate School of Engineering, together with Prof. Takashi Washio and Prof. Emer. Riichiro Mizoguchi at the Institute of Scientific and Industrial Research, Osaka University for their useful guidance and instructions giving basic knowledge for this dissertation.

I am also greatly indebted to my academic supervisor Asst. Prof. Shinsuke Ibi of the Sampei laboratory for accompanying me on every step of this research. His constructive criticism, insightful comments and valuable suggestions have helped to improve the overall presentation and technical content of this work.

I would like to express my deep appreciation to Assoc. Prof. Kei Sakaguchi of the Sampei laboratory for the warm encouragements, valuable suggestions and insightful comments.

I would like to thank all the former and current members of the Sampei laboratory for their helpful advice and fruitful discussions. I also would like to thank my Japanese, Vietnamese and international friends for their deep friendship that makes my journey enjoyable and memorable.

I would like to express my deep thanks to the Ministry and Education, Science, Sports and Culture of Japan, the Global Centers Of Excellence Program Osaka University, and Matsuda Yosahichi Memorial Foreign Student Scholarship Foundation for financial aids and granting the scholarship.

Finally, I would like to express my deep and sincere gratitude to my parents and brother for enduring my absence, believing in me and encouraging me every step of the way.

Table of Contents

List of Figures

List of Tables

List of Symbols

T_{s}	Symbol duration in s
T_{OFDM}	Symbol duration in OFDM transmission
T_{SC}	Symbol duration in SC transmission
B	System bandwidth in Hz
n	Time index of transmitted symbol sequence
$x(n)$	The n-th transmitted modulation symbol
$\delta(t)$	The Dirac delta function
$\check{x}(t)$	Baseband transmitted signal waveform
$\check{y}(t)$	Baseband received signal waveform
$y(n)$	The n-th received modulation symbol
$\check{\eta}(t)$	Noise waveform induced at receiver
$h(l)$	Complex-valued attenuation factor of the l-th propagation path
$\check{h}(t)$	Channel impulse response
$\tau(l)$	Propagation delay in s of the l-th propagation path
$p(l)$	Value of delay power profile at instant delay $\tau(l) = (l-1)T_{\mathrm{s}}$
L	Number of propagation paths
l	Time index of propagation paths
$\check{\xi}(f)$	Channel frequency response in instant frequency f
$\check{\xi}(f,t)$	Channel frequency response in at instant frequency f and time t
Ψ	Energy gain of the channel
τ_{rms}	Root mean square delay spread in s
$\tau(L)$	Maximum excess delay in s
Δf_{coh}	Coherence bandwidth
$\mathbb{E}\{\cdot\}$	Expectation or ensemble average of random variable
$J_0(\cdot)$	Zero-order Bessel function of the first kind
f_{D}	Doppler frequency in Hz
f_{c}	Carrier frequency in Hz
c	Speed of light
v	Speed of receiver's movement from transmitter

$\boldsymbol{F}_a$	$a \times a$ DFT matrix
$\boldsymbol{s}$	Transmitted data symbol block
$.^{\mathrm{H}}$	Conjugate transpose of a vector or matrix
K	Number of subchannels of the system band
$\boldsymbol{x}$	Transmitted modulation symbol block
$\boldsymbol{x}^{\mathrm{f}}$	Transmitted spectrum
$x^{\mathrm{f}}(k)$	Transmitted spectral component at the k-th subchannel
$\boldsymbol{x}_{+\mathrm{CP}}$	CP-appended transmitted symbol block
$\boldsymbol{y}_{+\mathrm{CP}}$	CP-appended received symbol block
$\boldsymbol{G}_{+\mathrm{CP}}$	CP insertion matrix
$\boldsymbol{G}_{-\mathrm{CP}}$	CP removal matrix
$\boldsymbol{H}$	Time-domain channel matrix
$\boldsymbol{H}_{\mathrm{IBI}}$	Time-domain channel matrix for IBI
$\boldsymbol{H}_{\mathrm{circ}}$	Circular time-domain channel matrix after CP removal
$\boldsymbol{I}_a$	$a \times a$ identity matrix
$\boldsymbol{0}_{a\times b}$	$a \times b$ matrix with zero entries
$\boldsymbol{\eta}$	Noise vector
$\boldsymbol{\eta}^{\mathrm{f}}$	Noise spectrum
$\boldsymbol{y}$	Received symbol block
$\boldsymbol{y}^{\mathrm{f}}$	Received spectrum
k	Subchannel index
$y^{\mathrm{f}}(k)$	Received spectral component at the k-th subchannel
$\boldsymbol{\Xi}$	Frequency-domain channel matrix
$\mathrm{diag}[\boldsymbol{a}]$	Diagonal matrix with diagonal elements are those of vector $\boldsymbol{a}$
L_{CP}	CP length in T_{s}
$\mathbb{C}^{a\times b}$	$a \times b$ matrix with complex-valued elements
$\mathbb{R}^{a\times b}$	$a \times b$ matrix with real-valued elements
$\mathcal{CN}(a, b)$	Complex-valued Gaussian variables with mean a and variance b
E_{s}	Average energy of each transmitted spectral component
N_0	Noise variance
γ_{t}	Transmitted SNR for all subchannels
$\gamma_{\mathrm{r}}(k)$	Received SNR at the k-th subchannel
X	Random variable for transmitted spectral component $x^{\mathrm{f}}(k)$
Y	Random variable for received spectral component $y^{\mathrm{f}}(k)$
Z	Random variable for noise spectral component $\eta^{\mathrm{f}}(k)$
e	Napier's constant
$\mathcal{H}(X)$	Entropy of random variable X
$\mathcal{H}(X\|Y)$	Conditional entropy of X given Y
$\mathcal{I}(X;Y)$	Mutual information between X and Y

C	CCMC capacity in bits/s/Hz or bits/symbol
$\mathcal{S}$	Discrete constellation set
$D_{\mathcal{S}}$	DCMC capacity for discrete constellation set $\mathcal{S}$ in bits/s/Hz or bits/symbol
x^+	$= \max(x, 0)$
K'	Number of signal spectral components or used subchannels
K'/K	Band activity ratio
k'	Index of signal spectral components in the frequency-domain
$\tilde{\boldsymbol{x}}^{\mathrm{f}}$	Transmitted spectrum after spectrum mapping and energy allocation
$\boldsymbol{M}$	Spectrum mapping matrix
$\tilde{\boldsymbol{y}}^{\mathrm{f}}$	Received spectrum before spectrum demapping
$\psi(k)$	Channel gain ranking function
$\psi^{-1}(k)$	Inverse function of $\psi(k)$
$\boldsymbol{o}$	Ascending order vector of $\psi^{-1}(1)$, $\psi^{-1}(2)$, ..., $\psi^{-1}(K')$
$\tilde{\xi}_{u,u}(k')$	CFR of effective channel for the S_u-D_u link at k'-th spectral component
$I_u(k')$	Energy of interference induced in k'-th spectral component at D_u-node
$\psi_u(k)$	Channel gain ranking function for the S_u-D_u link
$\psi_u^{-1}(k)$	Inverse function of $\psi_u(k)$
$\boldsymbol{o}_u$	Ascending order vector of $\psi_u^{-1}(1)$, $\psi_u^{-1}(2)$, ..., $\psi_u^{-1}(K')$
$\boldsymbol{\Xi}_{u,u'}$	Frequency-domain channel matrix of the $\mathrm{S}_{u'}$-D_u link
$\boldsymbol{\xi}_{u,u'}$	Channel frequency response of the $\mathrm{S}_{u'}$-D_u link
$\boldsymbol{M}_u$	Spectrum mapping matrix for the S_u-D_u link
$\boldsymbol{\eta}_u^{\mathrm{f}}$	Noise spectrum induced at the D_u-node
$\boldsymbol{z}_u^{\mathrm{f}}$	Noise and interference spectrum induced at the D_u-node
U	Number of links in the considered autonomous network
$L_{u,u'}$	Number of multipath components of the $\mathrm{S}_{u'}$-D_u link
$\boldsymbol{h}_{u,u'}$	Channel impulse response of the $\mathrm{S}_{u'}$-D_u link
$\boldsymbol{Z}_u^{\mathrm{f}}$	Covariance matrix of $\boldsymbol{z}_u^{\mathrm{f}}$
$\hat{\underline{\boldsymbol{h}}}_{u,u}^{\mathrm{LS}}$	LS channel predict for $\underline{\boldsymbol{h}}_{u,u}$
$\hat{\boldsymbol{\xi}}_{u,u}^{\mathrm{LS}}$	LS channel predict for CFR $\boldsymbol{\xi}_{u,u}$ of the S_u-D_u link
$\boldsymbol{e}_u$	Prediction error vector for the prediction of CFR $\boldsymbol{\xi}_{u,u}$
$\boldsymbol{\Omega}_{\boldsymbol{e}}$	Covariance matrix of $\boldsymbol{e}_u$
ε^2	Average mean squared error of LS channel prediction
$\boldsymbol{T}_u$	Toeplitz matrix for the LS channel prediction
λ_l	Eigenvalue of Toeplitz matrix $\boldsymbol{T}_u$
trace$\{\cdot\}$	Trace of a matrix
$\Delta k_{\max}$	Maximum bandwidth of continuously non-selected subchannels
M	Number of subchannels allocated uniformly in low gain frequency region

$\boldsymbol{x}_{\mathrm{S}}^{\mathrm{f}}$	Transmitted spectrum at the S-node
$\boldsymbol{y}_{\mathrm{R}}^{\mathrm{f}}$	Received spectrum at the R-node
$\boldsymbol{\eta}_{\mathrm{R}}^{\mathrm{f}}$	Noise spectrum induced at the R-node
$\boldsymbol{x}_{\mathrm{R}}^{\mathrm{f}}$	Transmitted spectrum at the R-node
$\boldsymbol{y}_{\mathrm{D}}^{\mathrm{f}}$	Received spectrum at the D-node
$\boldsymbol{\eta}_{\mathrm{D}}^{\mathrm{f}}$	Noise spectrum induced at the D-node
Ψ_{RS}	Average channel gain of the S-R link
Ψ_{DR}	Average channel gain of the R-D link
μ	Path loss exponent
d_{RS}	Transmission distance of the S-R link
d_{DR}	Transmission distance of the R-D link
N_{R}	Variance of noise induced at the R-node
N_{D}	Variance of noise induced at the D-node
$\boldsymbol{x}_{u}^{\mathrm{f}}$	Transmitted spectrum at the S_u-node
$\boldsymbol{y}_{u}^{\mathrm{f}}$	Received spectrum at the D_u-node
$\boldsymbol{\Xi}_{\mathrm{RS}}$	Frequency-domain channel matrix for the S-R link
$\boldsymbol{\Xi}_{\mathrm{DR}}$	Frequency-domain channel matrix for the R-D link
$\tilde{\boldsymbol{\Xi}}_{\mathrm{RS}}$	Effective frequency-domain channel matrix for the S-R link
$\tilde{\boldsymbol{\Xi}}_{\mathrm{DR}}$	Effective frequency-domain channel matrix for the R-D link
$\psi_{\mathrm{RS}}(k)$	Channel gain ranking function for the S-R link
$\psi_{\mathrm{RS}}^{-1}(k)$	Inverse function of $\psi_{\mathrm{RS}}(k)$
$\boldsymbol{o}_{\mathrm{S}}$	Ascending order vector of $\psi_{\mathrm{RS}}^{-1}(1)$, $\psi_{\mathrm{RS}}^{-1}(2)$, ..., $\psi_{\mathrm{RS}}^{-1}(K')$
$\psi_{\mathrm{DR}}(k)$	Channel gain ranking function for the R-D link
$\psi_{\mathrm{DR}}^{-1}(k)$	Inverse function of $\psi_{\mathrm{DR}}(k)$
$\boldsymbol{o}_{\mathrm{R}}$	Ascending order vector of $\psi_{\mathrm{DR}}^{-1}(1)$, $\psi_{\mathrm{DR}}^{-1}(2)$, ..., $\psi_{\mathrm{DR}}^{-1}(K')$
$C_{\mathrm{DRS}}^{\mathrm{DF}}$	End-to-end CCMC capacity of broadband DF relaying
$C_{\mathrm{DRS}}^{\mathrm{AF}}$	End-to-end CCMC capacity of broadband AF relaying
$\boldsymbol{M}_{\mathrm{S}}$	Spectrum mapping matrix at the S-node
$\boldsymbol{M}_{\mathrm{R}}$	Spectrum mapping matrix at the R-node
$\boldsymbol{G}_{\mathrm{S}}$	Energy allocation matrix at the S-node
$\boldsymbol{G}_{\mathrm{R}}$	Energy allocation matrix at the R-node
$\omega_{\mathrm{S}}^{\mathrm{JEA}}(k')$	Joint energy allocation at the S-node for the k' spectral component
$\omega_{\mathrm{R}}^{\mathrm{JEA}}(k')$	Joint energy allocation at the R-node for the k' spectral component
$\omega_{\mathrm{S}}^{\mathrm{CEA}}(k')$	Cascaded energy allocation at the S-node for the k' spectral component
$\omega_{\mathrm{R}}^{\mathrm{CEA}}(k')$	Cascaded energy allocation at the R-node for the k' spectral component
K'_{opt}	Optimal K' that maximizes DCMC capacity for AF relaying

List of Abbreviations

AF	Amplify-and-Forward
AWGN	Additive White Gaussian Noise
BAR	Band Activity Ratio
BER	Bit Error Rate
BPSK	Binary Phase Shift Keying
CBRM	Circular Buffer Rate Matching
CCMC	Continuous input Continuous output Memoryless Channel
CDF	Cumulative Distribution Function
CEA	Cascaded Energy Allocation
CFR	Channel Frequency Response
CIR	Channel Impulse Response
CP	Cyclic Prefix
CSI	Channel State Information
DCMC	Discrete input Continuous output Memoryless Channel
DF	Decode-and-Forward
DFT	Discrete Fourier Transform
DSC	Dynamic Spectrum Control
EA	Energy Allocation
FER	Frame Error Rate
IBI	Interblock Interference
IDFT	Inverse Discrete Fourier Transform
ISI	Intersymbol Interference
JEA	Joint Energy Allocation
LS	Least Square
MC	Multicarrier
MSE	Mean Square Error
NSC	Non Systematic Convolutional
OFDM	Orthogonal Frequency Division Multiplexing
PAPR	Peak to Average Power Ratio

PDF	Probability Distribution Function
QAM	Quadrature Amplitude Modulation
QPSK	Quaternary Phase Shift Keying
RF	Radio Frequency
SC	Single Carrier
SC/MMSE	Soft-Canceller with Minimum Mean Square Error
SINR	Signal to Noise plus Interference power Ratio
SM	Spectrum Mapping
SNR	Signal to Noise power Ratio
SP	Subchannel Pairing
WSSUS	Wide-Sense Stationary Uncorrelated Scattering

Chapter 1

Introduction

Since the first transatlantic radio transmission by G. Marconi in 1901 [1], wireless communication has experienced a long way of development with phenomenal success. Especially, over the last couple of decays, wireless communication has witnessed a boom in the number of wireless devices with over 10 billion mobile handsets worldwide and a diversification of services from mobile telephony to video streaming [2]. This unprecedented growth is attributed to two significant milestones, both interestingly happened in the same year of 1948: (1) the establishment of information theory by C. E. Shannon [3] and (2) the development of solid state bipolar transistor by Shockley, Bardeen and Brattain [4]. In the early 1940s, transmissions over a communication link were commonly thought to be erroneous. However, Shannon's noisy-channel coding theorem [5] surprised the communication theory community by proving that it is possible to transmit information asymptotically error-free. If the transmission rate is less than or equal to the instantaneous achievable rate characterized by the channel, then the information can be transmitted asymptotically error-free by appropriate processing. Conversely, if the transmission rate exceeds the instantaneous achievable rate, then significant errors must occur no matter what processing is employed. By doing so, the information theory provided the hints and momentum for establishing reliable links between wireless terminals. Meanwhile, the transistor technology paved the way for the development and proliferation of inexpensive and portable wireless devices, resulting in the diversification of wireless services today. As a result, wireless communication has facilitated human's work and life and, at the same time, has introduced many challenges to communication engineers and theorists, especially, the challenge to cope with an ever growing demand for high data rate.

According to information theory, a link can achieve any arbitrarily low probability of error if the transmission rate is less than or equal to the instantaneous achievable rate provided by the channel [5][6]. The instantaneous rate is given by $C = B\log_2(1 + \text{SINR})$ [bits/s], where B is the transmission bandwidth and SINR is the received signal to noise plus interference power ratio.

Therefore, in order to meet the ever growing demand for high data rate, widening the bandwidth B, i.e., broadbandization of wireless transmissions, is an essential solution. Broadbandization can be enabled by exploring alternative frequency bands, e.g., ultra wide band (UWB) [7][8] and millimeter wave [9]–[12]. However, despise successes in the exploration for new frequency bands, radio-frequency spectrum is the most precious wireless resource and needs to be utilized efficiently. Therefore, together with the broadbandization, enhancing the spectral efficiency, which is measured by C/B is also necessary. Since most wireless terminal is battery-powered, the spectral efficiency should be enhanced under transmit power constraints. More importantly, when signal bandwidth is enlarged while its transmit power is kept constant, transmit energy per signal spectral component decreases. Furthermore, as the transmission band is widened, the transmission suffers from a frequency selective fading [13] which influences the spectral efficiency of the transmission. In the background of broadbandization, how to exploit the characteristics of frequency selective channel to enhance the spectral efficiency is an important issue.

The frequency selective fading stems from the multipath nature of radio channels [13]. In a transmission over a radio channel, due to scattering, diffraction and reflection, the signal reaches the receiver via various propagation paths with different delay times [14]. In a broadband wireless transmission, since the symbol duration is very short, multipath components may exceed several to several tenth symbol durations. As a result, intersymbol interference (ISI) may occur in the received signal and causes a degradation in the link reliability.

Orthogonal frequency division multiplexing (OFDM) [15][16] is an effective countermeasure against ISI. OFDM transmits a high rate data stream in multiple low rate substreams by multiple subchannels so that ISI occurs on only a small portion of each substream. OFDM employs cyclic prefix (CP) to make the received signal a periodic function so that the received signal spectrum becomes discrete. As a result, orthogonality among subchannels is preserved. Therefore, each subchannel experiences frequency-flat fading, which can be compensated for by a simple one-tap equalizer, e.g., zero-forcing [17]. In contrast, single carrier (SC) block transmission [18][19] transmits a high rate data stream by using one carrier frequency. In order to facilitate frequency-domain signal processing at the receiver, SC also employs CP to make the signal spectrum discrete. As a consequence, a powerful frequency-domain equalizer, e.g., frequency-domain soft-canceller with minimum mean square error (FD-SC/MMSE) turbo equalizer [20][21] can be applied to mitigate the impact of ISI. In summary, frequency selective fading is no longer an impairment to wireless communications since it can be coped with by OFDM or SC block transmission.

Frequency selective fading is now can be seen as providing opportunity to significantly enhance the spectral efficiency. A frequency selective channel is mathematically modeled by a

channel impulse response (CIR) with multiple components in the time-domain [22][23]. As a consequence, the channel frequency response (CFR), which is the Fourier transform of the CIR, dynamically fluctuates in the frequency-domain both in gain and phase shift. This characteristic of the frequency selective fading is very important because the spectral efficiency can be improved if the transmit power is optimally distributed in the frequency-domain to best exploit frequency band with high channel gain. The signal spectrum must be optimized at the transmitters while knowledge on the CFR is known to the receivers. Hence, it is essential for the receivers to notify the transmitters of the information about the CFR, in total or in part. This dissertation deliberates the issue of optimizing signal spectrum to enhance the spectral efficiency for broadband transmissions with a reasonable overhead. Although all proposals in this dissertation are applicable to either SC transmission or OFDM, hereafter only OFDM will be used for the sake of simplicity.

Due to the channel gain variation in the frequency-domain, there are both high gain subchannels and low gain subchannels within the system band. Transmission over high gain subchannels results in high received energy while transmission over low gain subchannels results in low received energy. To maximize the spectral efficiency for a system band in transmit power constraint conditions, transmit energy allocation using water-filling principle [13][24] is theoretically the best way. In this water-filling principle, no energy is allocated to a certain number of subchannels with low channel gain whereas more energy is allocated to those with higher gain. This means in water-filling principle, only an appropriate ratio of subchannels having higher gain in the system band is activated for transmissions. In other words, band activity ratio (BAR), i.e., the ratio of the number of activated subchannels to the number of all subchannels of the system band, is set to an appropriate value, which is smaller than 1. The reduction of BAR from 1 might sound like a reduction of spectral efficiency since the transmission suffers from a reduction in transmission bandwidth. However, the reduction of BAR brings about a possibility to improve the spectral efficiency because the transmission enjoys an increase in the received SINR owing to the selection of high gain subchannels. The increase in SINR implies that one can send more information on each activated subchannel. As a result, the spectral efficiency can be enhanced if BAR is set to balance the decrease in transmission bandwidth and the increase in the received SINR. On the other hand, a BAR controlled transmission results in a low overhead because the receiver needs to notify the transmitter of only the information on activated/deactivated status of each subchannel. Based on this consideration, this dissertation deliberates the exploitation of BAR control to solve the issue of spectral efficiency enhancement with a reasonable notification overhead. In this dissertation, BAR control is discussed mainly via two scenarios below.

The first scenario is BAR control for autonomous spectrum sharing for private networks, which is quite different from centralized spectrum sharing schemes used in cellular systems. In a centralized spectrum sharing scheme, an operator assigns frequency bands to each link according to the link conditions of all links in the network on a centralized management basis. On the other hand, in the autonomous spectrum sharing, the usable frequency band is obtained individually by each link according to the conditions of spectrum based on a distributed manner. An effective way to achieve high spectral efficiency in a distributed radio resource management is the dynamic spectrum control (DSC) [25]–[28]. In DSC, each link selects a certain amount of subchannels with higher gain in the system band regardless of the interference conditions. The number of subchannels to be selected is determined by BAR. Meanwhile, BAR is optimized by the number of links that simultaneously use the system band. Owing to the subchannel selection, the transmission band is arranged randomly over the system band, because channel condition for each link varies independently to each other. Therefore, mutual interference among links occurs only on a limited part of spectrum of each link. In this scheme, because mutual interference statistically decreases with the decrease of BAR, we can expect higher SINR in each link. However, when BAR is set to be too small, although mutual interference can be sufficiently reduced, the achievable throughput is suppressed because the transmission bandwidth of each link becomes too narrow. Therefore, there is an optimum value of BAR that maximizes the spectral efficiency of the whole network. Furthermore, when the number of links increases, the value of BAR becomes smaller to suppress the mutual interference. In this scenario, the optimal BAR is relatively small, basically, from around 0.5 to close to 0 depending on the number of links.

In the DSC, the point is, each link occupies only a limited amount of subchannels of the system band for transmission, and channel condition is observable only for the subchannels using a pilot signal embedded in the transmitted packet [29]. However, for the DSC, channel condition for the non-selected subchannels is also necessary because each link has to know channel state information (CSI) for the entire system band, including the non-selected subchannels for each user. Specifically, of course, CSI for the selected subchannels can be detected by a pilot signal [29]. Thus, the problem is how to accurately estimate CSI for the non-selected subchannels using only a pilot signal embedded in the currently selected subchannels [30][31]. Practically, the channel prediction can be formulated and solved by non-uniform sampling theory [32]-[34]. This CSI prediction has a characteristic that the reliability of the predicted CSI severely deteriorates if the bandwidth of continuously non-selected subchannels exceeds a specific level [30]. Unfortunately, when BAR is relatively small in a network, bandwidth of continuously non-selected subchannels tends to be large. As a consequence, reliability of the CSI severely

deteriorates. In this case, the spectral efficiency degrades since subchannels having high gain may not be selected due to lower reliability of the predicted CSI [30][31]. To deal with this issue, this dissertation proposes a CSI reliability guaranteeing subchannel selection which selects high gain subchannels under a constraint that the bandwidth of continuously non-selected subchannels is kept to be lower than a threshold [30]. Numerical results show that BAR control based on the proposed subchannel selection significantly enhance the spectral efficiency when BAR is relatively small in a network with many links, e.g., a network with up to 10 links [35].

The second scenario considered in this dissertation treats a case when a frequency band is already allocated to a user and the user dynamically controls BAR in the assigned spectrum to maximize its throughput. In this scenario, because the assigned band is fixed, the challenge is how to guarantee a certain transmission quality in a given channel condition. In the case of single hop transmission, water-filling principle is known to give its optimum solution as already explained. On the other hand, when multi-hop transmission is introduced to keep a certain transmission quality for broadband wireless access systems, optimization becomes more complex.

Wireless relaying with the aid of relay nodes (R-nodes) combats link quality degradation by dividing a link into many shorter sublinks. Relay strategies are typically classified into two categories: decode-and-forward (DF) and amplify-and-forward (AF) [36][37]. In DF relay, R-nodes perform hard-decoding on the received signal, and forward the resultant signal to the next R-node or D-node. In AF relay, R-nodes simply amplify and may linearly process the received signal before forwarding it. Therefore, compared to AF relay, DF relay gives higher transmission reliability especially when channel coding is introduced in the S-node. However, there is a very important advantage of the AF relay: applicability of AF to any type of signals without knowledge on their channel coding, modulation, encryption or any other privacy protection processing. Thus, this dissertation focuses on AF relay.

In a two-hop broadband AF relay, the end-to-end (from the source node to the destination node) channel gain is given by the multiplication of channel gains of the source-to-relay and relay-to-destination links. Hence, an existence of low gain subchannels in one arbitrary link results in a degradation in the end-to-end spectral efficiency for this subchannel. Unfortunately, because the channel gains of the two links fluctuate independently in the frequency-domain, subchannels which have high gain in one link might have low gain in the other link. When the number of links increases in the relay, more subchannels tend to be attenuated. This leads to a severe deterioration in the overall end-to-end spectral efficiency [38][39] [40]. To deal with this issue, subchannel pairing (SP) is already proposed in a literature [41]. In the SP, spectral component transmitted via a subchannel with higher gain in the first link is relayed via a sub-

channels with higher gain in the following links so that severe channel attenuation occurs only in a part of signal spectrum. Practically, the order of signal spectral components is changed at every relay node so that components transmitted over high gain subchannels in the first link, will also be relayed over high gain subchannels in the following links. As a result, the end-to-end efficiency can be significantly enhanced. For further spectral efficiency enhancement, this dissertation studies a cascaded energy allocation (CEA) in which energy of signal spectral components is adjusted at the source and each relay node based on convex optimization [39][40]. Under the CEA, this dissertation confirms the spectral efficiency enhancement effectiveness of the SP [39].

However, there is a very serious disadvantage in the SP that it requires a heavy notification overhead because the information of the spectral component order needs to be passed from the relay node to the destination node to enable the data detection [38][42]. To reduce such a heavy overhead, this dissertation proposes an alternative which removes the usage of low gain subchannels by optimizing BAR instead of the spectral component order [38][42]. Specially, the proposed BAR control employs spectrum nulling to deactivate an appropriate number of low gain subchannels of each link so that all spectral components are consistently transmitted over relatively high gain subchannels of the two links. Because the removal of lower gain subchannels in each link corresponds to the removal of the cause of low end-to-end channel gain, the proposed scheme is expected to achieve almost the same spectral efficiency as SP [42]. More importantly, because the proposed scheme does not require the information of the spectral component order (instead, only the selected/non-selected status for each subchannels is necessary), it can reduce the required notification overhead. Numerical analyses confirm that the proposed BAR control achieves almost the same spectral efficiency with the SP with a drastically reduced notification overhead for broadband AF relay [38].

The rest of this dissertation is organized as follows.

- Chapter 2 introduces a signal model for two broadband wireless transmission schemes: single carrier and OFDM, which will be used throughout this dissertation. Then, this chapter outlines the importance of BAR control in the enhancement of spectral efficiency for the broadband transmissions. After that, this chapter clarifies the impacts of BAR control and the issue of channel prediction in autonomous spectrum sharing with the aid of DSC. Finally, this chapter presents the effectiveness of wireless relaying in spectral efficiency enhancement and clarifies the spectral efficiency degradation issue of broadband AF relay. The issues of channel prediction in autonomous spectrum sharing and the spectral efficiency degradation issue of broadband AF relay clarify the contributions of this dissertation.

- In Chapter 3, Section 3.3, we formulate the issue of channel prediction for the entire system band when only a part of the system band is allocated to each user [A1][B2] [†]. This channel prediction is quite important for autonomous spectrum sharing with the aid of DSC in which a limited part of the system band with higher gain is dynamically selected for each link. Then we explain the spectral efficiency degradation due to the deterioration of CSI reliability when BAR is relatively small [A1][B2]. Aiming at enhancing the spectral efficiency, in Section 3.4, we propose CSI reliability guaranteeing subchannel selection scheme [A1]. Numerical analysis is given in Section 3.5 to show that BAR control based on the proposed subchannel selection scheme significantly enhances the spectral efficiency when BAR is controlled to be relatively small in networks with many links [D2].

- In Chapter 4, Section 4.2, we explain the challenges for broadband AF relay under frequency selective fading [A2][B1][D1]. In Section 4.3, we introduce subchannel pairing in order to enhance the spectral efficiency for the broadband AF relay. To further enhance the performance, we investigate the energy allocations for subchannels on the basis of convex optimizations in Section 4.4 [B1][D1]. In Section 4.5, the effectiveness of subchannel pairing in spectral efficiency enhancement is verified via numerical analysis [B1]. After that, in Section 4.6, we proposes adaptive BAR control based on spectrum nulling as a low overhead alternative for subchannel pairing [A2][C1]. Numerical analyses are given in Section 4.7 to confirm that the proposed adaptive BAR control achieves almost the same spectral efficiency with the subchannel pairing with a drastically reduced notification overhead [A2].

- Chapter 5 highlights the main results and contributions of this dissertation.

[†] A literature denoted by an upper case alphabet followed by a number, e.g., [A1], [A2], [B1], is a publication of the author. These literatures are shown in the "List of Publications by the Author" (pp. 109–110). Meanwhile, literatures denoted by numbers are listed in the "Bibliography" (pp. 103–108).

Chapter 2

Band Activity Ratio Control Aided Broadband Wireless Transmissions

2.1 Introduction

In a broadband transmission, the signal spectrum undergoes a CFR that dynamically fluctuates in the frequency-domain in both gain and phase shift. In the time varying CFR, there are both high gain subchannels and low gain subchannels. To enhance the spectral efficiency, only an appropriate ratio of subchannels having higher gain in the system band should be activated for transmissions. In other words, band activity ratio (BAR), i.e., the ratio of the number of activated subchannels to the number of all subchannels of the system band, should be set to an appropriate number, which is smaller than 1. Such a BAR controlled transmission requires an affordable notification of binary values describing activated/deactivated status of subchannels. This chapter outlines effectiveness of BAR control and deliberates the exploitation of BAR control to solve the issue of spectral efficiency enhancement with a reasonable notification overhead.

Specifically, the impacts and issue of BAR control in autonomous spectrum sharing employing DSC is clarified. Then, the effectiveness of wireless relaying in spectral efficiency enhancement for single user link with fixed band is presented and the spectral efficiency degradation issue of broadband AF relaying is explained. By presenting the issues of BAR control in autonomous spectrum sharing and broadband AF relaying, this chapter clarifies the contributions of this dissertation.

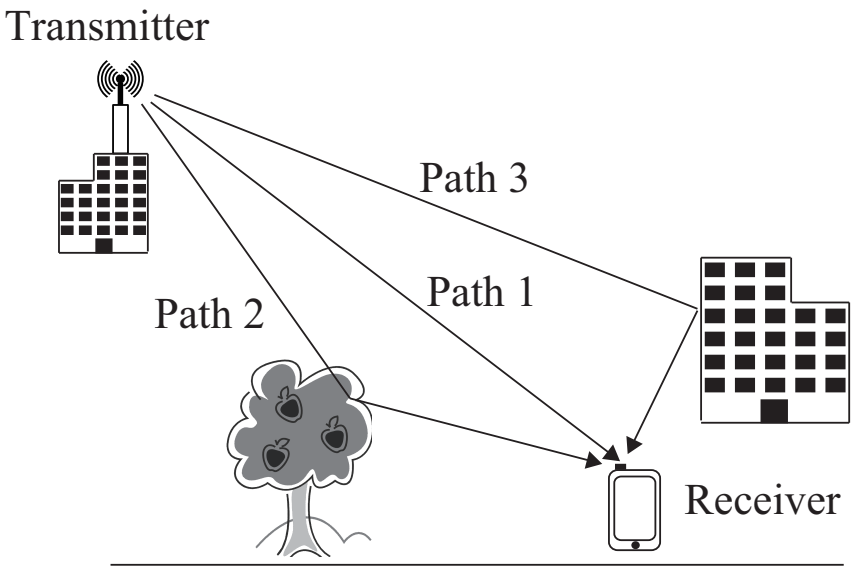

Figure 2.1: Illustration of the physical multipath environment.

2.2 Frequency Selective Fading Channels

2.2.1 Multipath Fading

Figure 2.1 illustrates a wireless communication under radio environment. Wireless signal reception is severely affected by multipath propagation as shown in Figure 2.1. Due to scattering, diffraction and reflection of electromagnetic wave, the transmitted signal follows many propagation paths before reaching the receiver's antenna. As a consequence, the received signal is a superposition of many signals with different delay times caused by the different path lengths of these signals. This leads to an interference pattern that varies over time and the transmission bandwidth. Thus, this section presents the statistical characteristics of this interference pattern.

An illustration of baseband transceiver for transmission over the multipath channel is described in Figure 2.2 in the next page. At the transmitter, a data bit sequence is divided into groups, each consists of several data bits. Each bit groups forms a data symbol which is then mapped into a waveform with interval T_s. The interval T_s is also called a symbol duration and its inversion $B = 1/T_s$ is the system bandwidth. Using the Dirac delta function $\delta(t)$ [13], the data symbol sequence $\check{x}(t)$ can be expressed as

$$\check{x}(t) = \sum_{n=-\infty}^{\infty} x(n) \cdot \delta(t - nT_s), \tag{2.1}$$

where t is instant time and $x(n)$ denotes the data symbol at the instant time nT_s. The data symbol sequence $\check{x}(t)$ is fed to the transmit filter to generate baseband transmitted signal. Let $g_T(t)$ be

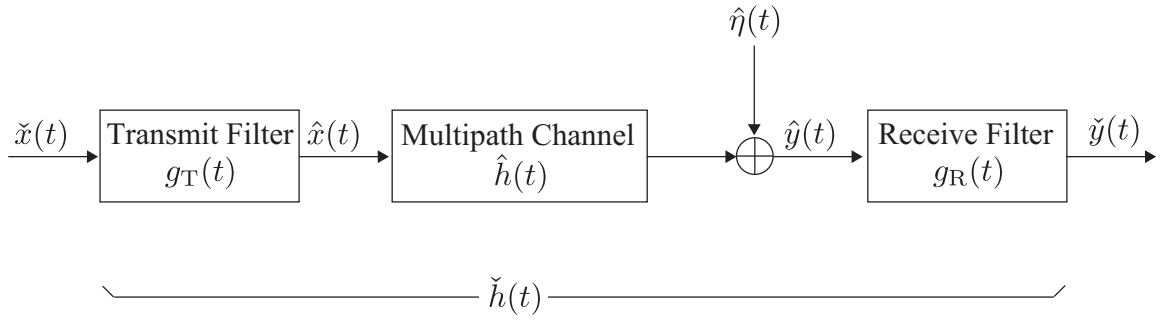

Figure 2.2: Baseband transceiver for transmission over multipath channel.

the impulse response of the transmit filter, the output of the transmit filter $\hat{x}(t)$ is given by

$$\hat{x}(t) = g_{\mathrm{T}}(t) \otimes \check{x}(t) = \sum_{n=-\infty}^{\infty} x(n) \cdot g_{\mathrm{T}}(t - nT_{\mathrm{s}}), \tag{2.2}$$

where $\otimes$ denotes convolution.

The signal $\hat{x}(t)$ is then transmitted to the receiver via the multipath channel. Let $\hat{h}(t)$ be the impulse response of the physical multipath channel, the received signal is expressed as

$$\hat{y}(t) = \hat{h}(t) \otimes \hat{x}(t) + \hat{\eta}(t) = \hat{h}(t) \otimes g_{\mathrm{T}}(t) \otimes \check{x}(t) + \hat{\eta}(t), \tag{2.3}$$

where $\hat{\eta}(t)$ is the baseband representation of random noise induced at the receiver.

At the receiver, the received signal $\hat{y}(t)$ is fed to the receive filter to generate received symbol sequence $\check{y}(t)$. Let $g_{\mathrm{R}}(t)$ be the impulse response of the receive filter, the received symbol sequence $\check{y}(t)$ is expressed as

$$\begin{aligned} \check{y}(t) &= g_{\mathrm{R}}(t) \otimes \hat{y}(t) \\ &= g_{\mathrm{R}}(t) \otimes \hat{h}(t) \otimes g_{\mathrm{T}}(t) \otimes \check{x}(t) + g_{\mathrm{R}}(t)\hat{\eta}(t) \\ &= \check{h}(t) \otimes \check{x}(t) + \check{\eta}(t) \end{aligned} \tag{2.4}$$

where $\check{\eta}(t) = g_{\mathrm{R}}(t)\hat{\eta}(t)$ is random noise which is known to follow a Gaussian distribution for most communication systems. More importantly, $\check{h}(t) = g_{\mathrm{R}}(t) \otimes \hat{h}(t) \otimes g_{\mathrm{T}}(t)$ is the CIR of the multipath channel including impact of physical environment as well as transmit and receive filters. As mentioned above, the transmitted signal reaches the receiver via multiple propagation paths. Thus, the CIR $\check{h}(t)$ can be represented by

$$\check{h}(t) = \sum_{l=1}^{L} h(l) \cdot \delta(t - \tau(l)), \tag{2.5}$$

where L is the number of propagation paths, $h(l)$ is complex-valued attenuation factor for the l-th path and $\tau(l)$ is the corresponding propagation delay. Without loss of generality, assuming $\tau(1) < \tau(2) < ... < \tau(L)$, then $\tau(L)$ is called the maximum excess delay of the multipath channel and the first path, i.e., $l = 1$, is the direct path with delay $\tau(1) = 0$.

From (2.4) and (2.5), the received symbol sequence is given by

$$\check{y}(t) = \sum_{l=1}^{L} h(l) \cdot \check{x}(t - \tau(l)) + \check{\eta}(t). \tag{2.6}$$

As shown in (2.6), $(L-1)$ echoes of the transmitted signal $\check{x}(t)$ arrive at the receiver and cause ISI in the received signal $\check{y}(t)$.

In the frequency-domain, the channel is characterized by the CFR which is the Fourier transform of CIR $\check{h}(t)$

$$\check{\xi}(f) = \int_{-\infty}^{\infty} \check{h}(t) \cdot \exp\left(-j2\pi f\tau\right) dt = \sum_{l=1}^{L} h(l) \cdot \exp\left(-j2\pi\tau(l)f\right). \tag{2.7}$$

In a mobile radio channel, the movement of transmitter and/or receiver causes the variation of the channel in the time-domain. In such a case, the CFR in (2.7) is a function of frequency and time which can be denoted as $\check{\xi}(f,t)$. Time variance of the channel is characterized by the autocorrelation of $\check{\xi}(f,t)$ which can be modeled by Jakes' model [43] as

$$\mathbb{E}\left[\check{\xi}^{*}(f,t) \cdot \check{\xi}(f,t+\Delta t)\right] = J_0(2\pi f_{\mathrm{D}}\Delta t), \tag{2.8}$$

where $J_0(\cdot)$ is the zero-order Bessel function of the first kind [13] and f_{D} is called Doppler frequency. The Doppler frequency f_{D} captures the rapidity with which the channel changes due to the movement of transmitter and/or receiver. The Doppler frequency f_{D} relates to the speed v of receiver's movement from transmitter as

$$f_{\mathrm{D}} = \frac{v}{c} \cdot f_{\mathrm{c}}, \tag{2.9}$$

where c is the speed of light and f_{c} is the carrier frequency.

2.2.2 Inter-Symbol Interference

The maximum excess delay $\tau(L)$ is defined by the characteristics of the physical multipath environment while the symbol duration T_{s} is determined by the required data rate. Relationship between them determines the severity of ISI in the received signal.

In a broadband transmission, the symbol duration T_s is very short, consequently the maximum excess delay $\tau(L)$ may exceed multiple symbol durations. In such a case, different multipath components can be resolved by the symbol duration T_s. Without loss of generality, assuming that $\tau(l) = (l-1)T_s$, the CIR is expressed as

$$\check{h}(t) = \sum_{l=1}^{L} h(l) \cdot \delta(\tau - (l-1)T_s). \tag{2.10}$$

From (2.6), the received signal is given by

$$\check{y}(t) = \sum_{l=1}^{L} h(l) \cdot \check{x}(t - (l-1)T_s) + \check{\eta}(t). \tag{2.11}$$

Consequently, received signal for $x(n)$ is given by

$$y(n) \equiv \check{y}(nT_s) = \sum_{l=1}^{L} h(l) \cdot x(n-l+1) + \eta(n), \tag{2.12}$$

where $\eta(n) \equiv \check{\eta}(nT_s)$. In this case ISI spans up to $(L-1)$ data symbols because the previous $(L-1)$ data symbols $x(n-1)$, ..., $x(n-L+1)$ are added in $y(n)$ as shown in equation (2.12). The CFR is given by

$$\check{\xi}(f) = \sum_{l=1}^{L} h(l) \cdot \exp\left(-\frac{j2\pi(l-1)f}{B}\right). \tag{2.13}$$

The channel is said to exhibit frequency selective fading because the CFR $\check{\xi}(f)$ fluctuates in the bandwidth B as shown in Equation (2.13).

By contrast, in a narrowband transmission, the symbol duration T_s is much longer than the maximum excess delay $\tau(l)$. In this case, since the multipath components arrive within a short fraction of the symbol duration, there is very little ISI. However, the received symbol is still distorted because the multipath components may add destructively. Because $\tau(l) \ll T_s$, from (2.7) it follows that the CFR is almost constant as $\check{\xi}(f) \approx \sum_{l=1}^{L} h(l)$ for $f \in [0, B)$. Thus, in this case the channel is said to exhibit frequency nonselective or flat fading.

Figure 2.3 illustrates the impact of ISI on broadband and narrowband transmissions. Figure 2.3 (a) describes an example of CIR. The CIR consists of a direct component and two delay components at delay T_s and $2T_s$, where T_s is the symbol duration as shown in Figure 2.3 (b). In the broadband transmission in Figure 2.3 (b), the symbol $x(1)$ arrives at the receiver together with echoes of the symbol $x(0)$ and $x(-1)$. In this case, the delay paths cause severe ISI on the whole received symbol. By contrast, in a narrow band transmission with long symbol duration $10T_s$ as shown in Figure 2.3 (c), the delay paths arrive within a short fraction of the received symbol and cause very little ISI.

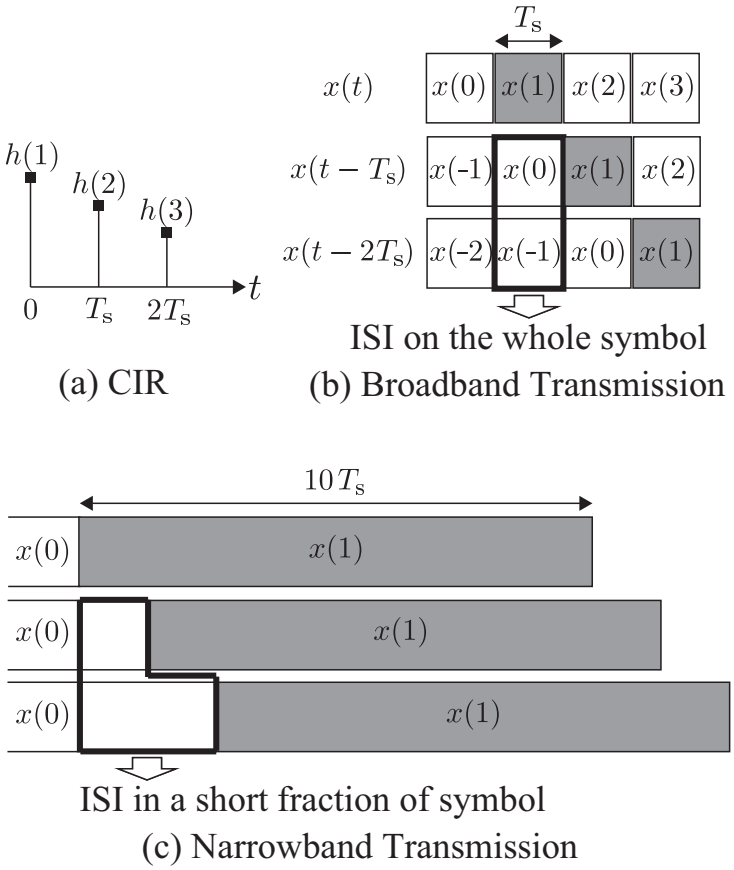

Figure 2.3: Impact of ISI on broadband and narrowband transmissions.

2.2.3 WSSUS Channel Model

In this section, we introduce a channel model for multipath fading for a broadband transmission. In such a case, the CIR is sampled by sampling interval T_s to generate discrete CIR $h(1)$, ..., $h(l)$, ..., $h(L)$ as mentioned in Section 2.2.2. Random fluctuations in the received symbol due to multipath fading is modeled by treating the discrete CIR $h(1)$, ..., $h(l)$, ..., $h(L)$ as random processes in time. A widely used model for the multipath channel was introduced by Bello [22] in which the time-varying nature of the CIR $h(l)$ is modeled as a wide-sense stationary uncorrelated scattering (WSSUS) random process, i.e., the variance of $h(l)$ is stationary and uncorrelated. As a result, $h(l)$ is modeled as uncorrelated Gaussian random variables with zero-mean and variance $\mathbb{E}\{|h(l)|^2\} = p(l)$, i.e., $h(l) \sim \mathcal{CN}(0, p(l))$. Note that $\mathbb{E}\{\cdot\}$ denotes the expected value of a random variable and $p(l)$ is the value of delay power profile at instant delay $\tau(l) = (l-1)T_s$.

The sum of all values of $p(l)$ expresses the energy gain for a signal when transmitted over

the channel which is denoted by

$$\sum_{l=1}^{L} p\left(l\right) = \sum_{l=1}^{L} \mathbb{E}\left\{\left|h\left(l\right)\right|^2\right\} = \Psi. \tag{2.14}$$

The energy gain Ψ is affected by path loss and shadowing [44][45][14]. Path loss can be represented by the path loss exponent μ whose value is normally in the range of 2 to 6. Besides multipath fading, this dissertation only focuses on path loss in the investigation of spectral efficiency enhancement effect of relaying, thus shadowing is omitted to avoid divergence of discussions. In such a case, the relation between energy gain Ψ and the distance d from the transmitter to the receiver can be expressed as

$$\Psi \propto d^{-\mu}. \tag{2.15}$$

A useful indicator for the performance of a wireless transmission under the multipath fading channel is the delay spread τ_{rms} which is given by

$$\tau_{\text{rms}} = \sqrt{\overline{\tau^2} - \overline{\tau}^2}, \tag{2.16}$$

where

$$\overline{\tau} = \frac{\sum_{l=1}^{L}\left(l-1\right)p\left(l\right)}{\Psi}, \qquad \overline{\tau^2} = \frac{\sum_{l=1}^{L}\left(l-1\right)^2 p\left(l\right)}{\Psi}. \tag{2.17}$$

It is verified via computer simulations that the bit error rate (BER) performance of a wireless transmission is practically identical if the delay spread τ_{rms} is the same, even if the delay power profiles $p\left(l\right)$ differ widely [46]. Using the delay spread, coherence bandwidth of the channel, i.e., the bandwidth in which the CFR is almost constant in the frequency-domain is roughly determined as

$$\Delta f_{\text{coh}} \approx \frac{1}{\tau_{\text{rms}}}. \tag{2.18}$$

Figure 2.4 describes delay power profiles for two widely used channel models. The power delay profile for the equal gain L path Rayleigh fading model in Figure 2.4 (a) is given by

$$p(l) = \begin{cases} \Psi/L & 1 \le l \le L \\ 0 & l > L \end{cases}, \tag{2.19}$$

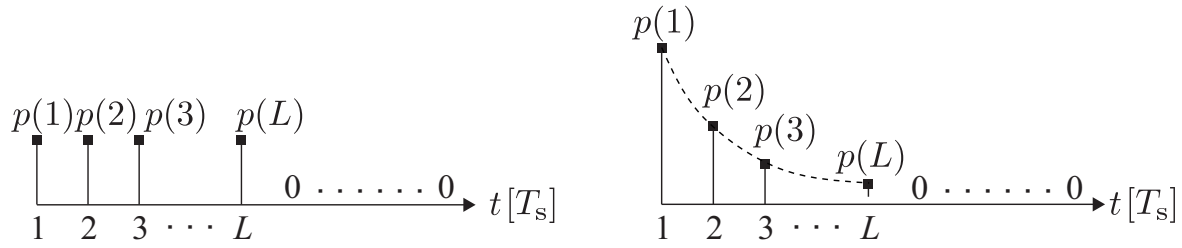

(a) Equal gain L path Rayleigh fading model

(b) υ dB exponentially decaying L path Rayleigh fading model

Figure 2.4: Delay power profiles of two widely used channel models.

and that for the υ dB exponentially decaying L path Rayleigh fading model in Figure 2.4 (b) is given by

$$p(l) = \begin{cases} \Psi \dfrac{10^{-(l-1)\upsilon/10} - 10^{-l\upsilon/10}}{1 - 10^{-L\upsilon/10}} & 1 \le l \le L \\ 0 & l > L \end{cases}. \tag{2.20}$$

Although the two models are quite different from real radio channels in practice, they are widely used in performance evaluations for many transmission systems. This is due to their simplicity and to the fact mentioned above that not the power delay profile but the delay spread influences the performances.

2.3 Broadband Wireless Transmissions

Countermeasure for ISI is a critical problem when realizing high data rate transmissions, i.e., those with short symbol duration T_s such that $T_s < \tau(L)$. Multicarrier (MC) and single carrier (SC) transmissions are two promising schemes to effectively mitigate the impact of ISI. The concept of MC and SC is described in Figure 2.5. As shown in Figure 2.5 (a), the MC scheme splits the data stream into K substreams of lower data rate such that the symbol duration becomes $KT_s(\gg \tau(L))$ and employs K subcarriers or subchannels to transmit substreams in parallel. MC scheme was considered impractical because it requires large hardware containing many modulation circuits and exact carrier frequency generators. Discrete Fourier transform (DFT) based orthogonal frequency division multiplexing (OFDM), which was proposed in 1971 [15][16], has open a possibility for realization of MC scheme. Due to the computational complexity reduction effect of DFT, the DFT based OFDM began to be adopted in many practical communication systems from 1979. By contrast, as illustrated in Figure 2.5 (b) the SC scheme [20] transmits the data stream with the original high symbol rate $T_s < \tau(L)$ and uses equalizer at

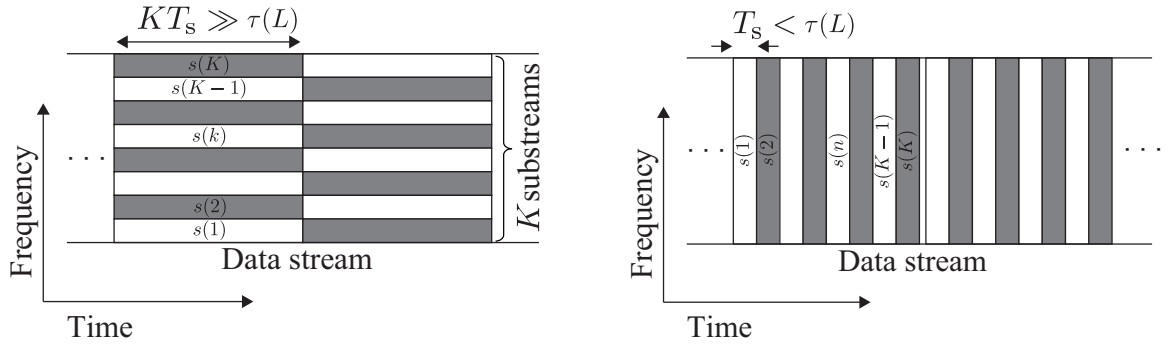

(a) Multicarrier scheme

(b) Single carrier scheme

Figure 2.5: The concept of broadband transmission schemes.

the receiver to mitigate the impact of ISI. The equalization in the time-domain is a computationally intense process. However, recently it was shown that by transforming the received signal to the frequency-domain using the DFT, we can in principle significantly reduce the computational complexity of the SC scheme.

Since the OFDM scheme transmits data in parallel subchannels, its receiver hardware is simple since one-tap equalizer can be employed to mitigate the impact of fading. However, since OFDM signal has high peak-to-average-power ratio (PAPR), the scheme requires amplifiers with wide linear region and high saturation power. By contrast, the SC scheme has lower PAPR and is more resistant to frequency offset error compared to OFDM. Of course, to mitigate the impact of ISI, SC receiver requires sophisticated equalizer. However, together with the evolution of semiconductor technology, the computational burden of SC receiver is no longer a serious problem at present. As a result, currently, the selection of OFDM or SC is based on backward compatibility of systems, required PAPR and some other preference factors for system designers rather than the computational burden of signal processing. Detailed comparisons between MC and SC schemes can be found in [47][18][19]. In the subsequent sections, we will give a detailed description of both OFDM and SC schemes.

2.3.1 OFDM

As an MC transmission, OFDM splits the incoming data stream with short symbol duration $T_s < \tau(L)$ into K substreams with longer symbol duration $T_{\text{OFDM}} = KT_s \gg \tau(L)$ and transmits these K substreams simultaneously via K orthogonal subchannels. Because each substream occupies a bandwidth of $\Delta f = 1/T_{\text{OFDM}}$, in the OFDM implementation by DFT [15] the carrier frequencies are chosen such that their spacing is equal to $\Delta f = 1/T_{\text{OFDM}}$. When $s(1)$, ...,

$s(k)$, ..., $s(K)$ are K data symbols transmitted during one OFDM symbol duration T_{OFDM}, the baseband transmitted signal is represented by

$$\check{x}(t) = \frac{1}{\sqrt{K}} \sum_{k=1}^{K} s(k) \cdot \exp\left(j2\pi(k-1)\Delta f t\right) \qquad (0 \le t < T_{\mathrm{OFDM}}). \tag{2.21}$$

Note that in the OFDM scheme, the data symbol index k corresponds to subchannel index.

Before transmission, the transmitted signal $\check{x}(t)$ is sampled in the time-domain with sampling interval $T_{\mathrm{OFDM}}/K = T_{\mathrm{s}}$. The n-th ($n \in \{1, 2, ..., K\}$) sampled time-domain transmitted signal is given by

$$x(n) \equiv \check{x}((n-1)T_{\mathrm{s}}) = \frac{1}{\sqrt{K}} \sum_{k=1}^{K} s(k) \cdot \exp\left(j\frac{2\pi(k-1)(n-1)}{K}\right). \tag{2.22}$$

Equation (2.22) shows that the sampled time-domain transmitted signals can be generated by inverse discrete Fourier transform (IDFT). The K samples of the time-domain signal $x(n)$ ($n \in \{1, 2, ..., K\}$) form an OFDM symbol whose vector representation is

$$\boldsymbol{x} = [x(1), ..., x(n), ..., x(K)]^{\mathrm{T}} = \boldsymbol{F}_K^{\mathrm{H}} \boldsymbol{s}. \tag{2.23}$$

Equation (2.23) implies that the data symbol vector $\boldsymbol{s} = [s(1), ..., s(k), ..., s(K)]^{\mathrm{T}}$ corresponds to the transmitted spectrum, i.e., the frequency-domain representation of $\boldsymbol{x}$. Note that $\cdot^{\mathrm{T}}$ is transpose of a matrix or a vector while $\cdot^{\mathrm{H}}$ indicates conjugate transpose of a matrix or a vector. The notation $\boldsymbol{F}_a$ expresses an $a \times a$ DFT matrix defined by

$$\boldsymbol{F}_a = \frac{1}{\sqrt{a}} \begin{bmatrix} \omega^{(0)(0)} & \omega^{(0)(1)} & \cdots & \omega^{(0)(a-1)} \\ \omega^{(1)(0)} & \omega^{(1)(1)} & \cdots & \omega^{(1)(a-1)} \\ \vdots & \vdots & \ddots & \vdots \\ \omega^{(a-1)(0)} & \omega^{(a-1)(1)} & \cdots & \omega^{(a-1)(a-1)} \end{bmatrix}, \tag{2.24}$$

where $\omega = \exp(-j2\pi/a)$. Equation (2.22) implies that the transmitted symbols are able to be multiplexed by IDFT and then de-multiplexed by DFT. This means that by using DFT/IDFT MC transmission is able to be implemented without a complex hardware consisting of many carrier frequency generators and bandpass filters.

For the ease of frequency-domain processing and mitigation of interblock interference (IBI) from the previous OFDM symbol, a cyclic prefix (CP), which is a copy of the last L_{CP} samples in the symbol vector $\boldsymbol{x}$ is appended to the head of the vector. The CP length L_{CP} must be longer than or equal to the maximum excess delay $(L-1)$ of the multipath channel to mitigate IBI from the previous OFDM symbol. Thus, $L_{\mathrm{CP}} = L-1$ will be used in the following. The CP-appended OFDM symbol $\boldsymbol{x}_{+\mathrm{CP}} \in \mathbb{C}^{(K+L-1)\times 1}$ is denoted by

$$\boldsymbol{x}_{+\mathrm{CP}} = [x_{+\mathrm{CP}}(1), ..., x_{+\mathrm{CP}}(n), ..., x_{+\mathrm{CP}}(K-L+1)]^{\mathrm{T}} = \boldsymbol{G}_{+\mathrm{CP}} \boldsymbol{x}, \tag{2.25}$$

where $\boldsymbol{G}_{+\mathrm{CP}} \in \mathbb{C}^{(K+L-1)\times K}$ is the CP insertion matrix which is determined by

$$\boldsymbol{G}_{+\mathrm{CP}} = \begin{bmatrix} \boldsymbol{0}_{(L-1)\times(K-L+1)} & \boldsymbol{I}_{(L-1)} \\ & \boldsymbol{I}_K \end{bmatrix}. \tag{2.26}$$

In (2.26), $\boldsymbol{0}_{a\times b}$ indicates an $a \times b$ matrix with zero entities and $\boldsymbol{I}_a$ indicates an $a \times a$ unit matrix.

Let the discrete representation for the CIR be a vector $\boldsymbol{h} \in \mathbb{C}^{L\times 1}$ denoted by

$$\boldsymbol{h} = [h(1), ..., h(l), ..., h(L)]^{\mathrm{T}}. \tag{2.27}$$

Being transmitted over the multipath channel, the CP-appended OFDM symbol $\boldsymbol{x}_{+\mathrm{CP}}$ is convoluted by the CIR $\boldsymbol{h}$ and multiplexed with the previous CP-appended OFDM symbol $\boldsymbol{x}'_{+\mathrm{CP}}$. As a result, the received signal vector $\boldsymbol{y}_{+\mathrm{CP}} \in \mathbb{C}^{(K+L-1)\times 1}$ is given by

$$\boldsymbol{y}_{+\mathrm{CP}} = \boldsymbol{H}_{\mathrm{IBI}}\boldsymbol{x}'_{+\mathrm{CP}} + \boldsymbol{H}\boldsymbol{x}_{+\mathrm{CP}} + \boldsymbol{\eta}_{+\mathrm{CP}}, \tag{2.28}$$

where the first term is IBI from the previous OFDM symbol, the second term is the desired signal, and the third is noise. In (2.28) $\boldsymbol{\eta}_{+\mathrm{CP}}$ denotes noise vector induced in the signal reception. Matrices $\boldsymbol{H}_{\mathrm{IBI}}$ and $\boldsymbol{H}$ are assumed to be constant during the transmissions of $\boldsymbol{x}'_{+\mathrm{CP}}$ and $\boldsymbol{x}_{+\mathrm{CP}}$, respectively. The matrix $\boldsymbol{H}_{\mathrm{IBI}}$ is defined by

$$\boldsymbol{H}_{\mathrm{IBI}} = \begin{bmatrix} \boldsymbol{0}_{(L-1)\times K} & \boldsymbol{\Delta} \\ \boldsymbol{0}_{K\times K} & \boldsymbol{0}_{K\times(L-1)} \end{bmatrix} \quad \left(\in \mathbb{C}^{(K+L-1)\times(K+L-1)}\right), \tag{2.29}$$

where $\boldsymbol{\Delta}$ is given by

$$\boldsymbol{\Delta} = \begin{bmatrix} h(L) & \cdots & h(2) \\ & \ddots & \vdots \\ & & h(L) \end{bmatrix} \quad \left(\in \mathbb{C}^{(L-1)\times(L-1)}\right). \tag{2.30}$$

Note that in (2.30) and other matrix notations hereafter, the blanks outside dots denote zeros. In (2.28) the matrix $\boldsymbol{H}$ is determined by

$$\begin{aligned} \boldsymbol{H} &= \begin{bmatrix} h(1) & & & & & \\ h(2) & \ddots & & & & \\ \vdots & & h(1) & & & \\ h(L) & & h(2) & h(1) & & \\ & \ddots & \vdots & \vdots & \ddots & \\ & & h(L) & h(L-1) & \cdots & h(1) \end{bmatrix} \\ &= \begin{bmatrix} \boldsymbol{H}_{11} & \boldsymbol{H}_{12} \\ \boldsymbol{H}_{21} & \boldsymbol{H}_{22} \end{bmatrix} \quad \left(\in \mathbb{C}^{(K-L+1)\times(K-L+1)}\right), \end{aligned} \tag{2.31}$$

where

$$\boldsymbol{H}_{11} = \begin{bmatrix} h(1) & & \\ \vdots & \ddots & \\ h(L-1) & \cdots & h(1) \end{bmatrix} \quad \left(\in \mathbb{C}^{(L-1)\times(L-1)}\right), \tag{2.32}$$

$$\boldsymbol{H}_{12} = \boldsymbol{0}_{(L-1)\times K}, \tag{2.33}$$

$$\boldsymbol{H}_{21} = \begin{bmatrix} h(L) & \cdots & h(2) \\ & \ddots & \vdots \\ & & h(L) \\ & & \\ & & \\ & & \end{bmatrix} \quad \left(\in \mathbb{C}^{K\times(L-1)}\right), \tag{2.34}$$

$$\boldsymbol{H}_{22} = \begin{bmatrix} h(1) & & & & & \\ h(2) & \ddots & & & & \\ \vdots & & h(1) & & & \\ h(L) & & h(2) & h(1) & & \\ & \ddots & \vdots & \vdots & \ddots & \\ & & h(L) & h(L-1) & \cdots & h(1) \end{bmatrix} \quad \left(\in \mathbb{C}^{K\times K}\right). \tag{2.35}$$

After that, CP is removed from the received signal $\boldsymbol{y}_{+\mathrm{CP}}$ by the CP removal matrix

$$\boldsymbol{G}_{-\mathrm{CP}} = \begin{bmatrix} \boldsymbol{0}_{K\times(L-1)} & \boldsymbol{I}_K \end{bmatrix} \qquad (\in \mathbb{C}^{K\times(K-L+1)}). \tag{2.36}$$

The received OFDM symbol after the CP removal is

$$\boldsymbol{y} = \boldsymbol{G}_{-\mathrm{CP}}\boldsymbol{y}_{+\mathrm{CP}} = \boldsymbol{G}_{-\mathrm{CP}}\left[\boldsymbol{H}_{\mathrm{IBI}}\boldsymbol{x}'_{+\mathrm{CP}} + \boldsymbol{H}\boldsymbol{x}_{+\mathrm{CP}} + \boldsymbol{\eta}_{+\mathrm{CP}}\right]. \tag{2.37}$$

From equations (2.29), (2.30), and (2.36) it follows that $\boldsymbol{G}_{-\mathrm{CP}}\boldsymbol{H}_{\mathrm{IBI}} = \boldsymbol{0}_{K\times(K+L_{\mathrm{CP}})}$, i.e., the CP insertion and removal eliminate IBI from the previous OFDM symbol. Hence, (2.37) yields

$$\boldsymbol{y} = \left[y(1), ..., y(n), ..., y(K)\right]^{\mathrm{T}} = \boldsymbol{H}_{\mathrm{circ}}\boldsymbol{x} + \boldsymbol{\eta}, \tag{2.38}$$

where noise vector is given by

$$\boldsymbol{\eta} = \left[\eta(1), ..., \eta(n), ..., \eta(K)\right]^{\mathrm{T}}, \tag{2.39}$$

and $\boldsymbol{H}_{\text{circ}}$ is a circulant matrix determined by

$$\boldsymbol{H}_{\text{circ}} = \boldsymbol{G}_{-\text{CP}}\boldsymbol{H}\boldsymbol{G}_{+\text{CP}} = \begin{bmatrix} h(1) & & & & h(L) & \cdots & h(2) \\ h(2) & \ddots & & & & \ddots & \vdots \\ \vdots & & \ddots & & & & h(L) \\ h(L) & & & h(1) & & & \\ & \ddots & & h(2) & h(1) & & \\ & & \ddots & \vdots & \vdots & \ddots & \\ & & & h(L) & h(L-1) & \cdots & h(1) \end{bmatrix} \quad (\in \mathbb{C}^{K\times K}). \tag{2.40}$$

The circular structure of $\boldsymbol{H}_{\text{circ}}$ implies that in the absence of noise the received OFDM symbol $\boldsymbol{y}$ is periodic. As a result, the received spectrum $\boldsymbol{y}^{\text{f}}$, which is the frequency-domain representation of $\boldsymbol{y}$ is able to be calculated by using DFT as

$$\begin{aligned} \boldsymbol{y}^{\text{f}} &= \left[y^{\text{f}}(1), ..., y^{\text{f}}(k), ..., y^{\text{f}}(K)\right]^{\text{T}} \\ &= \boldsymbol{F}_K \boldsymbol{y} \\ &= \boldsymbol{F}_K \boldsymbol{H}_{\text{circ}} \boldsymbol{F}_K^{\text{H}} \boldsymbol{s} + \boldsymbol{F}_K \boldsymbol{\eta} \\ &= \boldsymbol{\Xi}\, \boldsymbol{s} + \boldsymbol{\eta}^{\text{f}}, \end{aligned} \tag{2.41}$$

where $\boldsymbol{\eta}^{\text{f}} = \boldsymbol{F}_K\boldsymbol{\eta}$ is the noise spectrum vector and $\boldsymbol{\Xi} = \boldsymbol{F}_K\boldsymbol{H}_{\text{circ}}\boldsymbol{F}_K^{\text{H}}$ is the frequency-domain channel matrix.

In the following, we derive a simplified expression for $\boldsymbol{\Xi}$. From (2.24) and (2.40) we have

$$\boldsymbol{F}\boldsymbol{H}_{\text{circ}} = \frac{1}{\sqrt{K}} \begin{bmatrix} \omega^{(0)(0)}\xi(1) & \omega^{(0)(1)}\xi(1) & \cdots & \omega^{(0)(K-1)}\xi(1) \\ \omega^{(1)(0)}\xi(2) & \omega^{(1)(1)}\xi(2) & \cdots & \omega^{(1)(K-1)}\xi(2) \\ \vdots & \vdots & \ddots & \vdots \\ \omega^{(K-1)(0)}\xi(K) & \omega^{(K-1)(1)}\xi(1) & \cdots & \omega^{(K-1)(K-1)}\xi(K) \end{bmatrix}, \tag{2.42}$$

where $\xi(a) = \sum_{l=1}^{L} \omega^{(a-1)(l-1)}h(l)$ for $a \in \{1, 2, ..., K\}$. From (2.42), the element at the a-th row and the c-th column of matrix $\boldsymbol{F}\boldsymbol{H}_{\text{circ}}$ is

$$(\boldsymbol{F}\boldsymbol{H}_{\text{circ}})_{ac} = \frac{1}{\sqrt{K}}\omega^{(a-1)(c-1)}\xi(a). \tag{2.43}$$

The element at the a-th row and the b-th column of the matrix $\boldsymbol{\Xi}$ is derived as

$$\begin{aligned}\boldsymbol{\Xi}_{ab} &= \left(\left(\boldsymbol{F}_K \boldsymbol{H}_{\text{circ}}\right) \boldsymbol{F}_K^{\text{H}}\right)_{ab} \\ &= \sum_{c=1}^{K} \left(\boldsymbol{F}_K \boldsymbol{H}_{\text{circ}}\right)_{ac} \left(\boldsymbol{F}_K^{\text{H}}\right)_{cb} \\ &= \sum_{c=1}^{K} \left(\frac{1}{\sqrt{K}} \omega^{(a-1)(c-1)} \xi(a)\right)\left(\frac{1}{\sqrt{K}} \omega^{-(c-1)(b-1)}\right) \\ &= \frac{1}{K} \xi(a) \sum_{c=1}^{K} e^{(a-b)(c-1)}. \end{aligned} \tag{2.44}$$

On the other hand, for all $z \in \mathbb{C}$, we have

$$1 - z^K = (1 - z) \sum_{c=1}^{K} z^{c-1}. \tag{2.45}$$

Substituting $z = e^{j2\pi(a-b)/K}$ into (2.45), we get

$$1 - e^{j2\pi(a-b)} = (1 - e^{j2\pi(a-b)/K}) \sum_{c=1}^{K} e^{j2\pi(a-b)(c-1)/K}. \tag{2.46}$$

When $a \neq b$, the left hand side of (2.46) is zero while the first term of the right hand side is not zero. As a consequence the term $\sum_{c=1}^{K} e^{j2\pi(a-b)(c-1)/K} = 0$. Thus, according to (2.44) $\Xi(a, b) = 0$ for $a \neq b$, i.e., all the nondiagonal element of matrix $\boldsymbol{\Xi}$ are zeros. When $a = b$, according to (2.44)

$$\Xi(a, a) = \frac{1}{K} \xi(a) \sum_{c=1}^{K} e^{(a-b)(c-1)} = \frac{1}{K} \xi(a) \sum_{c=1}^{K} 1 = \xi(a). \tag{2.47}$$

Thus, $\boldsymbol{\Xi}$ is a diagonal matrix expressed by

$$\boldsymbol{\Xi} = \text{diag}\left[\xi(1), ..., \xi(k), ..., \xi(K)\right], \tag{2.48}$$

where $\xi(k)$ implies CFR at the k-th subchannel. CFRs of all K subchannels is modeled as

$$\boldsymbol{\xi} = \left[\xi(1), ..., \xi(k), ..., \xi(K)\right]^{\text{T}} = \sqrt{K} \boldsymbol{F}_K \boldsymbol{W} \boldsymbol{h}, \tag{2.49}$$

where matrix $\boldsymbol{W}$ is given by

$$\boldsymbol{W} = \begin{bmatrix} \boldsymbol{I}_L \\ \boldsymbol{0}_{(K-L)\times L} \end{bmatrix} \qquad \left(\in \mathbb{C}^{K \times L}\right). \tag{2.50}$$

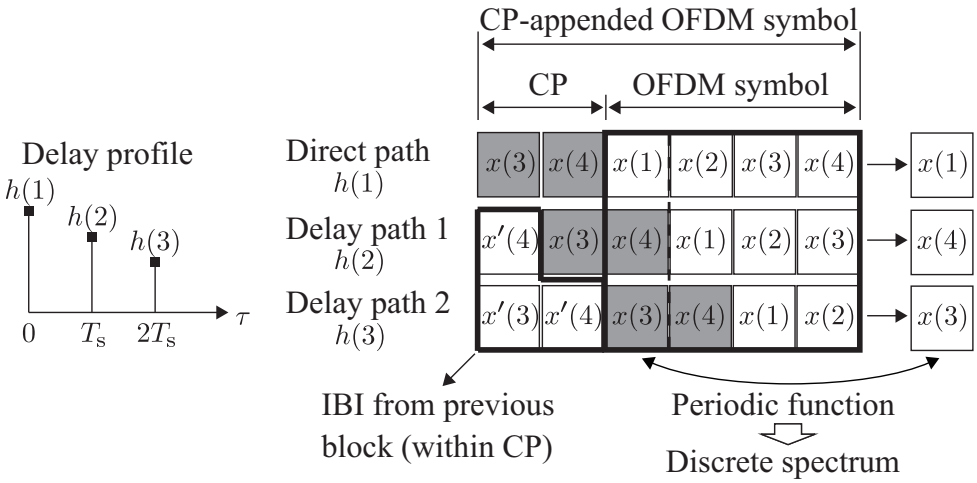

Figure 2.6: Illustration of functions of cyclic prefix for $K = 4$, $L = 3$.

The fact that $\boldsymbol{\Xi}$ is diagonal proves that all the K subchannels are orthogonal to each other and each subchannel experiences flat fading with CFR $\xi(k)$. This means we can apply a single tap equalizer for each subchannel to compensate for the flat fading.

It is necessary to rephrase that the CP has two functions that is very important to the implementation of OFDM: (1) eliminating IBI from previous OFDM symbol, and (2) preserving orthogonality among subchannels under ISI in each subchannel. Figure 2.6 illustrates these two functions for the case of $K = 4$ and $L = 3$ ($L_{\mathrm{CP}} = 2$). As shown in the figure, the received signal includes IBI from the previous OFDM symbol: $x'(4)$ arrived in the delay path 1, $x'(3)$ and $x'(4)$ arrived in the delay path 2. However, since this IBI is within the CP length, it is abandoned by the CP removal. The received signal corresponding to OFDM symbol block is a periodic function since if we extend the received OFDM block more 1 symbol, we will receive a symbol includes $x(1)$ in the direct path, $x(4)$ in the delay path 1 and $x(3)$ in the delay path 2, which is identical to the first symbol of the OFDM block. As a consequence, the signal spectrum is discrete and orthogonality among subchannels is preserved.

2.3.2 Single Carrier Transmission

In an SC scheme, the original data stream with short symbol duration $T_{\mathrm{SC}} = T_{\mathrm{s}} < \tau(L)$ is transmitted by a single carrier. Since the maximum excess delay $\tau(L)$ is longer than the symbol duration T_{s}, the received signal will suffer from severe ISI. ISI mitigation requires equalization at the receiver which is computationally complex in the time-domain but simpler in the frequency-domain. In order to facilitate the equalizer in the frequency-domain, data stream is

transmitted in blocks with a CP appended at the head of each block. The CP eliminates IBI from the previous symbol block and makes the received signal a periodic function so that the received signal spectrum becomes discrete.

Assume the CIR of the multipath channel is identical to that in the OFDM transmission in Section 2.3.1, i.e., the CIR defined by (2.27). Consider the transmission for a symbol block comprises of K data symbols $s(1)$, ..., $s(n)$, ..., $s(K)$. Vector representation for baseband signal of this block is given by

$$\boldsymbol{x} = [x(1), ..., x(n), ..., x(K)]^{\mathrm{T}} = \boldsymbol{s}, \tag{2.51}$$

where $x(n) = s(n)$. This relation is different from that in OFDM scheme where vector $\boldsymbol{x}$ is the IDFT of vector $\boldsymbol{s}$ as shown in (2.23). Note that in SC scheme, the data symbols are indexed by n since they are transmitted in serial in the time-domain.

Similar to OFDM scheme, a CP which is a copy of the last L_{CP} $(= L - 1)$ symbols of the symbol block $\boldsymbol{x}$ is appended to the head of $\boldsymbol{x}$. As a result, the CP-appended symbol block is K symbol periodic, thus the frequency-domain representation of $\boldsymbol{x}$ can be computed by using DFT

$$\boldsymbol{x}^{\mathrm{f}} = \left[x^{\mathrm{f}}(1), ..., x^{\mathrm{f}}(k), ..., x^{\mathrm{f}}(K)\right]^{\mathrm{T}} = \boldsymbol{F}_K \boldsymbol{s} \qquad \left(\in \mathbb{C}^{K\times 1}\right). \tag{2.52}$$

The CP-appended symbol block is then transmitted over the multipath channel. Note that in (2.52), $x^{\mathrm{f}}(k)$ represents the sample of transmitted spectrum at the discrete frequency $(k-1)/T_{\mathrm{SC}}$.

At the receiver, CP removal is applied to generate received symbol block in the time-domain

$$\boldsymbol{y} = [y(1), ..., y(n), ..., y(K)]^{\mathrm{T}} = \boldsymbol{H}_{\mathrm{circ}} \boldsymbol{x} + \boldsymbol{\eta}, \tag{2.53}$$

where $\boldsymbol{H}_{\mathrm{circ}}$ is the circulant matrix defined in (2.40) and $\boldsymbol{\eta}$ is noise vector given by (2.39).

To facilitate frequency-domain processing, the received block $\boldsymbol{x}$ is applied to DFT to generate the received spectrum in the frequency-domain as

$$\boldsymbol{y}^{\mathrm{f}} = \boldsymbol{\Xi}\boldsymbol{x}^{\mathrm{f}} + \boldsymbol{\eta}^{\mathrm{f}}, \tag{2.54}$$

where the frequency-domain channel matrix $\boldsymbol{\Xi}$ is identical to that in (2.48) and $\boldsymbol{\eta}^{\mathrm{f}}$ also denotes the noise spectrum induced in the signal reception.

Similar to OFDM, in the SC scheme, due to the fact that the frequency-domain channel matrix $\boldsymbol{\Xi}$ is diagonal, we can process all the spectral components of the received spectrum $\boldsymbol{y}^{\mathrm{f}}$ separately. This enables powerful equalizers, e.g., the frequency-domain turbo equalizer [21] to mitigate the impact of ISI for SC transmissions.

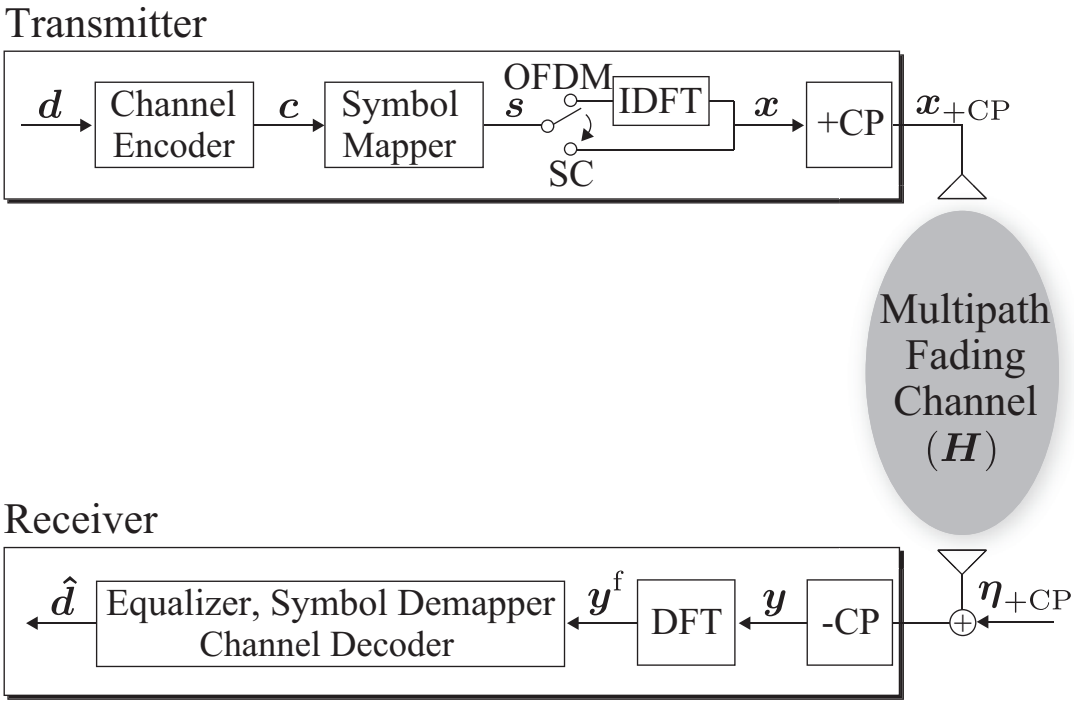

Figure 2.7: Block diagram for a broadband wireless transmission.

2.3.3 Generalized Signal Model

This section generalizes signal model for a broadband wireless link which employs either OFDM or SC as the transmission scheme. Hereafter, the concept of subchannel in OFDM scheme and the concept of discrete frequency in SC scheme are called subchannel for the sake of simplicity.

Block diagram for a generalized broadband wireless transmission is described in Figure 2.7. At the transmitter, an information bit sequence $\boldsymbol{d}$ is encoded by the channel encoder to protect the information bits from impact of the channel distortion and noise. The coded bit sequence $\boldsymbol{c}$ generated by the channel encoder is then fed to the symbol mapper to generate a data symbol block $\boldsymbol{s} \in \mathbb{C}^{K\times 1}$, where average energy of each data symbol is denoted by E_{s}. After that, the modulator, which is either OFDM or SC, converts the data symbol block $\boldsymbol{s}$ to a modulation symbol block $\boldsymbol{x}$. If OFDM scheme is employed, IDFT is applied to $\boldsymbol{s}$ to form $\boldsymbol{x}$. On the other hand, if SC scheme is employed, no process is required to generate $\boldsymbol{x}$. Hence,

$$\boldsymbol{x} = [x(1), ..., x(n), ..., x(K)]^{\mathrm{T}} = \begin{cases} \boldsymbol{F}_K^{\mathrm{H}} \boldsymbol{s} & \text{if OFDM} \\ \boldsymbol{s} & \text{if SC} \end{cases}. \tag{2.55}$$

After a CP is appended to the head of the modulation symbol block $\boldsymbol{x}$, the CP-appended block

is transmitted over the multipath channel.

At the receiver, after a CP removal is applied to generate the received symbol block $\boldsymbol{y}$, DFT is carried out to form the received spectrum $\boldsymbol{y}^{\mathrm{f}}$. Finally, the received spectrum is fed to the signal detector comprised of an equalizer, a symbol demapper and a channel decoder to yield an estimate $\hat{\boldsymbol{d}}$ for the information bit sequence.

The received spectrum is given by

$$\boldsymbol{y}^{\mathrm{f}} = \left[y^{\mathrm{f}}(1), ..., y^{\mathrm{f}}(k), ..., y^{\mathrm{f}}(K)\right]^{\mathrm{T}} = \boldsymbol{\Xi}\, \boldsymbol{x}^{\mathrm{f}} + \boldsymbol{\eta}^{\mathrm{f}}, \tag{2.56}$$

where the transmitted spectrum $\boldsymbol{x}^{\mathrm{f}}$ is determined by

$$\boldsymbol{x}^{\mathrm{f}} = \left[x^{\mathrm{f}}(1), ..., x^{\mathrm{f}}(k), ..., x^{\mathrm{f}}(K)\right]^{\mathrm{T}} = \begin{cases} \boldsymbol{s} & \text{if OFDM} \\ \boldsymbol{F}_K\, \boldsymbol{s} & \text{if SC} \end{cases}. \tag{2.57}$$

Note that since the determinant of DFT matrix is one, average energy of each spectral component of $\boldsymbol{x}^{\mathrm{f}}$ is also $\mathbb{E}\{x^{\mathrm{f}}(k)\} = E_{\mathrm{s}}$. Furthermore, the noise spectrum is denoted by

$$\boldsymbol{\eta}^{\mathrm{f}} = \left[\eta^{\mathrm{f}}(1), ..., \eta^{\mathrm{f}}(k), ..., \eta^{\mathrm{f}}(K)\right]^{\mathrm{T}} = \boldsymbol{F}_K\, \boldsymbol{\eta} \tag{2.58}$$

where $\boldsymbol{\eta}$ is noise vector denoted by

$$\boldsymbol{\eta} = [\eta(1), ..., \eta(n), ..., \eta(K)]^{\mathrm{T}}. \tag{2.59}$$

Elements of the noise vector $\eta(n)$ is modeled as independent and identically distributed (i.i.d.) complex Gaussian variables with zero mean and variance N_0, which is denoted by $\eta(n) \sim \mathcal{CN}(0, N_0)$. Since the determinant of DFT matrix is one, the noise spectrum is modeled as $\eta^{\mathrm{f}}(k) \sim \mathcal{CN}(0, N_0)$.

The frequency-domain channel matrix $\boldsymbol{\Xi}$ is given by (2.48)

$$\boldsymbol{\Xi} = \mathrm{diag}\left[\xi(1), ..., \xi(k), ..., \xi(K)\right], \tag{2.48 revisited}$$

where $\xi(k)$ is CFR at the k-th subchannel which is modeled in (2.49)

$$\boldsymbol{\xi} = [\xi(1), ..., \xi(k), ..., \xi(K)]^{\mathrm{T}} = \sqrt{K}\boldsymbol{F}_K \boldsymbol{W} \boldsymbol{h}. \tag{2.49 revisited}$$

In (2.49), matrix $\boldsymbol{W}$ is given by (2.50) and the discrete CIR is expressed in (2.27)

$$\boldsymbol{h} = [h(1), ..., h(l), ..., h(L)]^{\mathrm{T}}. \tag{2.27 revisited}$$

Due to the orthogonality of subchannels in OFDM and discrete spectral components in SC, the relationship between transmitted and received spectrum in (2.56) can be represented as

$$y^{\mathrm{f}}(k) = \xi(k) \cdot x^{\mathrm{f}}(k) + \eta^{\mathrm{f}}(k) \qquad (k \in \{1, 2, ..., K\}). \tag{2.60}$$

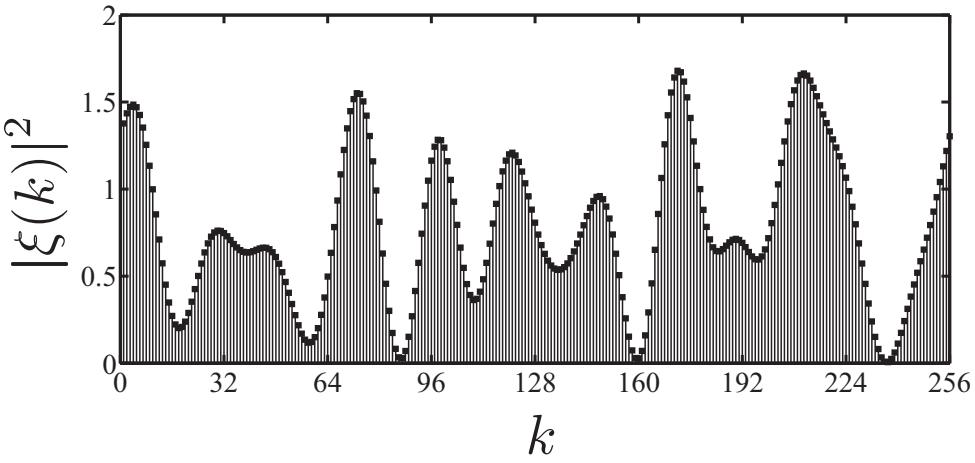

(a) A channel realization of equal gain 16 path Rayleigh fading model

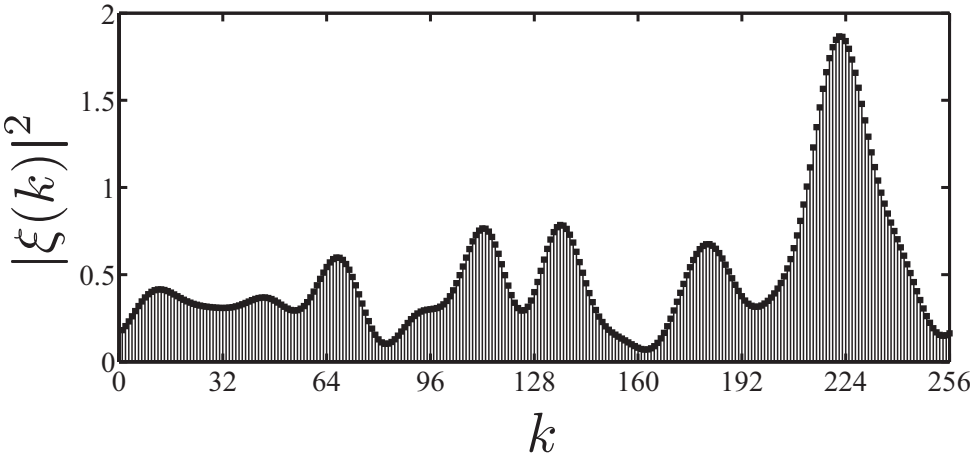

(b) A channel realization of 2 dB exponentially decaying 16 path Rayleigh fading model

Figure 2.8: Channel gain fluctuation over the frequency-domain.

The transmitted SNRs for all K subchannels are identical to

$$\gamma_{\mathrm{t}} = E_{\mathrm{s}}/N_0, \tag{2.61}$$

and received SNR for the k-th subchannel is

$$\gamma_{\mathrm{r}}(k) = |\xi(k)|^2 \cdot \frac{E_{\mathrm{s}}}{N_0}. \tag{2.62}$$

Figure 2.8 describes the fluctuation of channel gain $|\xi(k)|^2$ over the frequency-domain, which is denoted by subchannel index k for a realization of (a) equal gain 16 path and (b) that of 2 dB exponentially decaying 16 path Rayleigh fading models. The figures also shows that the channel gain $|\xi(k)|^2$ of the equal gain model fluctuate more dynamically in the frequency-domain than

that of the decaying gain model. This is due to the fact that delay spread of the equal gain model is longer than that of the decaying gain model.

2.4 Spectral Efficiency

The scalar signal model described in (2.60) implies that transmission over a frequency selective fading channel on a band with K subchannels can be viewed as transmissions over K parallel subchannels. Signal models for transmissions over these K subchannels are statistically identical and can be generalized as

$$Y = \xi(k) \cdot X + Z, \tag{2.63}$$

where $X \equiv x^{\mathrm{f}}(k)$, $Y \equiv y^{\mathrm{f}}(k)$, and $Z \equiv \eta^{\mathrm{f}}(k)$ in (2.60).

In a channel represented by (2.63), the transmitter packs information in symbol X and transmit it over the channel. The receiver acquires an observation Y in which X is distorted by the CFR $\xi(k)$ of the channel and impaired by the random noise Z induced in the signal reception. The task of the receiver is how to extract the information included in Y. The receiver is capable of capturing the CFR $\xi(k)$ by channel estimation but it is not able to observe the value of random variable Z. Hence, the transmission over the channel $\xi(k)$ was considered to be erroneous until before 1948. However, C. E. Shannon in his ground-breaking paper published in 1948 proved that the transmission can achieve any arbitrarily low probability of errors if the amount of information packed in the variable X is less than or equal to the instantaneous rate provided by the channel [5]. The instantaneous rate, which is the mutual information between X and Y [5], is a measurement for spectral efficiency of the channel. C. E. Shannon also defined channel capacity as the maximum value of the mutual information taken over all possible probability distribution of X. The channel capacity, hence can be viewed as the highest instantaneous rate at which the information can be transmitted over the channel with arbitrarily low probability of errors.

2.4.1 Mutual Information

To the receiver, the symbol X is an unknown random variable that needs to be interfered. The uncertainty of X can be measured by the concept of entropy $\mathcal{H}(X)$ which is the minimum number of bits that is needed to describe X. Mutual information between X and Y $\mathcal{I}(X;Y)$ is the reduction in the uncertainty of X due to the knowledge of Y.

To formulate the mutual information $\mathcal{I}(X;Y)$, let us begin from the entropy. Let X be a continuous random variable which is characterized by a probability density function (PDF) $p_X(x)$. The PDF $p_X(x)$ is a function that describes the relative likelihood for X to take value on a given vicinity of x, i.e.,

$$p_X(x) = \frac{d}{dx}\Pr(X \leq x), \tag{2.64}$$

where $\Pr(X \leq x)$ indicates the probability that X is smaller than or equal to the value x. Entropy of X is defined as *.

$$\mathcal{H}(X) = -\int_{-\infty}^{\infty} \log_2\left(p_X(x)\right) \cdot p_X(x)\, dx \qquad \text{[bits/symbol]}. \tag{2.65}$$

Note that the entropy $\mathcal{H}(X)$ is a function of the PDF $p_X(x)$ and does not depend on the actual values taken by X. Similarly, let $p_Y(y)$ be the PDF of random variable Y, the entropy of Y is

$$\mathcal{H}(Y) = -\int_{-\infty}^{\infty} \log_2\left(p_Y(y)\right) \cdot p_Y(y)\, dy \qquad \text{[bits/symbol]}. \tag{2.66}$$

Furthermore, let $p_{X|Y}(x|y)$ be the conditional PDF of X given $Y = y$. The conditional entropy of X given $Y = y$ is the entropy of the PDF $p_{X|Y}(x|y)$, i.e.,

$$\mathcal{H}(X|y) = -\int_{-\infty}^{\infty} \log_2\left(p_{X|Y}(x|y)\right) \cdot p_{X|Y}(x|y)\, dx \qquad \text{[bits/symbol]}. \tag{2.67}$$

The conditional entropy of X given Y is the average, over y, of the conditional entropy of X given $Y = y$, i.e.,

$$\begin{aligned} \mathcal{H}(X|Y) &= \int_{-\infty}^{\infty} \mathcal{H}(X|Y=y) \cdot p_Y(y)\, dy \\ &= -\int_{-\infty}^{\infty}\int_{-\infty}^{\infty} \log_2\left(p_{X|Y}(x|y)\right) \cdot p_{X|Y}(x|y) \cdot p_Y(y)\, dy dx \qquad \text{[bits/symbol]}. \end{aligned} \tag{2.68}$$

Let $p_{X,Y}(y,x)$ be the joint PDF of variables X and Y. According to Bayes' theorem [6]

$$\begin{aligned} \Pr\left[x \leq X < x+dx, y \leq Y < y+dy\right] &= \Pr\left[x \leq X < x+dx|y\right] \cdot \Pr\left[y \leq Y < y+dy\right] \\ \Leftrightarrow\ p_{X,Y}(x,y)\ dx\, dy &= \left(p_{X|Y}(x|y)\ dx\right)\left(p_Y(y)\, dy\right). \end{aligned} \tag{2.69}$$

Thus, $p_{X,Y}(x,y)$ can be expressed by

$$p_{X,Y}(x,y) = p_{X|Y}(x|y)\ p_Y(y). \tag{2.70}$$

*Although $X, Y \in \mathbb{C}$, integrals and derivatives in Section 2.4 are denoted for the case $X, Y \in \mathbb{R}$ for the ease of mathematical notations.

Substituting (2.70) into (2.68) yields

$$\mathcal{H}(X|Y) = -\int_{-\infty}^{\infty}\int_{-\infty}^{\infty} \log_2\left(p_{X|Y}(x|y)\right) \cdot p_{X,Y}(x,y)\, dydx \qquad \text{[bits/symbol]}. \tag{2.71}$$

Therefore, the mutual information between X and Y is given by

$$\begin{aligned} \mathcal{I}(X;Y) &= \mathcal{H}(X) - \mathcal{H}(X|Y) \\ &= -\int_{-\infty}^{\infty} p_X(x)\, \log_2\left(p_X(x)\right) dx - \left(-\int_{-\infty}^{\infty}\int_{-\infty}^{\infty} p_{X,Y}(x,y)\, \log_2\left(p_{X|Y}(x|y)\right) dydx\right) \\ &= \int_{-\infty}^{\infty}\int_{-\infty}^{\infty} p_{X,Y}(x,y)\, \log_2\left(\frac{p_{X|Y}(x|y)}{p_X(x)}\right) dydx \qquad \text{[bits/symbol]}. \end{aligned} \tag{2.72}$$

Furthermore, from the symmetry in Bayes' theorem

$$p_{Y,X}(y,x) = p_{Y|X}(y|x)\, p_X(x) = p_{X|Y}(x|y)\, p_Y(y), \tag{2.73}$$

it follows that

$$\mathcal{I}(X;Y) = \mathcal{H}(Y) - \mathcal{H}(Y|X) \qquad \text{[bits/symbol]}. \tag{2.74}$$

Equation (2.72) directly defines the mutual information $\mathcal{I}(X;Y)$, but in some cases it is more handy to use (2.74) for computational purposes. The mutual information $\mathcal{I}(X;Y)$ is the instantaneous rate of the channel.

The channel modeled by (2.63) is said to be a memoryless channel since the PDF of the output Y depends only on the input X at that time and is conditionally independent of previous channel inputs or outputs. The mutual information $\mathcal{I}(X;Y)$ depends on the chosen input PDF $p_X(x)$. The channel capacity of a memoryless channel is defined as the maximum of the mutual information $\mathcal{I}(X;Y)$ which is taken over all possible PDF $p_X(x)$ of the input symbol X, i.e.,

$$C = \max_{p_X(x)} \mathcal{I}(X;Y) = \max_{p_X(x)} \mathcal{H}(Y) - \mathcal{H}(Y|X) \qquad \text{[bits/symbol]}. \tag{2.75}$$

The channel capacity is the highest rate in bits per symbol at which information can be sent with arbitrarily low probability of error [5].

2.4.2 CCMC Capacity

When the input symbol X is a continuous variable under the assumption of Section 2.4.1 and the output Y is continuous, the channel is said to be a continuous input continuous output memoryless channel (CCMC). In this case, the instantaneous rate of such a channel is referred to

as CCMC capacity [48]. For a frequency flat channel modeled by (2.63), according to Shannon's theorem [5], the CCMC capacity reaches the channel capacity defined by (2.75) when random input symbol X follows a Gaussian distribution. The reason is that among all distributions with zero-mean and variance E_s, the Gaussian distribution has the maximum entropy. Hence, the PDF of random complex input symbol X is given by

$$p_X(x) = \frac{1}{\pi E_\mathrm{s}} \exp\left(-\frac{|x|^2}{E_\mathrm{s}}\right). \tag{2.76}$$

Furthermore, the complex noise Z can be modeled as an additive white Gaussian noise (AWGN) with zero-mean and variance N_0. Thus, the PDF of Z is given by

$$p_Z(z) = \frac{1}{\pi N_0} \exp\left(-\frac{|z|^2}{N_0}\right). \tag{2.77}$$

Note that assumptions on variances of X and Z are consistent with analysis in Section 2.3.3. Because X and Z are independent, the output random symbol Y follows a complex-valued Gaussian distribution with zero-mean and variance $\left(|\xi(k)|^2 E_\mathrm{s} + N_0\right)$. Thus, PDF of Y is given by

$$p_Y(y) = \frac{1}{\pi\left(|\xi(k)|^2 E_\mathrm{s} + N_0\right)} \exp\left(-\frac{|y|^2}{|\xi(k)|^2 E_\mathrm{s} + N_0}\right). \tag{2.78}$$

Thus, the maximum of the entropy of Y is given by

$$\max_{p_X(x)} \mathcal{H}(Y) = \log_2\left[2\pi e\left(|\xi(k)|^2 E_\mathrm{s} + N_0\right)\right] \qquad \text{[bits/symbol]}, \tag{2.79}$$

From (2.63), when given $X = x$, Y follows a complex Gaussian distribution with mean $\xi(k)\,x$ and variance N_0. Thus, the conditional PDF of Y given $X = x$ is expressed as

$$p_{Y|X}(y|x) = \frac{1}{\pi N_0} \exp\left(-\frac{|y - \xi(k)\,x|^2}{N_0}\right) = p_Z(y - \xi(k)\,x). \tag{2.80}$$

Hence, the conditional entropy $\mathcal{H}(Y|X)$ is expressed as

$$\begin{aligned} \mathcal{H}(Y|X) &= -\int_{-\infty}^{\infty}\int_{-\infty}^{\infty} p_{Y,X}(y,x)\,\log_2\left(p_Z(y - \xi(k)\,x)\right) dydx \\ &= \mathcal{H}(Y - \xi(k)\,X) \\ &= \mathcal{H}(Z) \\ &= \log_2(2\,\pi\,e\,N_0) \qquad \text{[bits/symbol]}. \end{aligned} \tag{2.81}$$

Substituting Equations (2.79) and (2.81) into (2.75), we derive the CCMC capacity

$$C = \max_{p_X(x)} \mathcal{H}(Y) - \mathcal{H}(Z) = \log_2\left[1 + \gamma_\mathrm{r}(k)\right] \qquad \text{[bits/symbol]}, \tag{2.82}$$

where $\gamma_\mathrm{r}(k)$ is the received SNR which is given by (2.62) as

$$\gamma_\mathrm{r}(k) = |\xi(k)|^2 \frac{E_\mathrm{s}}{N_0}. \tag{2.62 revisited}$$

2.4.3 DCMC Capacity

As mentioned in Section 2.4.2, CCMC capacity reaches the channel capacity given by (2.82) if the input symbol X follows a continuous complex Gaussian distribution. However, there are many cases in which the input symbol X is drawn from a discrete constellation set since practical communication systems employ discrete modulation schemes, e.g., binary phase shift keying (BPSK), quaternary phase shift keying (QPSK), or quadrature amplitude modulation (QAM). In such a case, the channel is called discrete input continuous output memoryless channel (DCMC). The instantaneous rate of such a channel is referred to as DCMC capacity [48].

To derive DCMC capacity for the channel modeled by (2.63), assume that the input symbol X is drawn with equal probability from a discrete constellation set $\mathcal{S}$ containing Q constellation points $\mathcal{S} = \{\mathcal{S}_1, \mathcal{S}_2, ..., \mathcal{S}_Q\}$. Among distributions that take values on $\mathcal{S}$, the uniform distribution gives the highest entropy. Therefore,

$$\Pr\left[X = \mathcal{S}_q\right] = \frac{1}{Q}. \tag{2.83}$$

In this case, the entropy of the input variable X is given by

$$\mathcal{H}(X) = -\sum_{q=1}^{Q} \log_2\left(\Pr\left[X = \mathcal{S}_q\right]\right) \cdot \Pr\left[X = \mathcal{S}_q\right] = \log_2 Q \qquad \text{[bits/symbol]}. \tag{2.84}$$

And the conditional entropy of X given Y is redefined as

$$\mathcal{H}(X|Y) = -\sum_{q=1}^{Q} \int_{-\infty}^{\infty} p_{X,Y}\left(\mathcal{S}_q, y\right) \cdot \log_2\left(\Pr\left[X = \mathcal{S}_q|y\right]\right) dy \qquad \text{[bits/symbol]}. \tag{2.85}$$

According to Bayes' theorem, we have

$$p_{Y,X}\left(y, \mathcal{S}_q\right) = p_{Y|X}\left(y|\mathcal{S}_q\right) \Pr\left[X = \mathcal{S}_q\right] = p_{Y|X}\left(y|\mathcal{S}_q\right) \frac{1}{Q}. \tag{2.86}$$

Furthermore,

$$\Pr\left[X = \mathcal{S}_q|y\right] = \frac{p_{Y|X}\left(y|\mathcal{S}_q\right) \Pr\left[X = \mathcal{S}_q\right]}{p_Y(y)} = \frac{p_{Y|X}\left(y|\mathcal{S}_q\right) \Pr\left[X = \mathcal{S}_q\right]}{\sum_{q'=1}^{Q} p_{Y|X}\left(y|\mathcal{S}_{q'}\right) \Pr\left[X = \mathcal{S}_{q'}\right]} = \frac{p_{Y|X}\left(y|\mathcal{S}_q\right)}{\sum_{q'=1}^{Q} p_{Y|X}\left(y|\mathcal{S}_{q'}\right)}. \tag{2.87}$$

Substituting Equations (2.86) and (2.87) into (2.85) yields the conditional entropy $\mathcal{H}(X|Y)$

$$\mathcal{H}(X|Y) = \frac{1}{Q} \sum_{q=1}^{Q} \int_{-\infty}^{\infty} p_{Y|X}\left(y|\mathcal{S}_q\right) \log_2\left[\sum_{q'=1}^{Q} \frac{p_{Y|X}\left(y|\mathcal{S}_{q'}\right)}{p_{Y|X}\left(y|\mathcal{S}_q\right)}\right] dy \qquad \text{[bits/symbol]}. \tag{2.88}$$

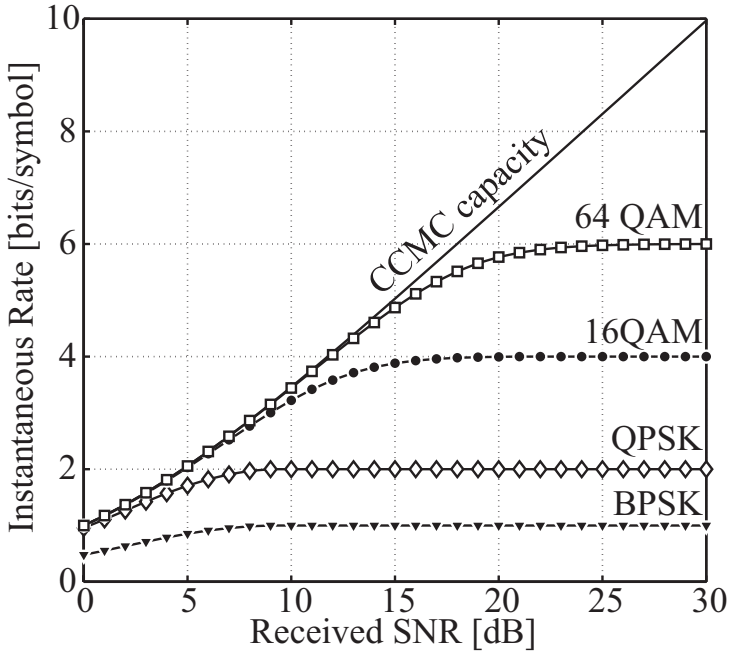

Figure 2.9: Maximum achievable rates for discrete modulation schemes in AWGN channel.

From Equations (2.84) and (2.88), the DCMC capacity is derived as

$$D_{\mathcal{S}} = \log_2 Q - \frac{1}{Q}\sum_{q=1}^{Q}\int_{-\infty}^{\infty} p_{Y|X}\left(y|\mathcal{S}_q\right)\log_2\left[\sum_{q'=1}^{Q}\frac{p_{Y|X}\left(y|\mathcal{S}_{q'}\right)}{p_{Y|X}\left(y|\mathcal{S}_q\right)}\right]dy \qquad \text{[bits/symbol]}. \tag{2.89}$$

Since calculations of DCMC capacity using (2.89) is complex, many approximations with high accuracies for computing DCMC capacity have been proposed. According to an approximation in [49], DCMC capacity for BPSK and M-QAM, e.g, QPSK, 16QAM, 64QAM, etc. can be calculated by

$$D_{\text{BPSK}} \approx \frac{1}{2}\log_2\left[1+\gamma_{\text{r}}(k)\right] - \frac{1}{4}\log_2\left[1+\frac{\gamma_{\text{r}}^2(k)}{16}\right] \qquad \text{[bits/symbol]}, \tag{2.90}$$

$$D_{M-\text{QAM}} \approx \log_2\left[1+\gamma_{\text{r}}(k)\right] - \frac{1}{2}\log_2\left[1+\frac{\gamma_{\text{r}}^2(k)}{M^2}\right] \qquad \text{[bits/symbol]}. \tag{2.91}$$

Figure 2.9 shows DCMC capacities for BPSK ($Q = 2^1$), QPSK ($Q = 2^2$), 16QAM ($Q = 2^4$), 64QAM ($Q = 2^6$) in comparison with CCMC capacity under additive white Gaussian noise (AWGN) channel, i.e., channel in which $\xi(k) = 1$. As shown in the figure, CCMC capacity is the highest instantaneous rate for the transmission and it increases steeply with the increase of received SNR. The instantaneous rates of discrete modulation schemes, i.e., DCMC capacities also increase when received SNR increases but they are bounded by the number

of bits transmitted in a symbol of each scheme. The instantaneous rates of the four discrete modulation are not higher than 1, 2, 4, 6 [bits/symbol], respectively.

2.4.4 Instantaneous Rate of Broadband Transmissions

A broadband transmission modeled by in (2.60) is equivalent to transmissions over K parallel flat fading channels modeled by (2.63). The broadband transmission occurs in an interval of KT_{s} [s] and occupies a bandwidth of $B = 1/T_{\mathrm{s}}$ [Hz]. As a result, the CCMC capacity for the broadband transmission can be computed in [bits/s/Hz] as

$$C = \frac{1}{K}\sum_{k=1}^{K}\log_2\left[1+\gamma_{\mathrm{r}}(k)\right] \qquad \text{[bits/s/Hz]}, \tag{2.92}$$

where the received SNR is determined by (2.62). The CCMC capacity in (2.92) shows how much information can be sent with arbitrarily low probability of error over the broadband transmission system. Thus, it can be viewed as a measurement for spectral efficiency of the channel. Furthermore, under the transmit power constraint, the CCMC capacity can be seen as a measurement for the spectral efficiency of the broadband transmission system. Note that, although all K input symbols to the channel follow Gaussian distributions, the CCMC capacity is not the channel capacity of the broadband transmission. The channel capacity is only achieved if transmit spectrum is optimized based on the water-filling principle [13][24] to maximize the CCMC capacity given by (2.92). The water-filling principle will be presented in section 2.4.5.

When all K input symbols to the channel are drawn from a discrete constellation, the instantaneous rate of the transmission is the DCMC capacity. For the case of BPSK modulation, the DCMC capacity is approximated as

$$D_{\mathrm{BPSK}} \approx \frac{1}{K}\sum_{k=1}^{K}\left\{\frac{1}{2}\log_2\left[1+\gamma_{\mathrm{r}}(k)\right]-\frac{1}{4}\log_2\left[1+\frac{\gamma_{\mathrm{r}}^2(k)}{16}\right]\right\} \qquad \text{[bits/s/Hz]}. \tag{2.93}$$

For the case of M-QAM, the DCMC capacity is

$$D_{M-\mathrm{QAM}} \approx \frac{1}{K}\sum_{k=1}^{K}\left\{\log_2\left[1+\gamma_{\mathrm{r}}(k)\right]-\frac{1}{2}\log_2\left[1+\frac{\gamma_{\mathrm{r}}^2(k)}{M^2}\right]\right\} \qquad \text{[bits/s/Hz]}, \tag{2.94}$$

where $\gamma_{\mathrm{r}}(k)$ is received SNR at the k-th subchannel defined in (2.62). The optimization of transmit spectrum for maximizing DCMC capacity is the so-called mercury/water-filling which is published in [50]. However, in this dissertation, the introduction of the mercury/water-filling algorithm is omitted to avoid divergence of discussions.

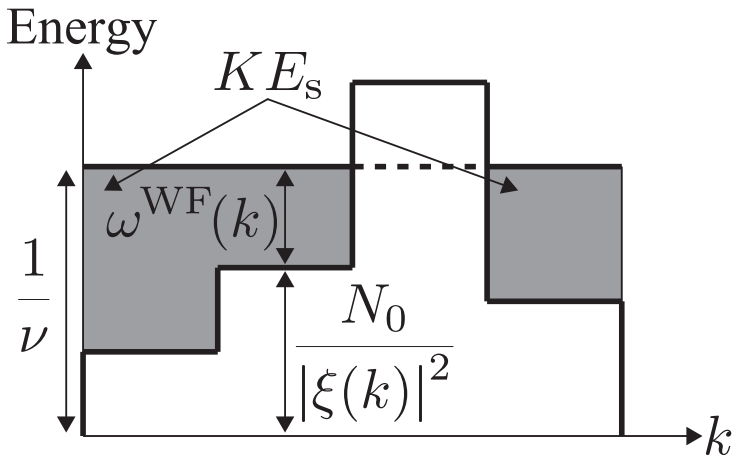

Figure 2.10: An illustration of water-filling principle based transmit spectrum optimization.

2.4.5 Water-filling Principle

In order to maximize CCMC capacity for a frequency selective fading channel, transmit spectrum should be manipulated based on the water-filling principle [24]. When transmit spectrum is manipulated, the average energy of the k-th spectral component is not E_{s} but varied to $\omega(k)$ given that the total energy of all K spectral components is preserved, i.e.,

$$\sum_{k=1}^{K} \omega(k) = KE_{\mathrm{s}}. \tag{2.95}$$

The CCMC capacity given by (2.92) becomes

$$C = \frac{1}{K} \sum_{k=1}^{K} \log_2 \left[1 + \frac{|\xi(k)|^2}{N_0} \cdot \omega(k) \right]^2. \tag{2.96}$$

To maximize the CCMC capacity (2.96) under the transmit energy constraint (2.95), the energy for the k-th subchannel is optimized as

$$\omega^{\mathrm{WF}}(k) = \left[\frac{1}{\nu} - \frac{N_0}{|\xi(k)|^2} \right]^+. \tag{2.97}$$

In (2.97), x^+ is defined as $\max(x, 0)$ and the water level $1/\nu$ is chosen such that the energy constraint (2.95) is satisfied. Thus, the water level $1/\nu$ is determined by the frequency variance of the CFR and the noise variance N_0.

An illustration of water-filling principle is shown in Figure 2.10. The value in the white area expresses $N_0/|\xi(k)|^2$ while the value in the gray area expresses optimal energy $\omega^{\mathrm{WF}}(k)$ of each spectral component. As shown in the figure, when $N_0/|\xi(k)|^2$ exceeds the water level $1/\nu$, no

Table 2.1: Simulation parameters for evaluation of water-filling principle.

Channel model	Equal gain 16 path Rayleigh fading model
Transmit SNR	3 dB, 7 dB, 10 dB
Number of trials	50000

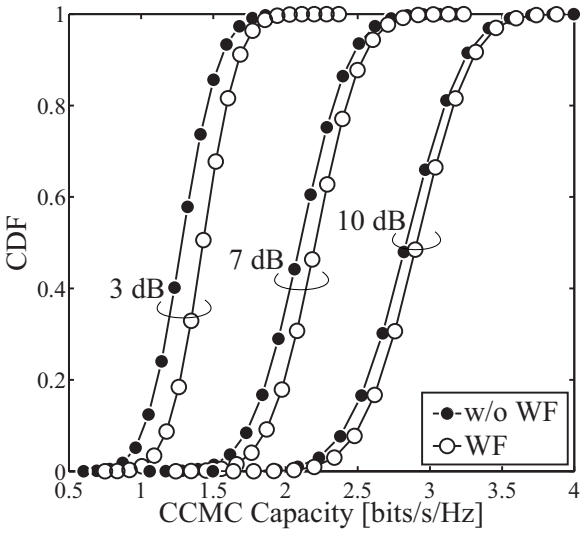

Figure 2.11: CCMC capacity of water-filling principle.

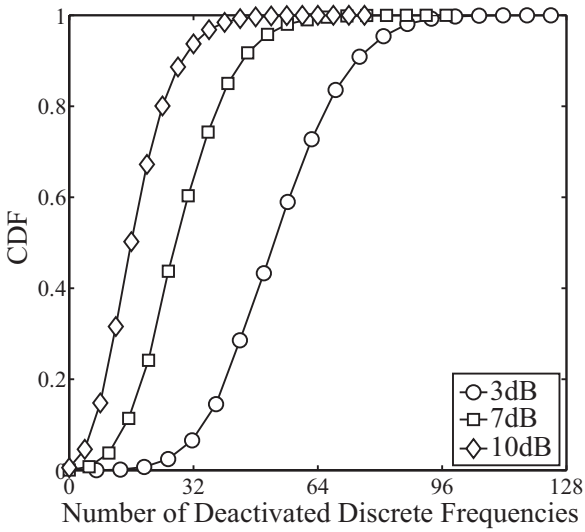

Figure 2.12: Number of subchannels deactivated by water-filling principle.

energy is allocated to such spectrum. The water-filling principle tells us two points to enhance the instantaneous rate as follows.

- Spectrum nulling should be carried out on very low gain subchannels to deactivate these subchannels and reassigns their energy to the remaining subchannels. The purpose of spectrum nulling is to concentrate more energy to higher gain subchannels.
- For energy allocation (EA) conducted, more energy is allocated to higher gain subchannels to increase the received signal level.

Since CCMC capacity is almost proportional to the logarithm of the received SNR, a small variation in the EA subchannels does not change the value of CCMC capacity so much. Therefore, a fine adjustment of energy in the EA would not contribute so much in CCMC capacity enhancement. On the other hand, creation of spectrum nulling would be more critical to enhance the capacity. To verify this argument, we investigate CCMC capacity enhancement and the number of subchannels deactivated in the water-filling principle. In this investigation, the

channel model is assumed to be equal gain 16 path Rayleigh fading model and the transmit SNR is 3 dB, 7 dB or 10 dB. Figure 2.11 in the previous page demonstrates enhancement in cumulative distribution function (CDF) of CCMC capacity of the water-filling principle. Meanwhile, the number of subchannels deactivated by water-filling principle is shown in Figure 2.12. When transmit SNR is as large as 10 dB, the EA becomes prominent because the number of deactivated discrete frequencies is small as shown in Figure 2.12. In such a case, Figure 2.11 shows that the CCMC capacity enhancement is small. This verifies that the EA makes a minor contribution to the capacity enhancement. On the other hand, in a low SNR case when transmit SNR is 3 dB, the spectrum nulling becomes prominent because the number of deactivated subchannels is large as shown in Figure 2.12. In this a case, Figure 2.11 shows that the CCMC capacity enhancement is large. This verifies that the spectrum nulling makes a significant contribution to the capacity enhancement.

In conclusion, the water-filling principle insists that we should use only a part of the assigned band with higher channel gain to enhance instantaneous rate for the frequency fading channel. This phenomenon suggests us that band activity ratio (BAR) control according to the frequency variance of the CFR is effective in achieving higher spectral efficiency.

2.5 Band Activity Ratio Control

In the BAR introduction, there are two scenarios. The first one is the case when a usable bandwidth that consists of K subchannels is already allocated to a system. In this case, BAR control can be realized by introducing spectrum nulling which deactivates $(K - K')$ subchannels having lower channel gain. In spectrum nulling, signal spectrum is transmitted over the activated K' subchannels having high channel gain. Note that, the subchannels deactivated by spectrum nulling are not re-assigned to other links. The second scenario is the case when multiple links in the same space simultaneously share a common system band. In this case, BAR control is conducted in cooperation with a dynamic spectrum control (DSC) [51]. DSC constructs transmission band for a link by dynamically selecting K' subchannels having higher channel gain in the system band which consists of K subchannels. In this scenario, the non-selected subchannels may be used by the other links. In these two scenarios, BAR is defined as K'/K. The value of BAR K'/K is determined to maximize throughput for each link. This section presents signal models and conditions for BAR control as the preliminary for the subsequent sections and chapters.

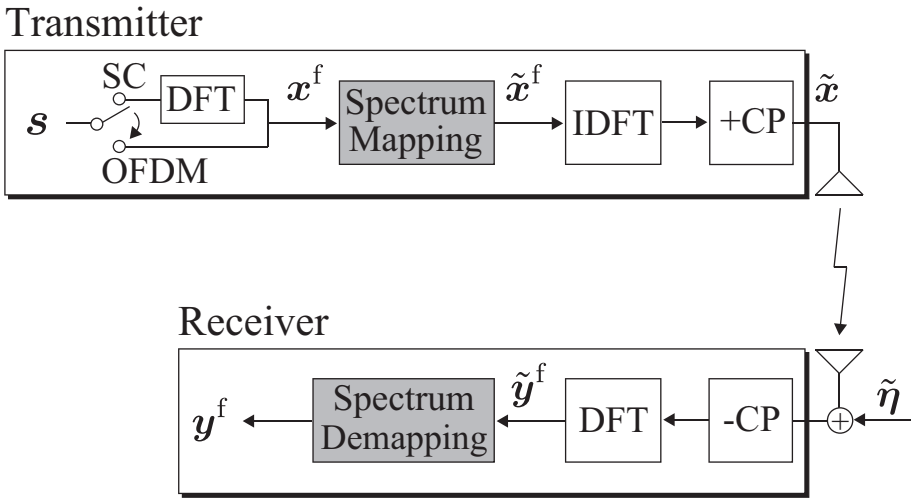

Figure 2.13: Simplified signal model to realize BAR Control.

2.5.1 Signal Model

Signal model for a broadband transmission employing BAR control is illustrated in Figure 2.13. As shown in the figure, compared to a common broadband transmission in Figure 2.7, a BAR control is conducted in a spectrum mapping (SM) at the transmitter and a spectrum demapping at the receiver. In this system, because the spectral component index and subchannel index are different, hereafter we use k' to index spectral components and k to index subchannels when BAR control is applied.

At the transmitter, each K' data symbols are segmented to generate a data symbol vector $\boldsymbol{s} \in \mathbb{C}^{K' \times 1}$ with average energy of each data symbol $\mathbb{E}\left\{|s(k)|^2\right\} = E_s$. Similar to Section 2.3.3, if an SC transmission is employed, DFT is applied to $\boldsymbol{s}$ to form a signal spectrum $\boldsymbol{x}^{\mathrm{f}}$. On the other hand, if an OFDM transmission is employed, no process is required to generate $\boldsymbol{x}^{\mathrm{f}}$. Hence,

$$\boldsymbol{x}^{\mathrm{f}} = \left[x^{\mathrm{f}}(1), ..., x^{\mathrm{f}}(k'), ..., x^{\mathrm{f}}(K')\right]^{\mathrm{T}} = \begin{cases} g\boldsymbol{F}_{K'}\boldsymbol{s} & \text{if SC} \\ g\boldsymbol{s} & \text{if OFDM} \end{cases}. \tag{2.98}$$

In (2.98), g is an amplification gain. For the case of DSC, $g = 1$. For the case of spectrum nulling, the energy of $(K - K')$ deactivated subchannels is reassigned to K' activated subchannels. Thus, g is set to $\sqrt{K/K'}$ to keep the total energy allocated to all assigned subchannels constant.

At the SM, the spectrum $\boldsymbol{x}^{\mathrm{f}}$ is then mapped onto K' subchannels having the highest channel gain of the system band. The SM yields the transmitted spectrum $\tilde{\boldsymbol{x}}^{\mathrm{f}}$ given by

$$\tilde{\boldsymbol{x}}^{\mathrm{f}} = \boldsymbol{M}\boldsymbol{x}^{\mathrm{f}} \qquad (\in \mathbb{C}^{K \times 1}), \tag{2.99}$$

where $\boldsymbol{M} \in \mathbb{C}^{K \times K'}$ denotes the SM matrix.

For a mathematical notation of the SM matrix $\boldsymbol{M}$, we define a channel gain ranking function $\psi(k)$ for the channel as $\psi(k) = \kappa$ ($\in \{1, ..., K\}$), in which $|\xi(k)|^2$ is the κ-th largest value among $|\xi(1)|^2$, $|\xi(2)|^2$, ..., $|\xi(K)|^2$. Reversely, $k = \psi^{-1}(\kappa)$ indicates that the κ-th largest value among $|\xi(1)|^2$, $|\xi(2)|^2$, ..., $|\xi(K)|^2$ is $|\xi(k)|^2$. Using the channel gain ranking function $\psi(k)$, the indexes of subchannels selected for the transmission of spectrum $\boldsymbol{x}^{\mathrm{f}}$ are determined as $\psi^{-1}(1)$, $\psi^{-1}(2)$, ..., $\psi^{-1}(K')$. For ease of mathematical notations, let us define $\boldsymbol{o} = [o(1), ..., o(k'), ..., o(K')]^{\mathrm{T}}$ as the ascending order vector for $\psi^{-1}(1)$, $\psi^{-1}(2)$, ..., $\psi^{-1}(K')$. Then at the SM, $x^{\mathrm{f}}(k')$ ($k' \in \{1, ..., K'\}$) is mapped onto the $o(k')$-th subchannel. As a consequence, the SM matrix $\boldsymbol{M}$ is determined by the following rules: the elements at the $o(k')$-th row and the k'-th column are ones, the others are zeros. Consequently, $\boldsymbol{M}^{\mathrm{T}}\boldsymbol{M} = \boldsymbol{I}_{K'}$.

Prior to transmission, IDFT is applied to the transmitted spectrum $\tilde{\boldsymbol{x}}^{\mathrm{f}}$, then CP is appended to generate the transmitted signal in the time-domain. With the assumption of perfect frequency and transmission timing synchronization, the received spectrum at the receiver after the CP removal is expressed as

$$\tilde{\boldsymbol{y}}^{\mathrm{f}} = \left[\tilde{y}^{\mathrm{f}}(1), ..., \tilde{y}^{\mathrm{f}}(k), ..., \tilde{y}^{\mathrm{f}}(K)\right]^{\mathrm{T}} = \boldsymbol{\Xi}\boldsymbol{M}\boldsymbol{x}^{\mathrm{f}} + \tilde{\boldsymbol{\eta}}^{\mathrm{f}}. \tag{2.100}$$

In (2.100), $\tilde{\boldsymbol{\eta}}^{\mathrm{f}} \in \mathbb{C}^{K \times 1}$ is noise spectrum vector whose entries are assumed to follow i.i.d. $\mathcal{CN}(0, N_0)$ and $\boldsymbol{\Xi}$ is the frequency-domain channel matrix given by (2.48)

$$\boldsymbol{\Xi} = \mathrm{diag}\left[\xi(1), ..., \xi(k), ..., \xi(K)\right]. \tag{2.48 revisited}$$

At the spectrum demapping, the spectrum $\tilde{\boldsymbol{y}}^{\mathrm{f}}$ is multiplied with $\boldsymbol{M}^{\mathrm{T}} \in \mathbb{C}^{K' \times K}$ to extract K' elements which convey data symbols. The data spectrum after the demapping is given by

$$\boldsymbol{y}^{\mathrm{f}} = \left[y^{\mathrm{f}}(1), ..., y^{\mathrm{f}}(k'), ..., y^{\mathrm{f}}(K')\right]^{\mathrm{T}} = \boldsymbol{M}^{\mathrm{T}}\boldsymbol{\Xi}\boldsymbol{M}\boldsymbol{x}^{\mathrm{f}} + \boldsymbol{M}^{\mathrm{T}}\tilde{\boldsymbol{\eta}}^{\mathrm{f}}. \tag{2.101}$$

Due to structure of the matrix $\boldsymbol{M}$, the term $\boldsymbol{M}^{\mathrm{T}}\boldsymbol{\Xi}\boldsymbol{M}$ in (2.101) is a diagonal matrix given by

$$\boldsymbol{M}^{\mathrm{T}}\boldsymbol{\Xi}\boldsymbol{M} = \mathrm{diag}\left[\xi(o(1)), ..., \xi(o(k')), ..., \xi(o(K'))\right]. \tag{2.102}$$

Thus, we define the effective channel matrix $\tilde{\boldsymbol{\Xi}} \in \mathbb{C}^{K' \times K'}$ for the transmission as

$$\tilde{\boldsymbol{\Xi}} = \mathrm{diag}\left[\tilde{\xi}(1), ..., \tilde{\xi}(k'), ..., \tilde{\xi}(K')\right] = \boldsymbol{M}^{\mathrm{T}}\boldsymbol{\Xi}\boldsymbol{M}, \tag{2.103}$$

where $\tilde{\xi}(k') = g(k')\,\xi(o(k'))$ is the CFR of the subchannel that transmits the spectral component $x^{\mathrm{f}}(k')$. As a result, (2.101) can be rewritten in a short form as

$$\boldsymbol{y}^{\mathrm{f}} = \tilde{\boldsymbol{\Xi}}\boldsymbol{x}^{\mathrm{f}} + \boldsymbol{\eta}^{\mathrm{f}}, \tag{2.104}$$

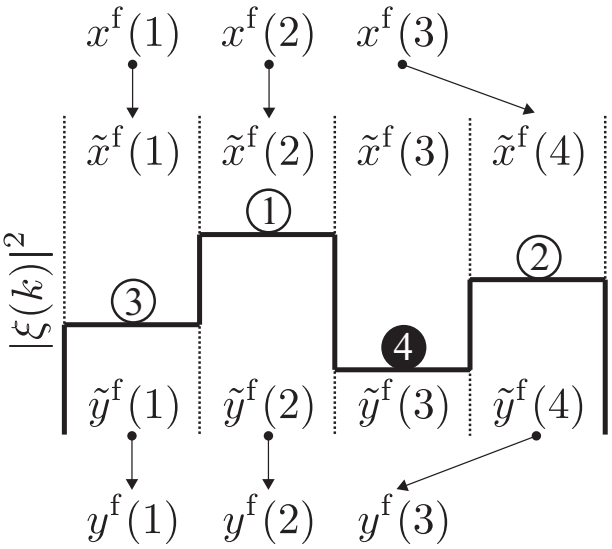

Figure 2.14: An example of SM for $K = 4$ and $K' = 3$.

where $\boldsymbol{\eta}^{\mathrm{f}} = \boldsymbol{M}^{\mathrm{T}}\tilde{\boldsymbol{\eta}}^{\mathrm{f}}$.

Figure 2.14 illustrates an example of SM for the case $K = 4$ and $K' = 3$. The numbers in the circles indicate values of the channel ranking function $\psi(k)$. As shown in the figure, indexes of $K' = 3$ subchannels with the highest channel gain are $\psi^{-1}(1) = 2$, $\psi^{-1}(2) = 4$ and $\psi^{-1}(3) = 1$, which make the ascending order vector become $\boldsymbol{o} = [1, 2, 4]^{\mathrm{T}}$. Thus, the SM assigns $x^{\mathrm{f}}(1)$, $x^{\mathrm{f}}(2)$ and $x^{\mathrm{f}}(3)$ to $\tilde{x}^{\mathrm{f}}(1)$, $\tilde{x}^{\mathrm{f}}(2)$ and $\tilde{x}^{\mathrm{f}}(4)$, respectively. Reversely, $\tilde{y}^{\mathrm{f}}(1)$, $\tilde{y}^{\mathrm{f}}(2)$ and $\tilde{y}^{\mathrm{f}}(4)$ are respectively assigned to $y^{\mathrm{f}}(1)$, $y^{\mathrm{f}}(2)$ and $y^{\mathrm{f}}(3)$ at the spectrum demapping. The SM matrix for the example in Figure 2.14 is

$$\boldsymbol{M} = \begin{bmatrix} 1 & 0 & 0 \\ 0 & 1 & 0 \\ 0 & 0 & 0 \\ 0 & 0 & 1 \end{bmatrix}. \tag{2.105}$$

2.5.2 Conditions for BAR Control Application

It is obvious that in order to select K' subchannels with the highest channel gain from K subchannels of the system band, CSI of the system band, i.e. knowledge on the channel matirx $\boldsymbol{\Xi}$ is necessary. To perform CSI acquisition, reference signal aided channel prediction [29] is widely used. The CSI acquisition is described in Figure 2.15. As shown in the figure, the transmitter transmits a reference signal over the channel. Reference signal is a signal that is known to both the transmitter and the receiver. Thus, the receiver is able to predict the channel

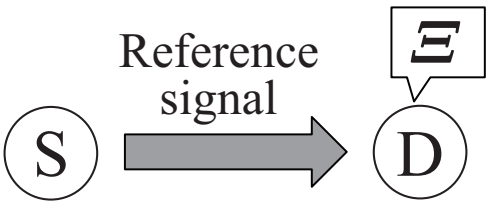

Figure 2.15: CSI acquisition.

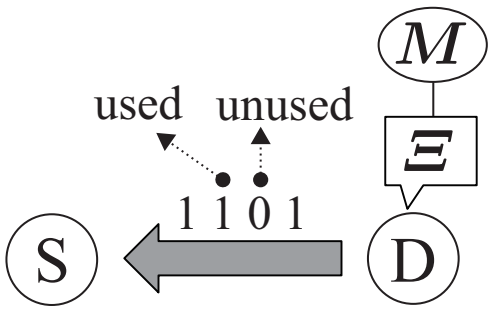

Figure 2.16: Notification for BAR control.

matrix $\boldsymbol{\Xi}$ from the received reference signal by using prediction criteria, e.g, least squares (LS) or minimum mean square error (MMSE) [29].

Figure 2.16 illustrates the notification for BAR control. As shown in the figure, after the CSI acquisition, the receiver selects K' subchannels having the highest channel gain and construct matrix $\boldsymbol{M}$. The receiver then needs to notify the transmitter of the information on $\boldsymbol{M}$ so that the transmitter is able to carry out the SM. The minimum necessary information on $\boldsymbol{M}$ is solely a block consisting of K bits in which one and zero respectively indicate the status of used/unused for K subchannels. Figure 2.16 illustrates notification for the BAR control described in Figure 2.14. Because only the third subchannel is not selected in this case, feedback information is given by $[1, 1, 0, 1]$.

Due to the CSI acquisition and notification mentioned above, BAR control is applicable to transmissions in quasi-static fading channels. In such an environment, the channel state is constant during the transmission one frame but varies slowly frame by frame. Thus, the notification of matrix $\boldsymbol{M}$ must be carried out every frame. Notification overhead caused by BAR control is affordable since it is about one symbol block while one frame consists of multiple symbol blocks. For fast varying channels, e.g., the channel state fluctuates within one frame, BAR control loses its effectiveness because CSI at the receiver and the SM matrix $\boldsymbol{M}$ become out-of-date.

2.6 Issue in Autonomous Spectrum Sharing

In the dynamically assigned band scenario in autonomous spectrum sharing, multiple independent links employ DSC to form their transmission bands from a common system band. Because each link chooses only a certain amount of high gain subchannels in the common system band, transmission band of each link is randomized. Due to impact of this transmission band

randomization, mutual interference occurs on a limited portion of the transmission band of each link. The mutual interference level, which depends on value of BAR, dominates the spectral efficiency of the whole network. In this section, the transmission band randomization effect of BAR control is described from spectral efficiency enhancement standpoint. After that, the issue of channel prediction which is encountered in this utilization of BAR control is presented.

2.6.1 BAR Control Aided Autonomous Spectrum Sharing

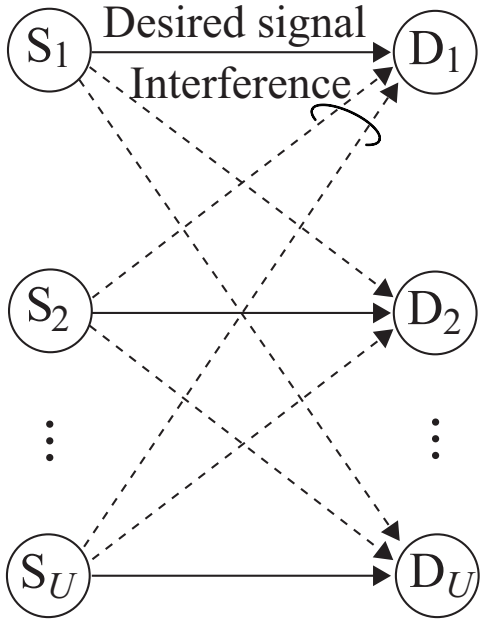

Figure 2.17: Network topology for autonomous spectrum sharing.

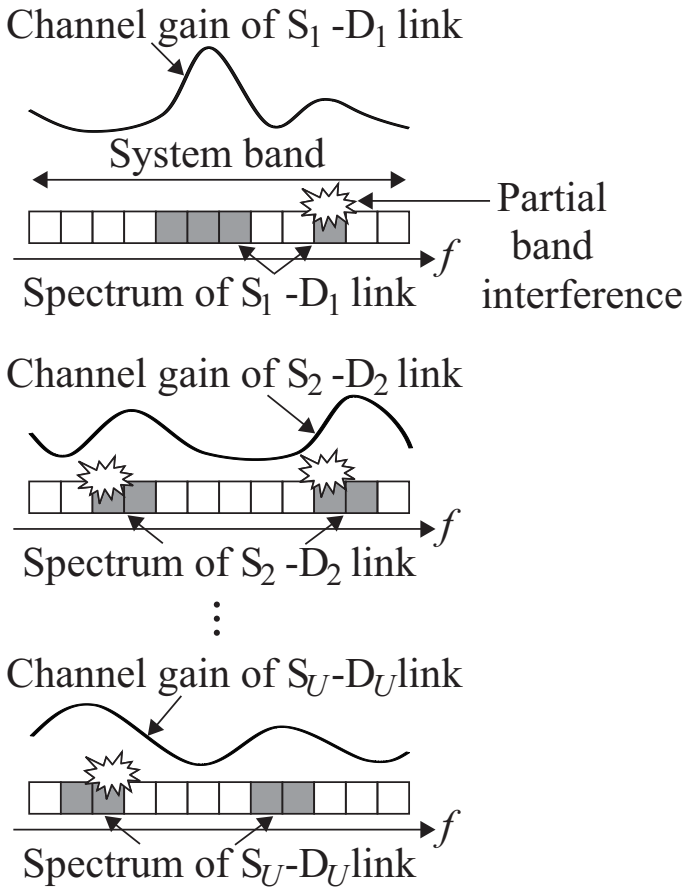

Figure 2.18: Autonomous spectrum sharing with the aid of DSC.

The considered network is illustrated in Figure 2.17. In the network, U source nodes S_1, S_2, ..., S_U simultaneously communicate with U destination nodes D_1, D_2, ..., D_U, respectively. The U links are assumed to autonomously share a common system band with the aid of DSC as shown in Figure 2.18. In Figure 2.18, gray boxes indicate the selected subchannels of each link

while white boxes express spectral-null subchannels. As shown in the figure, each link dynamically maps its spectral components onto a necessary amount of subchannels with the highest channel gain regardless of mutual interference. The number of subchannels of the system band is K and the number of spectral components of user signal is K' ($K' \leq K$). Consequently, BAR is defined as K'/K as in Section 2.5.

In the autonomous spectrum sharing, it is inevitable to have mutual interference from the other links. However, because each link uses only K' subchannels having the highest channel gain, transmission band of each link is scattered randomly over the system band. Due to the randomness of the transmission band, mutual interference among links occurs on only a portion of the transmission band of each link as shown in Figure 2.18. Although partial band interference may cause performance degradation, introduction of forward error correction can mitigate the impact of such partial band interference [52][53]. When state-of-the-art signal detection techniques, e.g., turbo code, turbo equalization, etc. are employed at the receiver, interference may be acceptable as long as it occurs in a sufficiently small portion of the transmission band [52][53][54].

Because mutual interference can be mitigated at the receiver, how to control mutual interference to enhance spectral efficiency becomes an important problem. It is obvious that the smaller the BAR, the lower the probability of interference. Thus, the mutual interference level, in average, decreases when BAR decreases from 1. Furthermore, in such a case average received signal energy increases because each link uses only a certain amount of subchannels with the highest channel gain. As a consequence, SINR of each link increases with the decrease of BAR. If the value of BAR is set to be small enough, mutual interference can be sufficiently reduced. Therefore, the spectral efficiency of the whole network can be enhanced by the BAR control. Furthermore, when the number of links U increases, the value of BAR should be small enough to lower the mutual interference level.

We investigate the variation in sum CCMC capacity of the whole network and that in the CCMC capacity of each link when value of BAR varies from 0 to 1. In this investigation, all nodes in the network are assumed to be uniformly distributed in a square area whose diagonal satisfies a reference transmit SNR of 5 dB. Path loss exponent is set to $\mu = 3.5$ and the 16 path Rayleigh fading model is employed. The number of links in the network is varied as $U = 2, 4, 6, 8$, and 10. CCMC capacity of each link per used subchannel and sum CCMC capacity of the network are demonstrated in Figure 2.19 and Figure 2.20, respectively. As shown in Figure 2.19, for $U = 2$, when BAR decreases from 1, the CCMC capacity per link per used subchannel increases due to the increase in received SINR. Thus, the sum CCMC capacity for $U = 2$ links starts to increase as BAR decreases as shown in Figure 2.20. There is an optimal

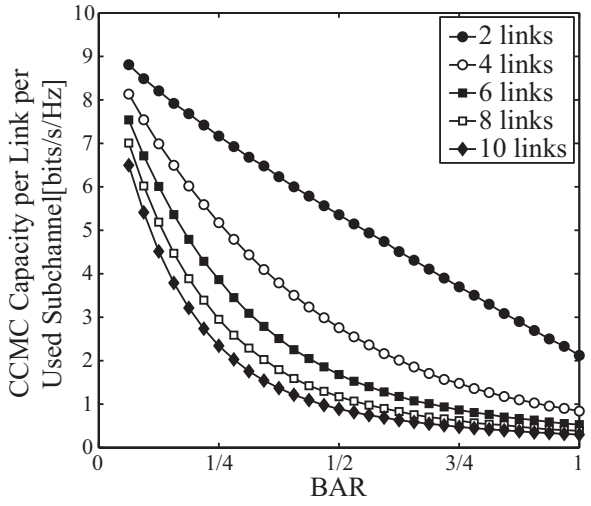

Figure 2.19: CCMC capacity per used subchannel of each link as a function of BAR.

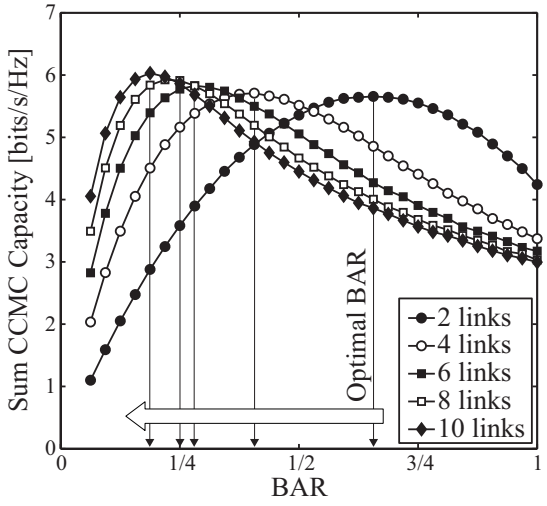

Figure 2.20: Sum CCMC capacity as a function of BAR.

value of BAR at which the sum CCMC capacity reaches its maximum. However, when BAR decreases further from the optimal value, the sum CCMC capacity starts to decrease. In this case, although CCMC capacity per link per used subchannel increases as shown in Figure 2.19, the sum CCMC capacity degrades from its maximum because the number of used subchannels is too small. As a result, for each value of U, there is an optimal value of BAR that maximizes the sum CCMC capacity. Furthermore, for each value of BAR, the CCMC capacity per used subchannel decreases when U increases because in such a case received SINR decreases. Consequently, the optimal value of BAR that maximizes the sum CCMC decreases when U increases as demonstrated in Figure 2.20. More importantly, the optimal values of BAR are relatively small, basically in the range between 0 and around 0.5.

2.6.2 Issue of Channel Prediction

To enable the subchannel selection in DSC for multi-user spectrum sharing cases, each link needs to capture CFR of the whole system band every certain interval. This means channel prediction for the entire system band including currently non-selected subchannels is necessary. This is not a problem if each link is able to send reference signals over the entire system band to carry out a channel prediction. However, in autonomous wireless networks, sending such reference signals reduces frame efficiency and may cause extra interference to neighboring links. Therefore, in Chapter 3, this dissertation studies a channel prediction scheme for the whole system band using a pilot signal embedded in the selected subchannels for data transmission. This

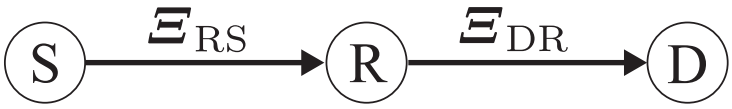

Figure 2.21: A two-hop relay transmission.

channel prediction problem will be formulated and solved by non-uniform sampling theory. However, when the number of simultaneously used links gets larger, because BAR should be set to be relatively small, the bandwidth of continuously non-selected subchannels tends to be relatively large. As a consequence, ill-conditioned channel prediction problem [34] arises and causes a severe deterioration in channel prediction reliability. Since DSC relies on the predicted CFR to select subchannels, the spectral efficiency of the next frame decreases and a drop in the overall spectral efficiency comes as a consequence. To deal with this problem, we propose a CSI reliability guaranteeing subchannel selection which selects higher gain subchannels while keeping the bandwidth of continuously non-selected subchannels below a specific threshold.

2.7 Issue in Broadband AF Relay

In the fixed assigned band scenario, because each link is able to observe CFR over the whole system band, CSI acquisition is not a problem. In this case, because the assigned system band is fixed rather than dynamically varied, it is a challenge to guarantee a certain transmission quality under attenuation due to path loss. Wireless relaying is one of straightforward solutions to reduce the path loss by dividing a link into many shorter sublinks. This section introduces two typical relaying categories: DF and AF [36][37] to explain their effectiveness in the spectral efficiency enhancement. After that, the spectral efficiency degradation issue in broadband AF relay will be clarified.

2.7.1 DF Relay

Figure 2.21 illustrates a typical two-hop relay transmission constituted by one source node (S-node), one relay node (R-node) and one destination node (D-node). For the sake of simplicity, received signal level of the direct link, i.e., the source-to-destination (S-D) link is assumed to be negligibly low. Transmitted signals from the S-node and the R-node are mutually independent in two orthogonal time slots or frequency bands. The source-to-relay (S-R) link and the relay-to-destination (R-D) link are assumed to be subject to quasi-static frequency selective fading

due to the broadband signaling. The number of subchannels of both links are assumed to be K. In the figure, $\boldsymbol{\Xi}_{\mathrm{RS}}$ and $\boldsymbol{\Xi}_{\mathrm{DR}}$ indicate the frequency-domain channel matrices of the S-R and R-D links which are given by

$$\boldsymbol{\Xi}_{\mathrm{RS}} = \mathrm{diag}\left[\xi_{\mathrm{RS}}(1), ..., \xi_{\mathrm{RS}}(k), ..., \xi_{\mathrm{RS}}(K)\right], \tag{2.106}$$

$$\boldsymbol{\Xi}_{\mathrm{DR}} = \mathrm{diag}\left[\xi_{\mathrm{DR}}(1), ..., \xi_{\mathrm{DR}}(k), ..., \xi_{\mathrm{DR}}(K)\right], \tag{2.107}$$

where $\xi_{\mathrm{RS}}(k)$ and $\xi_{\mathrm{DR}}(k)$ respectively denote CFRs of the S-R link and the R-D link over the k-th subchannel. Note that the expected values of channel gain $|\xi_{\mathrm{RS}}(k)|^2$ over the time-domain are the same for all K subchannels of the link. This expected value is denoted by $\mathbb{E}\left\{\frac{1}{K}\sum_{k=1}^{K}|\xi_{\mathrm{RS}}(k)|^2\right\} = \Psi_{\mathrm{RS}}$. Therefore, Ψ_{RS} expresses the average channel gain over all subchannels of the S-R link. When shadowing is not considered, $\Psi_{\mathrm{RS}} \propto d_{\mathrm{RS}}^{-\mu}$, where d_{RS} is the transmission distance of the S-R link and μ denotes path loss exponent. Similarly, $\mathbb{E}\left\{\frac{1}{K}\sum_{k=1}^{K}|\xi_{\mathrm{DR}}(k)|^2\right\} = \Psi_{\mathrm{DR}}$, where $\Psi_{\mathrm{DR}} \propto d_{\mathrm{DR}}^{-\mu}$ with d_{DR} is the transmission distance of the R-D link.

Let $\boldsymbol{x}_{\mathrm{S}}^{\mathrm{f}} = \left[x_{\mathrm{S}}^{\mathrm{f}}(1), ..., x_{\mathrm{S}}^{\mathrm{f}}(k), ..., x_{\mathrm{S}}^{\mathrm{f}}(K)\right]^{\mathrm{T}}$ denote the transmitted spectrum at the S-node. The transmitted spectrum $\boldsymbol{x}_{\mathrm{S}}^{\mathrm{f}}$ is subject to a transmit energy constraint $\mathbb{E}\left\{\frac{1}{K}\sum_{k=1}^{K}\left|x_{\mathrm{S}}^{\mathrm{f}}(k)\right|^2\right\} = E_{\mathrm{s}}$. Note that since BAR control is not applied in this section, we use k to index both spectral components and subchannels of the channels. The received spectrum at the R-node is $\boldsymbol{y}_{\mathrm{R}}^{\mathrm{f}} = \left[y_{\mathrm{R}}^{\mathrm{f}}(1), ..., y_{\mathrm{R}}^{\mathrm{f}}(k), ..., y_{\mathrm{R}}^{\mathrm{f}}(K)\right]^{\mathrm{T}}$, where each spectral component is given by

$$y_{\mathrm{R}}^{\mathrm{f}}(k) = \xi_{\mathrm{RS}}(k)\, x_{\mathrm{S}}^{\mathrm{f}}(k) + \eta_{\mathrm{R}}^{\mathrm{f}}(k). \tag{2.108}$$

In (2.108), $\eta_{\mathrm{R}}^{\mathrm{f}}(k)$ is the spectral component of noise induced in signal reception at the R-node over the k-th subchannel. We assume that $\eta_{\mathrm{R}}^{\mathrm{f}}(k) \sim \mathcal{CN}(0, N_{\mathrm{R}})$, where N_{R} is power spectral density of the noise induced at the R-node.

After the reception of $\boldsymbol{y}_{\mathrm{R}}^{\mathrm{f}}$, the R-node detects the information included in $\boldsymbol{x}_{\mathrm{S}}^{\mathrm{f}}$. Assuming perfect signal detection, the R-node then regenerates spectrum $\boldsymbol{x}_{\mathrm{R}}^{\mathrm{f}} = \boldsymbol{x}_{\mathrm{S}}^{\mathrm{f}}$ and transmits it to the D-node. The received spectrum at the D-node is $\boldsymbol{y}_{\mathrm{D}}^{\mathrm{f}} = \left[y_{\mathrm{D}}^{\mathrm{f}}(1), ..., y_{\mathrm{D}}^{\mathrm{f}}(k), ..., y_{\mathrm{D}}^{\mathrm{f}}(K)\right]^{\mathrm{T}}$, where each spectral component is given by

$$y_{\mathrm{D}}^{\mathrm{f}}(k) = \xi_{\mathrm{DR}}(k)\, x_{\mathrm{S}}^{\mathrm{f}}(k) + \eta_{\mathrm{D}}^{\mathrm{f}}(k). \tag{2.109}$$

In (2.109), $\eta_{\mathrm{D}}^{\mathrm{f}}(k)$ is the spectral component of noise induced in signal reception at the D-node over the k-th subchannel. We assume that $\eta_{\mathrm{D}}^{\mathrm{f}}(k) \sim \mathcal{CN}(0, N_{\mathrm{D}})$, where N_{D} is power spectral density of the noise induced at the D-node.

From (2.108) and (2.109), CCMC capacities for the transmissions over the S-R and R-D links

are given by

$$C_{\mathrm{RS}} = \frac{1}{K}\sum_{k=1}^{K}\log_2\left[1+\frac{|\xi_{\mathrm{RS}}(k)|^2 E_{\mathrm{s}}}{N_{\mathrm{R}}}\right], \tag{2.110}$$

$$C_{\mathrm{DR}} = \frac{1}{K}\sum_{k=1}^{K}\log_2\left[1+\frac{|\xi_{\mathrm{DR}}(k)|^2 E_{\mathrm{s}}}{N_{\mathrm{D}}}\right]. \tag{2.111}$$

DF relay can be considered as the extension of two single-hop transmissions: the S-R link and the R-D link. Therefore, end-to-end CCMC capacity of the transmission from the S-node via the R-node to the D-node is limited by the minimum value of C_{RS} and C_{DR} as

$$C_{\mathrm{DRS}}^{\mathrm{DF}} = \frac{1}{2}\min\left(C_{\mathrm{RS}}, C_{\mathrm{DR}}\right). \tag{2.112}$$

The coefficient 1/2 indicates that two time slots, or frequency bands, are occupied by the relay transmission.

2.7.2 AF Relay

In AF relay, the R-node does not regenerate the transmitted spectrum $\boldsymbol{x}_{\mathrm{S}}^{\mathrm{f}}$ of the S-node but just amplifies the received spectrum $\boldsymbol{y}_{\mathrm{R}}^{\mathrm{f}}$ before forwarding it to the D-node. In conventional AF relay, the R-node amplifies all K elements of $\boldsymbol{y}_{\mathrm{R}}^{\mathrm{f}}$ by the same amplification gain g_{R}. Thus, elements of the transmitted spectrum at the R-node are $x_{\mathrm{R}}^{\mathrm{f}}(k) = g_{\mathrm{R}} y_{\mathrm{R}}^{\mathrm{f}}(k)$, where they are subject to a transmit energy constraint $\mathbb{E}\left\{\frac{1}{K}\sum_{k=1}^{K}\left|x_{\mathrm{R}}^{\mathrm{f}}(k)\right|^2\right\} = E_{\mathrm{s}}$. As a result, the amplification gain is given by

$$g_{\mathrm{R}} = \sqrt{\frac{KE_{\mathrm{s}}}{\sum_{k=1}^{K}\left(|\xi_{\mathrm{RS}}(k)|^2 E_{\mathrm{s}} + N_{\mathrm{R}}\right)^2}}. \tag{2.113}$$

The spectral component of the received spectrum at the D-node over the k-th subchannel is given by

$$y_{\mathrm{D}}^{\mathrm{f}}(k) = \tilde{\xi}(k)\, x_{\mathrm{S}}^{\mathrm{f}}(k) + \eta^{\mathrm{f}}(k), \tag{2.114}$$

where the composite CFR $\tilde{\xi}(k)$ and the equivalent noise term $\eta^{\mathrm{f}}(k)$ are given by

$$\tilde{\xi}(k) = g_{\mathrm{R}}\,\xi_{\mathrm{DR}}(k)\,\xi_{\mathrm{RS}}(k), \tag{2.115}$$

$$\eta^{\mathrm{f}}(k) = g_{\mathrm{R}}\,\xi_{\mathrm{DR}}(k)\,\eta_{\mathrm{R}}^{\mathrm{f}}(k) + \eta_{\mathrm{D}}^{\mathrm{f}}(k). \tag{2.116}$$

Because $\eta_{\mathrm{R}}^{\mathrm{f}}(k)$ and $\eta_{\mathrm{D}}^{\mathrm{f}}(k)$ are also zero-mean Gaussian variables with variances N_{R} and N_{D}, respectively, $\eta(k)$ is a zero-mean Gaussian variable with variance

$$N_{\eta}(k) = g_{\mathrm{R}}^{2} \left|\xi_{\mathrm{DR}}(k)\right|^{2} N_{\mathrm{R}} + N_{\mathrm{D}}. \tag{2.117}$$

As a result, the end-to-end CCMC capacity of the AF relay is determined by

$$C_{\mathrm{DRS}}^{\mathrm{AF}} = \frac{1}{2K} \sum_{k=1}^{K} \log_2 \left[1 + \frac{g_{\mathrm{R}}^{2} \left|\xi_{\mathrm{DR}}(k)\right|^{2} \left|\xi_{\mathrm{RS}}(k)\right|^{2} E_{\mathrm{s}}}{g_{\mathrm{R}}^{2} \left|\xi_{\mathrm{DR}}(k)\right|^{2} N_{\mathrm{R}} + N_{\mathrm{D}}} \right]. \tag{2.118}$$

2.7.3 CCMC Capacity Evaluation

Numerical analysis is carried out to demonstrate the effectiveness and issues of relay in the spectral efficiency enhancement for broadband wireless transmissions with fixed assigned band. The end-to-end CCMC capacity of a relaying system is dominated by the relative position of the R-node in comparison with the S-node and the D-node. Basically, when the R-node moves from the S-node to the D-node, the CCMC capacity reaches its largest value when the R-node is right in the middle of the two nodes. Since this section evaluates CCMC capacity enhancement effect of relaying schemes, the R-node is assumed to be right in the middle of the S-node and the D-node. In this case, since average channel gain of the S-R and R-D links are equal, we normalize these average channel gains as $\Psi_{\mathrm{RS}} = \Psi_{\mathrm{DR}} = 1$ for the sake of simplicity.

To verify effectiveness of relaying schemes it is necessary to consider CCMC capacity for the direct link from the S-node to the D-node. Let $\boldsymbol{\Xi}_{\mathrm{DS}} = \mathrm{diag}\left[\xi_{\mathrm{DS}}(1), ..., \xi_{\mathrm{DS}}(k), ..., \xi_{\mathrm{DS}}(K)\right]$ be the frequency-domain channel matrix of the S-D link, where $\xi_{\mathrm{DS}}(k)$ is the CFR of the S-D link at the k-th subchannel. Hence, CCMC capacity of the direct link is calculated by

$$C_{\mathrm{DS}} = \frac{1}{K} \sum_{k=1}^{K} \log_2 \left[1 + \frac{\left|\xi_{\mathrm{DS}}(k)\right|^{2} E_{\mathrm{s}}}{N_{\mathrm{D}}} \right]. \tag{2.119}$$

The average channel gain of the S-D link is denoted by $\mathbb{E}\left\{\left|\xi_{\mathrm{DS}}(k)\right|^{2}\right\} = \Psi_{\mathrm{DS}}$. Because the R-node is right in the middle of the S-node and the D-node, Ψ_{DS} is given by

$$\Psi_{\mathrm{DS}} = \frac{\Psi_{\mathrm{RS}}}{2^{\mu}} = \frac{\Psi_{\mathrm{DR}}}{2^{\mu}} = \frac{1}{2^{\mu}}. \tag{2.120}$$

Figure 2.22 shows average CCMC capacity comparison between the relay schemes and the direct transmission for a network topology shown in Figure 2.21 with parameters is given in Table 2.2. In order to confirm path loss reduction effect of the relaying schemes, a severe path loss environment with large path loss exponent $\mu = 3.5$ is used in this evaluation. For the sake

Table 2.2: Simulation parameters for CCMC capacity evaluation of DF and AF relay.

Channel model	Equal gain 16 path Rayleigh fading model
Transmit SNR per link	E_s/N_0 = 10 dB
Number of trials	50000

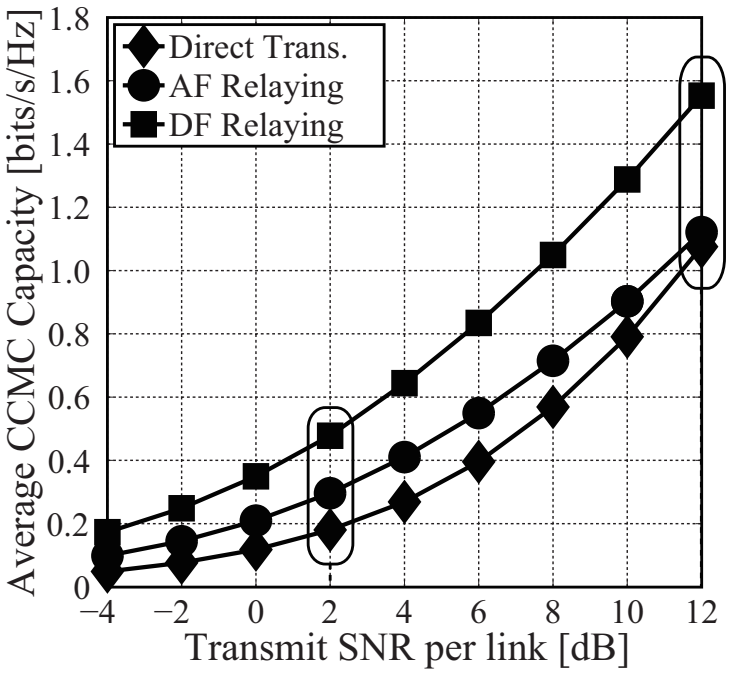

Figure 2.22: CCMC capacity comparison between relaying schemes and direct transmission.

of simplicity, variances of each noise spectral component are assumed as $N_R = N_D = N_0$. As a result, transmit SNR for the S-R, R-D and S-D links are the same as E_s/N_0. The transmit SNR per link is set to $E_s/N_0 = 10$ dB and an equal gain 16 path Rayleigh fading channel model is employed. As shown in the figure, for all values of transmit SNR per link, DF relay exhibits best CCMC capacity performance. The capacity curve of DF relay has almost the same inclination with that of the direct transmission. Meanwhile the capacity curve of AF relay has smaller inclination compared to those of DF relay and the direct transmission. AF relay has an enhanced capacity compared to the direct transmission but AF relay loses its effectiveness as SNR increases.

2.7.4 Spectral Efficiency Degradation of AF Relay

It is obvious that in high SNR regime, value of noise variance does not dominate the CCMC capacity performances. Thus, the fact that AF relay loses its effectiveness in high SNR regime implies that the degradation of AF relay stems from the frequency-variance of CFR of the S-R and R-D links. The reason of AF relay's degradation can be explained as follows. In the two-hop AF relay system, as shown in (2.116), end-to-end channel gain is given by the multiplication of channel gains of the S-R and R-D links. Hence, an existence of low gain subchannels in one of the two links results in a bottleneck issue in terms of spectral efficiency. Unfortunately, because the channel gains of the S-R and R-D links fluctuate independently in the frequency-domain, higher gain subchannels in the S-R link may have lower channel gain in the R-D link, and vice versa. This leads to a severe deterioration in the spectral efficiency of the whole signal spectrum.

To improve the end-to-end spectral efficiency for the AF relay, the number of received spectral components which experience deep fading throughout the relay transmission should be reduced. To this end, spectral components which are transmitted over high gain subchannels even in the S-R link should be consistently transmitted over high gain subchannels in the R-D link, and vice versa. In Chapter 4, we study transmit spectrum optimization at the S-node and the R-node to realize this idea.

2.8 Concluding Remarks

Due to the channel gain variance in the frequency-domain, in order to enhance the spectral efficiency, not all subchannels of the system band but only an appropriate ratio of high gain subchannels should be activated for transmissions. This means BAR should be set to an optimal value which is smaller than 1. This chapter outlined the effectiveness of BAR control and deliberated the exploitation of BAR control to solve the issue of spectral efficiency enhancement through two scenarios: autonomous spectrum sharing and broadband AF relay with fixed assigned band.

In the autonomous spectrum sharing scenario where multiple links are autonomously sharing a common system band by using DSC, this chapter showed that we can achieve an enhanced spectral efficiency while making mutual interference a tolerable one by selecting a relatively small BAR according to the number of links.

In order to select subchannels having high channel gain from the system band, CSI of all subchannels in the system band needs to be known prior to the subchannel selection. In an autonomous spectrum sharing, each link is able to observe CSI for the currently selected sub-

channels. Therefore, this chapter pointed out that channel prediction for the entire system band from only subchannels selected for the current data transmission is necessary to realize the BAR control aided autonomous spectrum sharing.

In the scenario of AF relay with fixed assigned band, the signal spectrum experiences deep fading at different subchannels every time the signal spectrum is relayed by a relay node. Thus, there may be many spectral components which experienced deep fading in the received signal spectrum at the destination node, and a deterioration in spectral efficiency comes as an consequence. In order to deal with this issue, this chapter showed that spectral components which are transmitted over high gain subchannels of one link should be also consistently transmitted over high gain subchannels of the other links.

By pointing out the issues of BAR control in autonomous spectrum sharing and broadband AF relay, this chapter clarified the contributions of this dissertation.

Chapter 3

Band Activity Ratio Control for Autonomous Spectrum Sharing

3.1 Introduction

In the autonomous spectrum sharing with the aide of DSC, in order to enhance the spectral efficiency for the whole network, BAR is controlled according to the number of links in the network. The optimal value of BAR is chosen to balance the decrease in transmission bandwidth and the increase in the received SINR. The optimal value of BAR is relatively small, basically, from around 0.5 to close to 0 when the number of links is varied from 2 to 10. To realize such a BAR control aided autonomous spectrum sharing, channel prediction for the entire system band from transmission band sparsely selected by DSC is required. However, due to the sparse spectrum, deterioration of the channel prediction reliability arises and causes a drop in the overall spectral efficiency averaged over multiple transmissions. This chapter clarifies the spectral efficiency degradation due to the deterioration of the channel prediction reliability. In order to enhance the spectral efficiency, this chapter proposes a subchannel selection technique which guarantees the channel prediction reliability while selecting high gain subchannels. Numerical analyses are given to verify effectiveness of the proposed subchannel selection.

3.2 DSC Aided Autonomous Spectrum Sharing

3.2.1 Signal Model

This section considers signal model based on the network model shown in Figure 2.17. Figure 3.1 represents a signal model of DSC for the link between the S_u ($u \in \{1, 2, ..., U\}$) node and the D_u node (S_u-D_u link). At the S_u node, each K' data symbols are segmented to generate

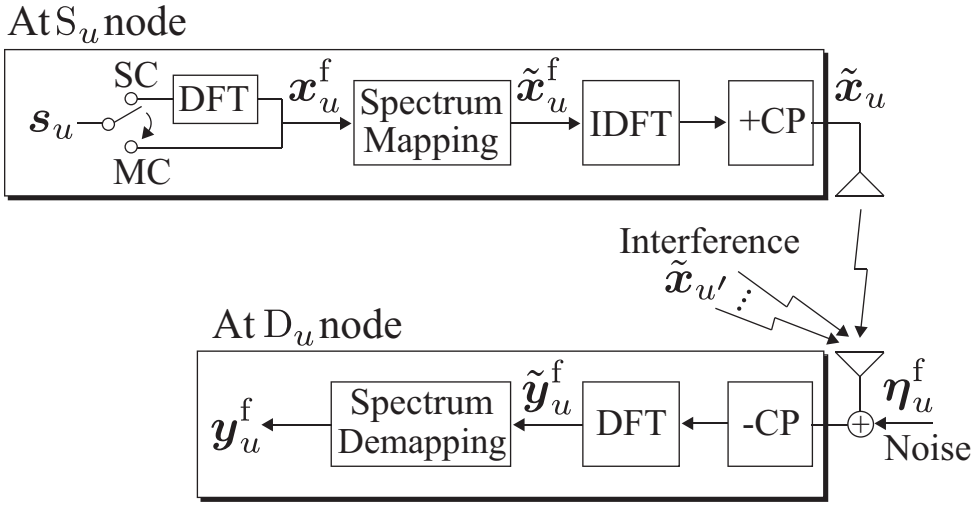

Figure 3.1: Signal model of DSC for S_u-D_u link.

transmitted symbol vector $\boldsymbol{s}_u \in \mathbb{C}^{K' \times 1}$. Note that average energy of each data symbol is E_s. Then the data spectrum $\boldsymbol{x}_u^f$ is generated by

$$\boldsymbol{x}_u^f = \left[x_u^f(1), ..., x_u^f(k'), ..., x_u^f(K')\right]^T = \begin{cases} \boldsymbol{F}_{K'} \boldsymbol{s}_u & \text{if SC} \\ \boldsymbol{s}_u & \text{if OFDM} \end{cases}. \tag{3.1}$$

Note that (3.1) is the same as (2.98) when it is applied to DSC of the S_u-D_u link with $g = 1$. Recall that $\boldsymbol{F}_a$ is $a \times a$ DFT matrix given by (2.24). Since determinant of $\boldsymbol{F}_{K'}$ is one, average energy of each spectral component $x_u^f(k')$ is equal to E_s.

At the SM, the data spectrum is mapped onto K' subchannels of the transmission band of the S_u-D_u link. The transmission band is comprised of K' subchannels with the highest channel gain selected from K subchannels in the S_u-D_u link. Similar to discussion in Section 2.5, let $\psi_u(k)$ be the channel gain ranking function for the S_u-D_u link and define $\boldsymbol{o}_u = [o_u(1), ..., o_u(k'), ..., o_u(K')]$ as the ascending order vector for $\psi_u^{-1}(1)$, ..., $\psi_u^{-1}(k')$, ..., $\psi_u^{-1}(K')$. Hence, $x_u^f(k')$ ($k' \in \{1, 2, ..., K'\}$) is mapped onto the $o_u(k')$-th subchannel. As a result, the transmitted spectrum after the spectrum mapper is $\tilde{\boldsymbol{x}}_u^f = \boldsymbol{M}_u \boldsymbol{x}^f$. The spectrum mapping matrix $\boldsymbol{M}_u \in \mathbb{C}^{K \times K'}$ is determined by the following rules: the elements at the $o_u(k')$-th row and the k'-th column are ones, and the other elements are zeros.

Prior to transmission, a K point IDFT is applied to the transmitted spectrum $\tilde{\boldsymbol{x}}_u^f$, then CP is appended to generate the transmitted signal in the time-domain. The signal transmitted from the S_u node $\tilde{\boldsymbol{x}}_u^f$ is multiplexed with those coming from the $S_{u'}$ ($u' \in \{1, 2, ..., U\}$, $u' \neq u$) node. The received signal is applied to a K point DFT to generate received spectrum $\tilde{\boldsymbol{y}}_u^f$ and then $\tilde{\boldsymbol{y}}_u^f$ is demapped by multiplication with $\boldsymbol{M}_u^T$ to return it to the original order. Under the assumption of

perfect transmission timing and carrier frequency synchronization, the data spectrum after the demapping is given by

$$\boldsymbol{y}_u^{\mathrm{f}} = \left[y_u^{\mathrm{f}}(1), ..., y_u^{\mathrm{f}}(k'), ..., y_u^{\mathrm{f}}(K')\right]^{\mathrm{T}} = \boldsymbol{M}_u^{\mathrm{T}} \boldsymbol{\Xi}_{u,u} \boldsymbol{M}_u \boldsymbol{x}_u^{\mathrm{f}} + \sum_{\substack{u'=1 \\ u' \neq u}}^{U} \boldsymbol{M}_u^{\mathrm{T}} \boldsymbol{\Xi}_{u,u'} \boldsymbol{M}_{u'} \boldsymbol{x}_{u'}^{\mathrm{f}} + \boldsymbol{\eta}_u^{\mathrm{f}}. \tag{3.2}$$

In (3.2), $\boldsymbol{\eta}_u^{\mathrm{f}} \in \mathbb{C}^{K' \times 1}$ is the noise spectrum vector whose entries are i.i.d. complex Gaussian random variables with zero-mean and variance N_0. Furthermore, $\boldsymbol{\Xi}_{u,u'}$ ($u' \in \{1, 2, ..., U\}$) is the frequency-domain channel matrix of the $\mathrm{S}_{u'}$-D_u link defined as

$$\boldsymbol{\Xi}_{u,u'} = \mathrm{diag}\left[\xi_{u,u'}(1), ..., \xi_{u,u'}(k), ..., \xi_{u,u'}(K)\right]. \tag{3.3}$$

In (3.3), $\xi_{u,u'}(k)$ is CFR of the $\mathrm{S}_{u'}$-D_u link at the k-th subchannel which is modeled as

$$\boldsymbol{\xi}_{u,u'} = \left[\xi_{u,u'}(1), ..., \xi_{u,u'}(k), ..., \xi_{u,u'}(K)\right]^{\mathrm{T}} = \sqrt{K} \boldsymbol{F}_K \boldsymbol{W}_{u,u'} \boldsymbol{h}_{u,u'}, \tag{3.4}$$

where $\boldsymbol{h}_{u,u'} = \left[h_{u,u'}(1), ..., h_{u,u'}(L_{u,u'})\right]^{\mathrm{T}} \in \mathbb{C}^{L_{u,u'} \times 1}$ is delay profile vector and $L_{u,u'}$ is the number of multipath components of the $\mathrm{S}_{u'}$-D_u link. Furthermore, $\boldsymbol{W}_{u,u'} \in \mathbb{R}^{K \times L_{u,u'}}$ is given by

$$\boldsymbol{W}_{u,u'} = \begin{bmatrix} \boldsymbol{I}_{L_{u,u'}} \\ \boldsymbol{0}_{(K - L_{u,u'}) \times L_{u,u'}} \end{bmatrix}. \tag{3.5}$$

To simplify (3.2), let

$$\boldsymbol{z}_u^{\mathrm{f}} = \left[z_u^{\mathrm{f}}(1), ..., z_u^{\mathrm{f}}(k'), ..., z_u^{\mathrm{f}}(K')\right]^{\mathrm{T}} = \sum_{\substack{u'=1 \\ u' \neq u}}^{U} \boldsymbol{M}_u^{\mathrm{T}} \boldsymbol{\Xi}_{u,u'} \boldsymbol{M}_{u'} \boldsymbol{x}_{u'}^{\mathrm{f}} + \boldsymbol{\eta}_u^{\mathrm{f}} \tag{3.6}$$

express spectrum vector of interference plus noise at the D_u node. The spectrum vector $\boldsymbol{z}_u^{\mathrm{f}} \in \mathbb{C}^{K' \times 1}$ can be modeled as a complex Gaussian random vector with zero-mean and covariance matrix $\boldsymbol{Z}_u = \mathbb{E}\left\{\boldsymbol{z}_u^{\mathrm{f}} \left(\boldsymbol{z}_u^{\mathrm{f}}\right)^{\mathrm{H}}\right\} = \mathrm{diag}\left[Z_u(1), ..., Z_u(k'), ..., Z_n(K')\right]$. Note that $Z_u(k')$ is the energy of interference plus noise induced in the reception of the spectral component $x_u^{\mathrm{f}}(k')$, which is transmitted over the $o_u(k')$-th subchannel. Therefore, (3.2) is rewritten as

$$\boldsymbol{y}_u^{\mathrm{f}} = \left[y_u^{\mathrm{f}}(1), ..., y_u^{\mathrm{f}}(k'), ..., y_u^{\mathrm{f}}(K')\right]^{\mathrm{T}} = \boldsymbol{M}_u^{\mathrm{T}} \boldsymbol{\Xi}_{u,u} \boldsymbol{M}_u \boldsymbol{x}_u^{\mathrm{f}} + \boldsymbol{z}_u^{\mathrm{f}}. \tag{3.7}$$

From (3.7) the k'-th element ($k' \in \{1, 2, ..., K'\}$) of $\boldsymbol{y}_u^{\mathrm{f}} \in \mathbb{C}^{K' \times 1}$ is given by

$$y_u^{\mathrm{f}}(k') = \xi_{u,u}\left(o_u(k')\right) x_u^{\mathrm{f}}(k') + z_u^{\mathrm{f}}(k'). \tag{3.8}$$

Hence, average CCMC capacity over K' subchannels used by the $\mathrm{S}_{u'}$-D_u link is

$$C_u(K') = \frac{1}{K'} \sum_{k'=1}^{K'} \log_2 \left[1 + \frac{\left|\xi_{u,u}\left(o_u(k')\right)\right|^2 E_{\mathrm{s}}}{Z_u(k')}\right]. \tag{3.9}$$

Finally, the sum CCMC capacity averaged over all K subchannels of the system band for all U links is given by

$$C_{\text{sum}}(K') = \frac{1}{K}\sum_{u=1}^{U}\sum_{k'=1}^{K'}\log_2\left[1+\frac{\left|\xi_{u,u}\left(o_u\left(k'\right)\right)\right|^2 E_{\text{s}}}{Z_u\left(k'\right)}\right] = \frac{K'}{K}\sum_{u=1}^{U} C_u\left(K'\right). \tag{3.10}$$

The probability that the $\text{S}_{u'}$-node transmits its signal on the $o_u(k')$-th subchannel is K'/K. Hence the expected value of $Z_u(k')$ can be roughly calculated by

$$\overline{Z}_u\left(k'\right) = \frac{K'}{K}\sum_{\substack{u'=1\\u'\neq u}}^{U}\left|\xi_{u,u'}\left(k'\right)\right|^2 E_{\text{s}} + N_0. \tag{3.11}$$

It is apparent that $\overline{Z}_u(k')$ is reduced when BAR is reduced. Meanwhile value of $\left|\xi_{u,u}\left(o_u\left(k'\right)\right)\right|^2$ increases since the signal spectrum $\boldsymbol{x}_u^{\text{f}}$ is transmitted over K' subchannels with the highest channel gain of the S_u-D_u link. As a result, when BAR decreases, the CCMC capacity per used subchannel of each link $C_u(K')$ increases as shown in Figure 2.19 of Section 2.6.1. As a demerit of BAR reduction, the bandwidth that exploited for data transmission decreases. Thus, the sum capacity in (3.10) can be enhanced as shown in Figure 2.20 if BAR is controlled to balance the increase in $C_u(K')$ and the decrease in transmission bandwidth. Furthermore, as implied in (3.11), when the number of links U increases, the average interference plus noise energy $\overline{Z}_u(k')$ increases. Therefore, for a large U, BAR must be set to a small value to sufficiently reduce the interference level. The optimal values of BAR are relatively small, basically in the range between 0 and around 0.5 as mentioned in the discussion of Figure 2.19 and Figure 2.20.

3.2.2 Requirement for Channel Prediction in DSC

In order to carry out the subchannel selection in DSC, the D_u-node is required to predict CFR of the entire system band. However, in the considered autonomous network, sending reference signal over the whole system band reduces frame efficiency and may cause extra interference to the neighboring links. Therefore, this dissertation focuses on channel prediction of the entire system band using reference signals whose spectral components are sparsely assigned by DSC.

Figure 3.2 illustrates reference signal and data spectrum distribution for the S_u-D_u link. In the autonomous spectrum sharing, all the wireless channels are subject to quasi-static fading channels, i.e., the channel states are constant during the transmission of one frame, but vary slowly frame by frame. In the transmission of one frame, the S_u node transmits reference

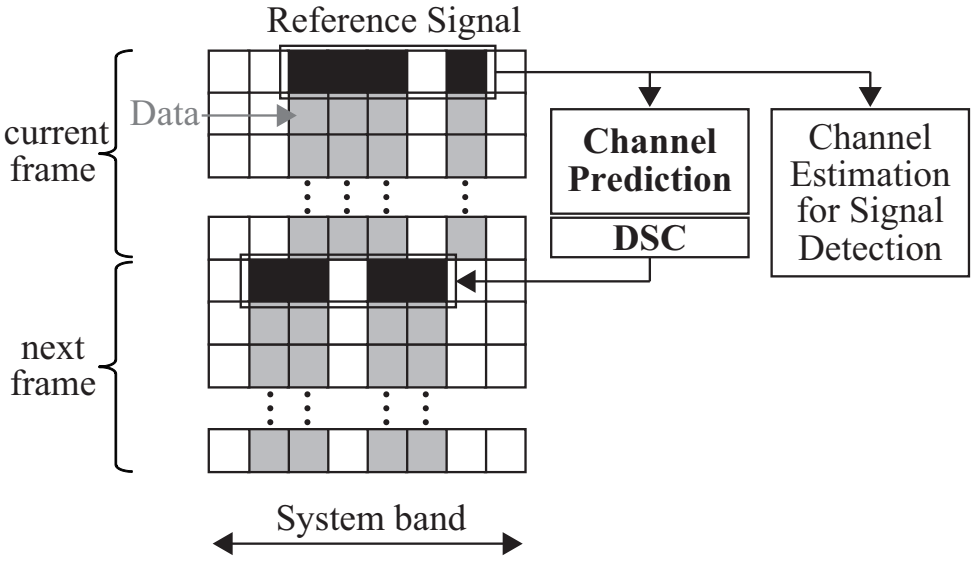

Figure 3.2: Reference signal spectrum placement for channel prediction.

signal and data over the same subchannels selected by the DSC. The D_u node uses the received reference signal to perform channel estimation for coherent signal detection. The D_u node also exploits the reference signal to carry out channel prediction for the entire system band which is necessitated by the DSC. After that, the D_u node uses the predicted CFR to select K' subchannels with higher channel gain for transmission in the next frame. The D_u node notifies the S_u node of the status of selected/non-selected for all K subchannels of the system band. As mentioned in Section 2.5.2, this notification can be fulfilled if the D_u node feedback one block consisting of K bits in which one and zero respectively indicate selected and non-selected subchannels. Following this notification, the S_u node transmits reference signal and data for the next frame over the selected subchannels.

As shown in (3.8), among K discrete elements of the CFR $\boldsymbol{\xi}_{u,u}$ the D_u-node can observe only K' samples which are contained in $\boldsymbol{y}_u^{\mathrm{f}} \in \mathbb{C}^{K' \times 1}$. Hence, the primary problem is how to predict K discrete CFRs $\xi_{u,u}(1)$, ..., $\xi_{u,u}(k)$, ..., $\xi_{u,u}(K)$ using only K' ($K' < K$) spot-wise spectral components of the received reference signal $y_u^{\mathrm{f}}(1)$, ..., $y_u^{\mathrm{f}}(k')$, ..., $y_u^{\mathrm{f}}(K')$. Using (3.8), we derive signal model for the channel prediction as

$$\boldsymbol{y}_u^{\mathrm{f}} = \boldsymbol{X}_u^{\mathrm{f}} \boldsymbol{M}_u^{\mathrm{T}} \boldsymbol{\xi}_{u,u} + \boldsymbol{z}_u^{\mathrm{f}}, \tag{3.12}$$

where

$$\boldsymbol{X}_u^{\mathrm{f}} = \mathrm{diag}\left[x_u^{\mathrm{f}}(1), ..., x_u^{\mathrm{f}}(k'), ..., x_u^{\mathrm{f}}(K')\right]. \tag{3.13}$$

3.3 Channel Prediction for DSC

3.3.1 Constrained LS Channel Prediction

According to (3.4), $\boldsymbol{\xi}_{u,u} = \sqrt{K}\boldsymbol{F}_K\boldsymbol{W}_{u,u}\boldsymbol{h}_{u,u}$. This means that determination of vector $\boldsymbol{\xi}_{u,u} \in \mathbb{C}^{K\times 1}$ is equivalent to that of vector $\boldsymbol{h}_{u,u} \in \mathbb{C}^{L_{u,u}\times 1}$. Thus, instead of predicting vector $\boldsymbol{\xi}_{u,u}$, we will predict vector $\boldsymbol{h}_{u,u}$, which consists of only $L_{u,u}$ elements. In practice, the number of multipath components $L_{u,u}$ of the channel is unknown. However, supposing that the maximum excess delay $L_{u,u}$ is smaller than or equal to the CP length, we can redefine vector $\boldsymbol{\xi}_{u,u}$ as

$$\boldsymbol{\xi}_{u,u} = \sqrt{K}\boldsymbol{F}_K\boldsymbol{W}\underline{\boldsymbol{h}}_{u,u}. \tag{3.14}$$

Note that

$$\boldsymbol{W} = \begin{bmatrix} \boldsymbol{I}_{L_{\mathrm{CP}}} \\ \boldsymbol{0}_{(K-L_{\mathrm{CP}})\times L_{\mathrm{CP}}} \end{bmatrix} \in \mathbb{R}^{K\times L_{\mathrm{CP}}}, \tag{3.15}$$

where L_{CP} is the CP length. Furthermore, $\underline{\boldsymbol{h}}_{u,u} = \left[h_{u,u}(1), ..., h_{u,u}(L_{u,u}), 0, ..., 0\right]^{\mathrm{T}} \in \mathbb{C}^{L_{\mathrm{CP}}\times 1}$.

Substituting (3.14) into (3.12), we have

$$\boldsymbol{y}_u^{\mathrm{f}} = \sqrt{K}\,\boldsymbol{X}_u^{\mathrm{f}}\boldsymbol{Q}_u\,\underline{\boldsymbol{h}}_{u,u} + \boldsymbol{z}_u^{\mathrm{f}}, \tag{3.16}$$

where

$$\boldsymbol{Q}_u = \boldsymbol{M}_u^{\mathrm{T}}\boldsymbol{F}_K\boldsymbol{W} \qquad (\in \mathbb{C}^{K'\times L_{\mathrm{CP}}}). \tag{3.17}$$

Thus, the channel prediction can be formulated as a constrained LS problem which exploits the fact that the maximum excess delay of the channel is shorter than the CP length L_{CP} as follows [33][32]

$$\underline{\hat{\boldsymbol{h}}}_{u,u}^{\mathrm{LS}} = \arg\min_{\underline{\hat{\boldsymbol{h}}}_{u,u}} \left|\boldsymbol{y}_u^{\mathrm{f}} - \sqrt{K}\,\boldsymbol{X}_u^{\mathrm{f}}\boldsymbol{Q}_u\,\underline{\hat{\boldsymbol{h}}}_{u,u}\right|^2. \tag{3.18}$$

From (3.18) it follows

$$\boldsymbol{Q}_u\,\underline{\hat{\boldsymbol{h}}}_{u,u}^{\mathrm{LS}} = \frac{1}{\sqrt{K}}\left(\boldsymbol{X}_u^{\mathrm{f}}\right)^{-1}\boldsymbol{y}_u^{\mathrm{f}}. \tag{3.19}$$

Because $\boldsymbol{Q}_u \in \mathbb{C}^{K\times L_{\mathrm{CP}}}$ is an irregular matrix, we use its left pseudo-inverse [55] $\left(\boldsymbol{Q}_u^{\mathrm{H}}\boldsymbol{Q}_u\right)^{-1}\boldsymbol{Q}_u^{\mathrm{H}}$ to solve (3.18). Thus, solution to (3.18) is given by

$$\underline{\hat{\boldsymbol{h}}}_{u,u}^{\mathrm{LS}} = \frac{1}{\sqrt{K}}\left(\boldsymbol{Q}_u^{\mathrm{H}}\boldsymbol{Q}_u\right)^{-1}\boldsymbol{Q}_u^{\mathrm{H}}\left(\boldsymbol{X}_u^{\mathrm{f}}\right)^{-1}\boldsymbol{y}_u^{\mathrm{f}}. \tag{3.20}$$

Hence, the predicted CFR is

$$\hat{\boldsymbol{\xi}}_{u,u}^{\mathrm{LS}} = \boldsymbol{F}_K \boldsymbol{W} \left(\boldsymbol{Q}_u^{\mathrm{H}} \boldsymbol{Q}_u\right)^{-1} \boldsymbol{Q}_u^{\mathrm{H}} \left(\boldsymbol{X}_u^{\mathrm{f}}\right)^{-1} \boldsymbol{y}_u^{\mathrm{f}}. \tag{3.21}$$

From (3.21), $\boldsymbol{Q}_u$ is necessary in computation of $\hat{\boldsymbol{\xi}}_{u,u}^{\mathrm{LS}}$. In order to define $\boldsymbol{Q}_u$, we need information on $\boldsymbol{W}$ determined by the CP length L_{CP}, and $\boldsymbol{M}_u$ defined by distribution of subchannels sparsely selected by DSC.

3.3.2 MSE of Predicted CSI

From (3.21), we have

$$\hat{\boldsymbol{\xi}}_{u,u}^{\mathrm{LS}} = \boldsymbol{\xi}_{u,u} + \boldsymbol{F}_K \boldsymbol{W} \left(\boldsymbol{Q}_u^{\mathrm{H}} \boldsymbol{Q}_u\right)^{-1} \boldsymbol{Q}_u^{\mathrm{H}} \left(\boldsymbol{X}_u^{\mathrm{f}}\right)^{-1} \boldsymbol{z}_u^{\mathrm{f}}. \tag{3.22}$$

Thus, the prediction error vector is given by

$$\boldsymbol{e}_u = \hat{\boldsymbol{\xi}}_{u,u}^{\mathrm{LS}} - \boldsymbol{\xi}_{u,u} = \boldsymbol{F}_K \boldsymbol{W} \left(\boldsymbol{Q}_u^{\mathrm{H}} \boldsymbol{Q}_u\right)^{-1} \boldsymbol{Q}_u^{\mathrm{H}} \left(\boldsymbol{X}_u^{\mathrm{f}}\right)^{-1} \boldsymbol{z}_u^{\mathrm{f}}. \tag{3.23}$$

Consequently, covariance matrix of the prediction error is

$$\boldsymbol{\Omega}_{\boldsymbol{e}} = \mathbb{E}\left\{\boldsymbol{e}_u \boldsymbol{e}_u^{\mathrm{H}}\right\} = \boldsymbol{F}_K \boldsymbol{W} \boldsymbol{T}_u^{-1} \boldsymbol{Q}_u^{\mathrm{H}} \left(\boldsymbol{X}_u^{\mathrm{f}}\right)^{-1} \boldsymbol{Z}_u \left(\left(\boldsymbol{X}_u^{\mathrm{f}}\right)^{-1}\right)^{\mathrm{H}} \boldsymbol{Q}_u \boldsymbol{T}_u^{-1} \boldsymbol{W}^{\mathrm{T}} \boldsymbol{F}_K^{\mathrm{H}}. \tag{3.24}$$

In (3.24), $\boldsymbol{T}_u \in \mathbb{C}^{L_{\mathrm{CP}} \times L_{\mathrm{CP}}}$ is a Hermitian Toeplitz matrix which is defined as

$$\boldsymbol{T}_u = \boldsymbol{Q}_u^{\mathrm{H}} \boldsymbol{Q}_u = \begin{bmatrix} t_0 & t_{-1} & \cdots & t_{-L_{\mathrm{CP}}+1} \\ t_1 & t_0 & & \vdots \\ \vdots & \vdots & \ddots & t_{-1} \\ t_{L_{\mathrm{CP}}-1} & t_{L_{\mathrm{CP}}-2} & \cdots & t_0 \end{bmatrix}, \tag{3.25}$$

where t_l ($l \in \{0, ..., L_{\mathrm{CP}} - 1\}$) is given by

$$t_l = \sum_{k'=1}^{K'} \exp\left(j \frac{2\pi o_u(k')\, l}{K}\right). \tag{3.26}$$

Recall that $o_u(k')$ ($o_u(k') \in \{1, 2, ..., K\}, k' \in \{1, 2, ..., K'\}$) are indexes of subchannels over which spectral components are mapped by DSC. Since in practical systems, the number of spectral components K' is larger than the CP length L_{CP}, $\boldsymbol{T}_u$ is full-rank and invertible [33].

Because in autonomous spectrum sharing, the number of spectral components K' is relatively smaller than that of the number of subchannels K of the system band, interference occurs in a

small portion of the received spectrum and covariance matrix of $\boldsymbol{z}_u^{\mathrm{f}}$ can be approximated as $\boldsymbol{Z}_u \approx N_0 \boldsymbol{I}_{K'}$. As a result, (3.24) becomes

$$\boldsymbol{\Omega_e} \approx \frac{N_0}{E_{\mathrm{s}}} \boldsymbol{F}_K \boldsymbol{W} \boldsymbol{T}_u^{-1} \boldsymbol{W}^{\mathrm{T}} \boldsymbol{F}_K^{\mathrm{H}}. \tag{3.27}$$

Note that the covariance matrix of prediction error $\boldsymbol{\Omega_e}$ does not depend on statistics of the channel but only on the distribution of subchannels selected by DSC and covariance matrix of noise plus interference.

Finally, average mean squared error (MSE) over all K subchannels of the system band is expressed as

$$\begin{aligned}
\varepsilon^2 &= \frac{1}{K}\mathrm{trace}\left\{\boldsymbol{\Omega_e}\right\} \\
&\approx \frac{1}{K}\mathrm{trace}\left\{\frac{N_0}{E_{\mathrm{s}}} \boldsymbol{F}_K \left(\boldsymbol{W} \boldsymbol{T}_u^{-1} \boldsymbol{W}^{\mathrm{T}}\right) \boldsymbol{F}_K^{\mathrm{H}}\right\} \\
&= \frac{N_0}{KE_{\mathrm{s}}}\mathrm{trace}\left\{\boldsymbol{W} \boldsymbol{T}_u^{-1} \boldsymbol{W}^{\mathrm{T}}\right\} \\
&= \frac{N_0}{KE_{\mathrm{s}}}\mathrm{trace}\left\{\begin{bmatrix} \boldsymbol{T}_u^{-1} & \boldsymbol{0}_{L_{\mathrm{CP}}\times(K-L_{\mathrm{CP}})} \\ \boldsymbol{0}_{(K-L_{\mathrm{CP}})\times L_{\mathrm{CP}}} & \boldsymbol{0}_{(K-L_{\mathrm{CP}})\times(K-L_{\mathrm{CP}})} \end{bmatrix}\right\} \\
&= \frac{N_0}{KE_{\mathrm{s}}}\mathrm{trace}\left\{\boldsymbol{T}_u^{-1}\right\}.
\end{aligned} \tag{3.28}$$

3.3.3 Dependence of MSE on Bandwidth of Continuously Non-Selected Subchannels

According to [34], the average MSE ε^2 is dominated by the bandwidth of continuously non-selected subchannels which is defined as

$$\Delta k_{\max} = \max_{k' \in \{1,2,\ldots,K'\}} \{\Delta k_{k'}\}, \tag{3.29}$$

where

$$\Delta k_{k'} = o_u(k'+1) - o_u(k'),\ k' \in \{1, 2, ..., K'-1\}, \tag{3.30}$$

and

$$\Delta k_{K'} = K + o_u(1) - o_u(K'). \tag{3.31}$$

Because the number of used subchannels K' is set to be larger than the CP length L_{CP} in practical systems, $\boldsymbol{T}_u$ is full-rank, i.e., $\boldsymbol{T}_u$ has L_{CP} nonzero eigenvalues. Let $\lambda_1 \geq \lambda_2 \geq ... \geq \lambda_{L_{\mathrm{CP}}}$

are L_{CP} eigenvalues of $\boldsymbol{T}_u$. Because $\boldsymbol{T}_u$ is Hermitian, λ_1, ..., $\lambda_{L_{\mathrm{CP}}} > 0$ and average MSE can be expressed as

$$\varepsilon^2 = \frac{N_0}{KE_{\mathrm{s}}}\mathrm{trace}\left\{\boldsymbol{T}_u^{-1}\right\} = \frac{N_0}{KE_{\mathrm{s}}}\sum_{l=1}^{L_{\mathrm{CP}}}\frac{1}{\lambda_l}. \tag{3.32}$$

Since determination of λ_l's is analytically intractable, we employ a theorem in [56] to find an upper bound on ε^2. Let

$$T(\lambda) = \sum_{l=-L_{\mathrm{CP}}+1}^{L_{\mathrm{CP}}-1} t_l \exp(-jl\lambda) \qquad (\lambda \in [0, 2\pi]) \tag{3.33}$$

then $\lambda_1, ..., \lambda_{L_{\mathrm{CP}}} \geq \min_{\lambda\in[0,2\pi]} T(\lambda)$. Substituting (3.26) into (3.33), we derive

$$\begin{aligned}
T(\lambda) &= \sum_{l=-L_{\mathrm{CP}}+1}^{L_{\mathrm{CP}}-1}\sum_{k'=1}^{K'} \exp\left(j2\pi o_u(k')\, l/K\right)\cdot\exp(-jl\lambda) \\
&= \sum_{k'=1}^{K'}\left\{\sum_{l=-L_{\mathrm{CP}}+1}^{L_{\mathrm{CP}}-1}\exp\left[j\left(2\pi o_u(k')/K-\lambda\right)l\right]\right\} \\
&= \sum_{k'=1}^{K'}\frac{\exp\left[-j\left(L_{\mathrm{CP}}-1\right)\left(2\pi o_u(k')/K-\lambda\right)\right]-\exp\left[j\left(L_{\mathrm{CP}}-1\right)\left(2\pi o_u(k')/K-\lambda\right)\right]}{1-\exp\left[j\left(2\pi o_u(k')/K-\lambda\right)\right]} \\
&= \sum_{k'=1}^{K'}\frac{\exp\left[j\left(L_{\mathrm{CP}}-1/2\right)\left(2\pi o_u(k')/K-\lambda\right)\right]-\exp\left[-j\left(L_{\mathrm{CP}}-1/2\right)\left(2\pi o_u(k')/K-\lambda\right)\right]}{\exp\left[j\left(2\pi o_u(k')/K-\lambda\right)/2\right]-\exp\left[-j\left(2\pi o_u(k')/K-\lambda\right)/2\right]} \\
&= \sum_{k'=1}^{K'}\frac{\sin\left[\left(2\pi o_u(k')/K-\lambda\right)\left(L_{\mathrm{CP}}-1/2\right)\right]}{\sin\left[\left(2\pi o_u(k')/K-\lambda\right)/2\right]}.
\end{aligned} \tag{3.34}$$

Thus,

$$T(\lambda) = \sum_{k'=1}^{K'} T_{o_u(k')}(\lambda), \tag{3.35}$$

where

$$T_{o_u(k')}(\lambda) = \frac{\sin\left[\left(2\pi o_u(k')/K-\lambda\right)\left(L_{\mathrm{CP}}-1/2\right)\right]}{\sin\left[\left(2\pi o_u(k')/K-\lambda\right)/2\right]}. \tag{3.36}$$

Figure 3.3 characterizes behavior of $T_{o_u(k')}(\lambda)$ when $K = 256$, $o_u(k') = 83$ and $L_{\mathrm{CP}} = 16$. As shown in the figure, $T_{o_u(k')}(\lambda)$ has one main lobe with maximum at $\lambda = 2\pi o_u(k')/K$ and the width of the lobe is $2\pi/(L_{\mathrm{CP}} - 1/2)$.

Table 3.1: $\varepsilon^2_{\max}$ when $\delta > 0$.

δ	10^{-1}	10^{-2}	10^{-3}	10^{-10}
$\varepsilon^2_{\max}$	$0.09 \cdot \frac{N_0}{E_s}$	$0.17 \cdot \frac{N_0}{E_s}$	$0.45 \cdot \frac{N_0}{E_s}$	$0.47 \cdot \frac{N_0}{E_s}$

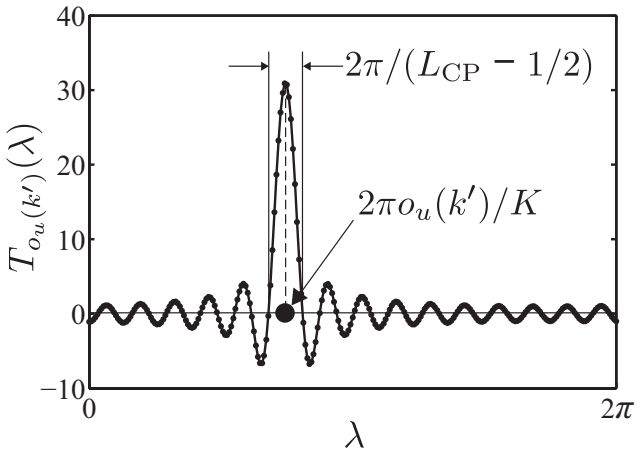

Figure 3.3: $T_{o_u(k')}(\lambda)$ when $K = 256$, $o_u(k') = 83$ and $L_{\mathrm{CP}} = 16$.

Let $o_u(k'_0)$ and $o_u(k'_0 + 1)$ are indexes of two adjacent subchannels selected by DSC that their spacing is the maximum, i.e., $o_u(k'_0 + 1) = o_u(k'_0) + \Delta k_{\max}$. We consider the minimum of $T(\lambda)$ in domain $D_0 = \left[2\pi o_u(k'_0)/K, 2\pi o_u(k'_0 + 1)/K\right]$. Figures 3.4 (a), (b) and (c) respectively characterize behavior of $T(\lambda)$ in domain $0 \le \lambda < 2\pi$ in three cases: $\Delta k_{\max} < K/(L_{\mathrm{CP}} - 1/2)$, $\Delta k_{\max} = K/(L_{\mathrm{CP}} - 1/2)$ and $\Delta k_{\max} > K/(L_{\mathrm{CP}} - 1/2)$. As shown in Figure 3.4 (a), $T(\lambda)$ is superposition of $T_{o_u(k'_0)}(\lambda)$ and $T_{o_u(k'_0+1)}(\lambda)$. When, $\Delta k_{\max} < K/(L_{\mathrm{CP}} - 1/2)$, $\Delta\lambda = 2\pi\Delta k_{\max}/K < 2\pi/(L_{\mathrm{CP}} - 1/2)$ and $\min_{\lambda\in D_0} T(\lambda) > 0$. In Figure 3.4 (b), when $\Delta k_{\max} = K/(L_{\mathrm{CP}} - 1/2)$, $\min_{\lambda\in D_0} T(\lambda) = 0$. Finally, in Figure 3.4 (c), when $\Delta k_{\max} > K/(L_{\mathrm{CP}} - 1/2)$, $\min_{\lambda\in D_0} T(\lambda) < 0$.

Let $\delta = K/(L_{\mathrm{CP}} - 1/2) - \Delta k_{\max}$. As can be seen from these figures, when $\delta > 0$, $\min_{\lambda\in D_0} T(\lambda) > 0$ and ε^2 is upper bounded as

$$\varepsilon^2 = \frac{N_0}{KE_s} \sum_{l=1}^{L_{\mathrm{CP}}} \frac{1}{\lambda_l} \le \varepsilon^2_{\max} \equiv \frac{L_{\mathrm{CP}}}{K \min_{\lambda\in D_0} T(\lambda)} \cdot \frac{N_0}{E_s}. \tag{3.37}$$

Due to our numerical analysis shown in Table 3.1, even when δ is slightly higher than 0, e.g., $\delta = 10^{-10}$, ε^2 is still small, e.g., its upper bound is of the order of N_0/E_s. On the other hand, when $\delta \le 0$, $\min_{\lambda\in D_0} T(\lambda) \le 0$. Hence, it is impossible to determine any upper bound on ε^2. In this case, there is no concrete evidences show magnitude of ε^2 [34].

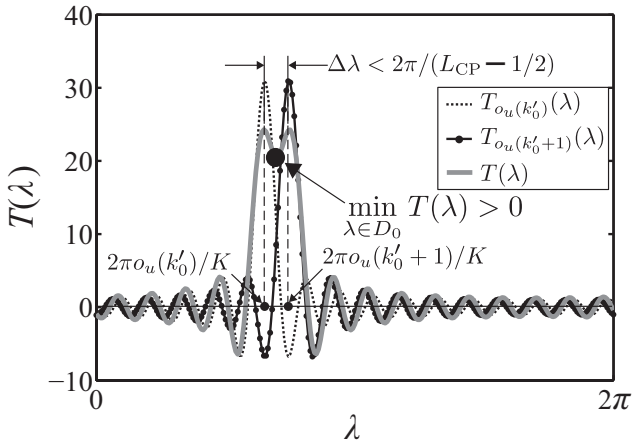

(a) $\Delta k_{\max} < K/(L_{\mathrm{CP}} - 1/2)$

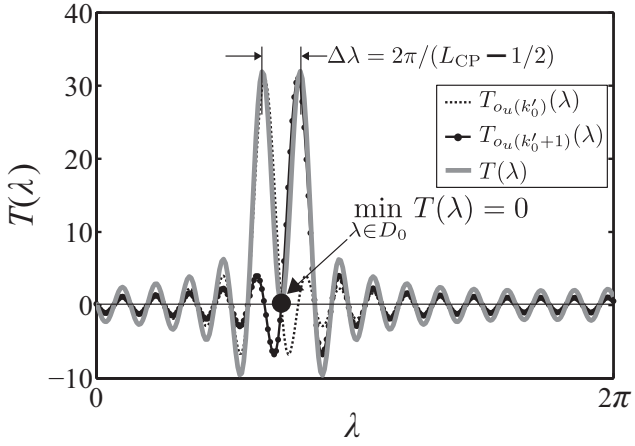

(b) $\Delta k_{\max} = K/(L_{\mathrm{CP}} - 1/2)$

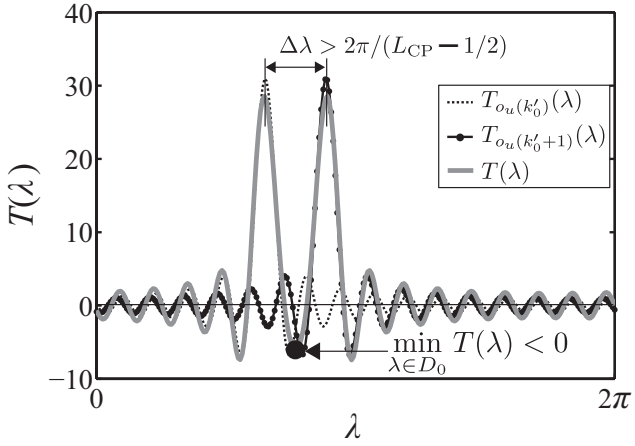

(c) $\Delta k_{\max} > K/(L_{\mathrm{CP}} - 1/2)$

Figure 3.4: Minimum of $T(\lambda)$ in D_0 when $\Delta k_{\max}$ varies.

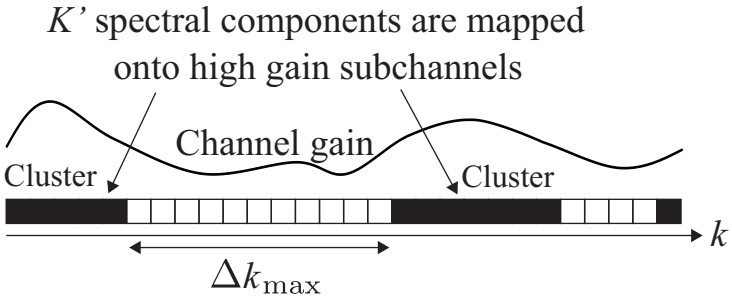

Figure 3.5: Cluster-featured transmission band in DSC.

Therefore, although it is not allowed to argue that ε^2 is extremely large if $\Delta k_{\max} \geq K/(L_{\mathrm{CP}} - 1/2)$, we can conclude that ε^2 is small if $\Delta k_{\max} < K/(L_{\mathrm{CP}} - 1/2)$.

3.3.4 Ill-conditioned LS Channel Prediction in DSC

In practice, CFR has relatively wide coherence bandwidth because maximum excess delay of the channel is much smaller than DFT window size K. As a consequence, transmission band of each link in DSC forms several clusters as shown in Figure 3.5. In other words, when value of BAR is relatively small in the BAR control aided autonomous spectrum sharing, the bandwidth of continuously non-selected subchannels $\Delta k_{\max}$ is relatively large. Therefore, $\Delta k_{\max}$ exceeds the threshold $K/(L_{\mathrm{CP}} - 1/2)$ with a high probability. An investigation on value of $\Delta k_{\max}$ is conducted to verify this argument. In this investigation, similar to the other sections, an equal gain 16 path Rayleigh model is employed. The CP length L_{CP} is set to 16. BAR is set to 0.125, 0.25, 0.375 and 0.5. Number of subchannels of the system band, i.e., the DFT window size, is $K = 256$. According to these assumptions, the threshold $K/(L_{\mathrm{CP}} - 1/2) \approx 16.52$. Figure 3.6 demonstrates CDF of $\Delta k_{\max}$ for relatively small values of BAR. As demonstrated in Figure 3.6, when BAR is in the range from 0.125 to 0.5, $\Delta k_{\max}$ is relatively large such that the probability the K exceeds the threshold 16.52 is almost 1.

Thus, when $\Delta k_{\max}$ is relatively large, the predicted CFR at non-selected subchannels could be less reliable. As a result, some of subchannels that should be selected to use might not be selected by DSC for the next frame even if they have actually high channel gain. This phenomenon tends to continue in the following frames and causes reduction of overall spectral efficiency averaged over multiple frames.

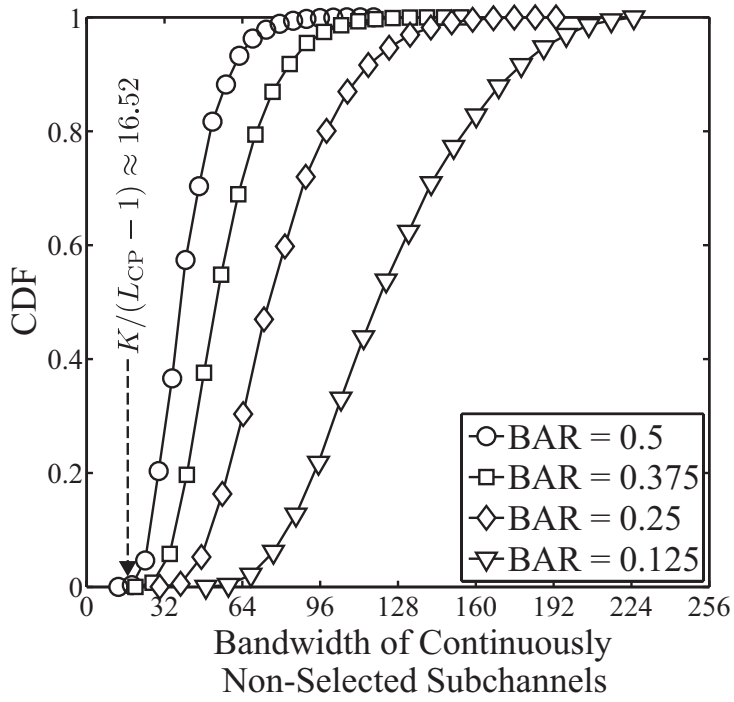

Figure 3.6: CDF of bandwidth of continuously non-selected subchannels $\Delta k_{\max}$ for relatively small BARs.

3.4 CSI Reliability Guaranteeing Subchannel Selection

3.4.1 Subchannel Selection

In order to improve the overall spectral efficiency under the presence of channel prediction error, this dissertation proposes a subchannel selection technique to guarantee the channel prediction reliability while enhancing the spectral efficiency for the current frame. The proposed subchannel selection scheme is described in Figure 3.7. In the proposed scheme, among K' spectral components of the transmitted signal, $(K' - M)$ spectral components are mapped onto subchannels with the highest predicted channel gain to enhance the spectral efficiency, whereas the rest of M spectral components are allocated uniformly onto the remaining subchannels regardless of channel gain to improve reliability of channel prediction, i.e., to reduce $\Delta k_{\max}$. In this scheme, if M is too large, the spectral efficiency is, of course, degraded. However, if M is too small, even if channel gain of non-selected subchannels becomes sufficiently high, it would be more probable not to be accurately estimated for channel gains of non-selected subchan-

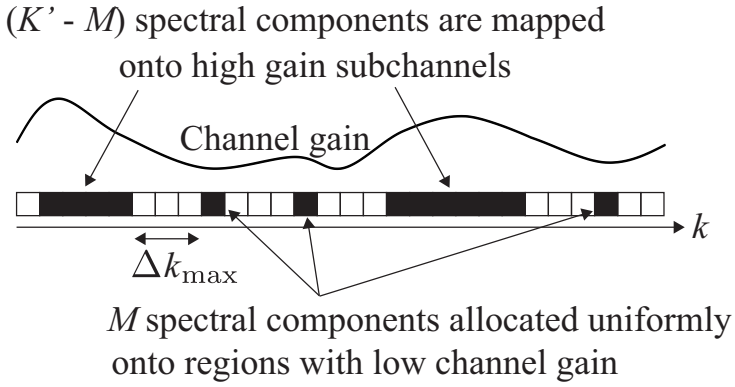

Figure 3.7: Channel prediction reliability guaranteeing subchannel selection.

nels, thereby subchannels in non-selected spectrum region might not be selected. Thus, it is mandatory to optimize M based on channel conditions for each timing.

We consider a private network with two links S_1-D_1 and S_2-D_2. The number of subchannels in the system band and the number of selected subchannels for each link are $K = 256$ and $K' = 64$, respectively, i.e., BAR is 0.25. In this analysis, we assume that distances from S_1 to D_1, from S_1 to D_2, from S_2 to D_1, and S_2 to D_2 are the same. Channel variations for all links in the considered network are subject to quasi-static frequency selective fading channels with equal gain 16 path Rayleigh model and transmitted E_s/N_0 is set to 10 dB. Maximum Doppler frequency f_D normalized by a frame duration is 0.05, i.e., the autocorrelation of CFR in the time-domain shown in (2.8) for all links is as high as 0.999. This setting guarantees the slow time-variance of all the links, which is the required condition for the application of DSC. Path loss and shadowing are not considered for the sake of simplicity. We also assume that the maximum excess delay of the channel is equal to L_{CP}.

Average CCMC capacity per used discrete frequency of one particular link, which is defined by (3.9), with a parameter of M is shown in Figure 3.8. As can be seen from Figure 3.8 in the next page, there is an optimum M at around 12 that maximizes the average CCMC capacity. When M increases from 0 to the optimum value, the capacity increases because MSE of channel prediction for currently non-selected subchannels gets large. When M increases further from the optimum value, capacity starts to decrease because higher gain subchannels are less probable to be selected. Hence, there is an optimum value of M which maximizes the overall CCMC capacity over transmission of multiple frames.

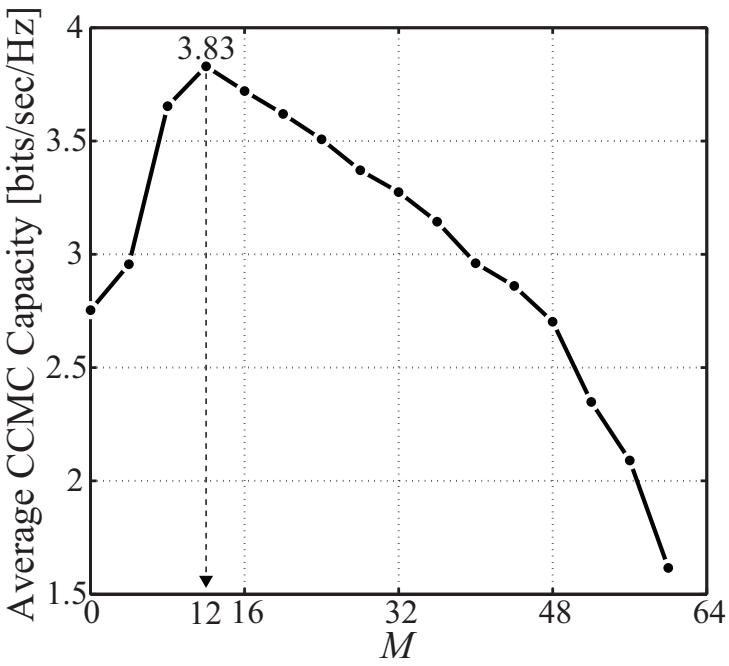

Figure 3.8: Average channel capacity when M varies.

3.4.2 Optimization of Subchannel Selection

Since the optimal value of M plays an important role in enhancement of average CCMC capacity of DSC, we examine a criterion to determine the optimal value.

We investigate variation of CCMC capacity for the present frame and that of MSE of channel prediction for the next frame when M varies. The simulation parameters are the same as those in Section 3.4.1. Figures 3.9 and 3.10 in the next page respectively show CCMC capacity and MSE of channel prediction for the present frame for various values of M. As shown in Figure 3.9, CCMC capacity for the present frame decreases almost linearly with the increase of M. While in Figure 3.10, average MSE of channel prediction in the next frame decreases exponentially when M starts to increase until it reaches a certain value. That is to say, MSE of channel prediction for the next frame is more sensitive to M than CCMC capacity of the present frame. Therefore, we define M to minimize MSE of channel prediction to be smaller than a certain level.

Eigenvalue analysis for the Hermitian Toeplitz matrix $\boldsymbol{T}_u$ in Section 3.3.3 shows that if the bandwidth of continuously non-selected subchannels $\Delta k_{\max}$ is smaller than $K/(L_{\mathrm{CP}} - 1/2)$, average MSE is small. $\Delta k_{\max}$ varies frame by frame since it depends not only on value of M but also on the selection of subchannels with high channel gain. According to the fluctuation of channel gain in the frequency-domain, the group of $(K' - M)$ subchannels with higher channel

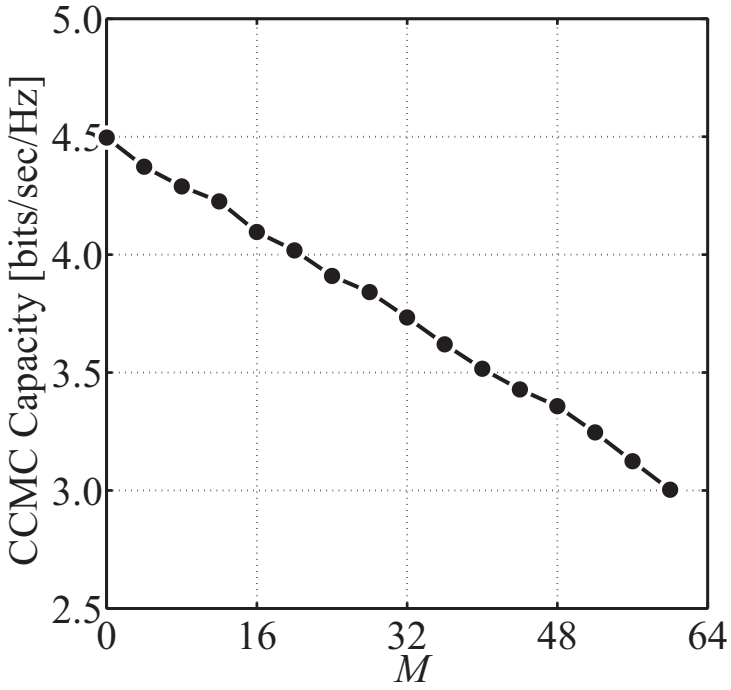

Figure 3.9: CCMC capacity for the present frame when M varies.

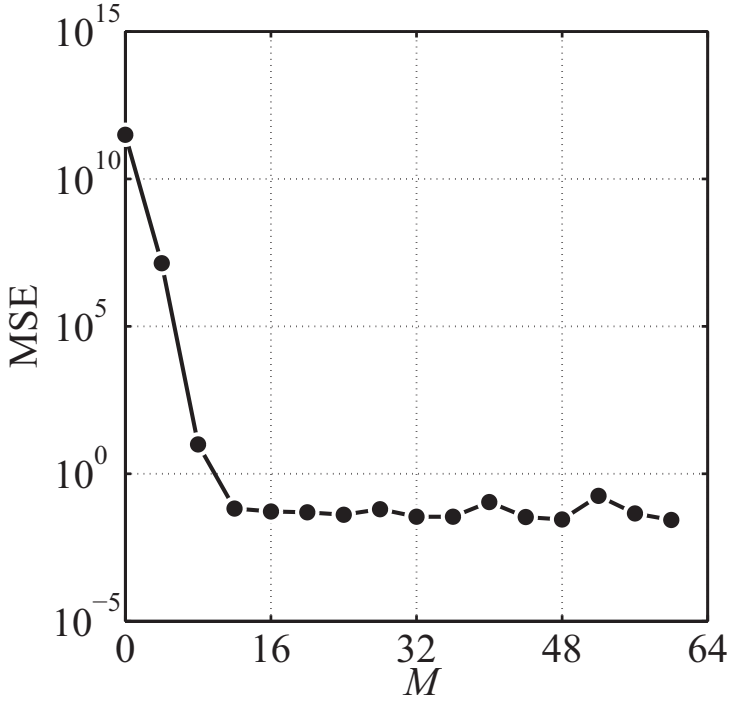

Figure 3.10: MSE of channel prediction for the next frame when M varies.

gain may form one or two or more clusters. When the group of $(K' - M)$ subchannels with higher channel gain forms one cluster, $\Delta k_{\max}$ reaches its largest value. Thus, an upper bound on $\Delta k_{\max}$ is derived as

$$\Delta k_{\max} \leq \frac{K - K' + M}{M + 1}. \tag{3.38}$$

Therefore, we define an optimal value of M so that upper bound on $\Delta k_{\max}$ is slightly smaller than $K/(L_{\mathrm{CP}} - 1/2)$, i.e.,

$$M = \left\lceil \frac{(K - K' - 1)(L_{\mathrm{CP}} - 1/2)}{K - L_{\mathrm{CP}} + 1/2} \right\rceil - 1. \tag{3.39}$$

The criterion described by (3.39) is applicable in practice because it requires only information on the number of selected subchannels K', the number of subchannels of the system band K and the CP length L_{CP} to determine the suboptimal value of M.

3.4.3 CCMC Capacity per Link

In this section, we evaluate the effectiveness of the proposed subchannel selection in enhancement of overall CCMC capacity achieved over transmission of multiple frames. The overall CCMC capacity is time-averaged value of the CCMC capacity given in (3.9), not that of the sum CCMC capacity given in (3.10). Evaluation for the sum CCMC capacity of the whole network is given in Section 3.5.2. All the parameters for numerical analysis in this section are the same as those in Section 3.4.1, except that K' is varied as 128, 96, 64, and 32, i.e., BAR is 0.5, 0.375, 0.25, and 0.125, respectively.

Figure 3.11 demonstrates average CCMC of DSC for the following four schemes:

- All spectral components are allocated onto subchannels with the highest channel gain ($M = 0$).
- M is determined by exhaustive search to maximize the average CCMC capacity (Exhaustive Search). To implement this scheme, all simulation parameters must be known and calculations with high computational burden must be conducted prior to transmissions.
- M is determined by (3.39) (Proposed).
- Perfect CSI is assumed to be available and it is used in subchannel selection (Perfect CSI). Different from the three cases above, in this case, channel prediction is unnecessary. Thus, all spectral components are allocated onto subchannels with the highest channel gain, i.e., $M = 0$.

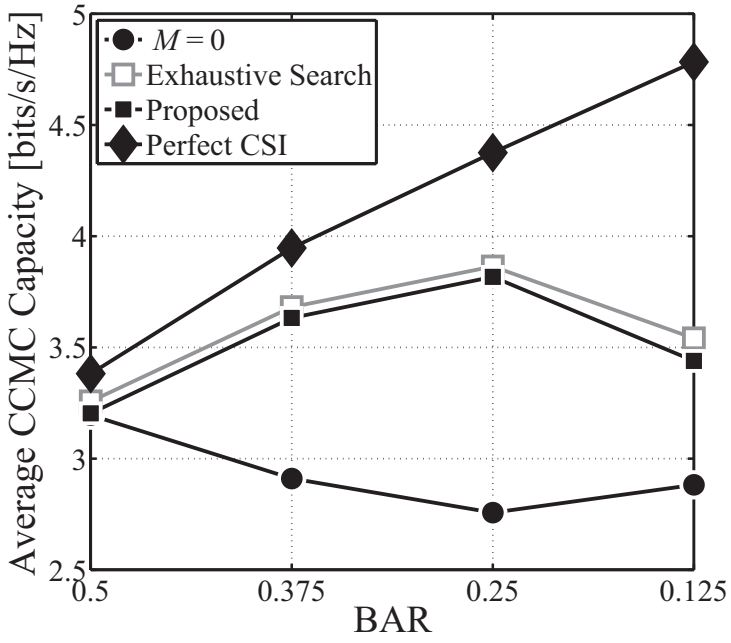

Figure 3.11: CCMC capacity per link per used subchannel for various values of BAR.

As can be seen from the figure, capacity for the proposed subchannel selection is very close to that for the exhaustive search. Channel capacity obtained by the proposed subchannel selection degrades from that for the perfect CSI case by 3.2%, 5.4%, 10.9% and 28.7% for BAR of 0.5, 0.375, 0.25 and 0.125, respectively. That is, when BAR is set to be relatively small, we need to increase M to reduce $\Delta k_{\max}$ for CCMC capacity enhancement of the next frame. On the other hand, when BAR is getting higher, it is acceptable to reduce M because $\Delta k_{\max}$ is getting smaller as demonstrated in Figure 3.6. Thus, MSE of channel prediction for the next frame is sufficiently small even with a small M.

As can also be observed from the figure, capacity improvement of the proposed subchannel selection from DSC with $M = 0$ are 1.2 %, 30.6%, 37.7% and 9.9% for the BAR of 0.5, 0.375, 0.25 and 0.125, respectively. This means that we can significantly improve the overall spectral efficiency by employing the suboptimal value of M.

3.5 BAR Control with CSI Reliability Guaranteeing Subchannel Selection

3.5.1 BAR Control

This section describes BAR control for autonomous spectrum sharing with the aid of CSI reliability guaranteeing subchannel selection. The BAR control is performed via computer simulation prior to transmissions. The procedure is as follows.

1. For each $K' \in \{1, 2, ..., K\}$, generate CFRs for all links in the network.
2. Each link in the network select K' subchannels based on CSI reliability guaranteeing subchannel selection which is proposed in Section 3.4.1. Note that value of M is optimized by (3.39) in Section 3.4.2.
3. Compute sum CCMC capacity for the whole network by (3.10) $C_{\text{sum}}(K')$.
4. Steps 1, 2 and 3 mentioned above is to compute $C_{\text{sum}}(K')$ for one channel realization. Repeat these steps for many channel realizations and calculate the average sum CCMC capacity $\overline{C}_{\text{sum}}(K')$. Note that $\overline{C}_{\text{sum}}(K')$ is the average value of $C_{\text{sum}}(K')$ over many channel realizations.
5. After completing the calculation of average sum CCMC capacity $\overline{C}_{\text{sum}}(K')$ for all $K' \in \{1, 2, ..., K\}$, search for $K'_{\text{opt}} = \arg \max_{K' \in \{1,2,...,K\}} \overline{C}_{\text{sum}}(K')$.

The predetermined K'_{opt} is used in transmissions as a parameter.

3.5.2 Sum CCMC Capacity Evaluation

In this section sum CCMC capacity of the whole network is evaluated to verify effectiveness of BAR control based on the proposed subchannel selection. All parameters in this evaluation are identical to those in Section 2.6.1. This means, all nodes of the network are assumed to be uniformly distributed in a square area whose diagonal satisfies a reference transmit SNR of 5 dB. Path loss exponent is $\mu = 3.5$ and the 16 path Rayleigh fading model is employed. The number of links in the network is varied as $U = 2, 4, 6, 8$, and 10.

Figure 3.12 portrays sum CCMC capacity vs. the number of simultaneously transmitted links for the following three BAR control schemes:

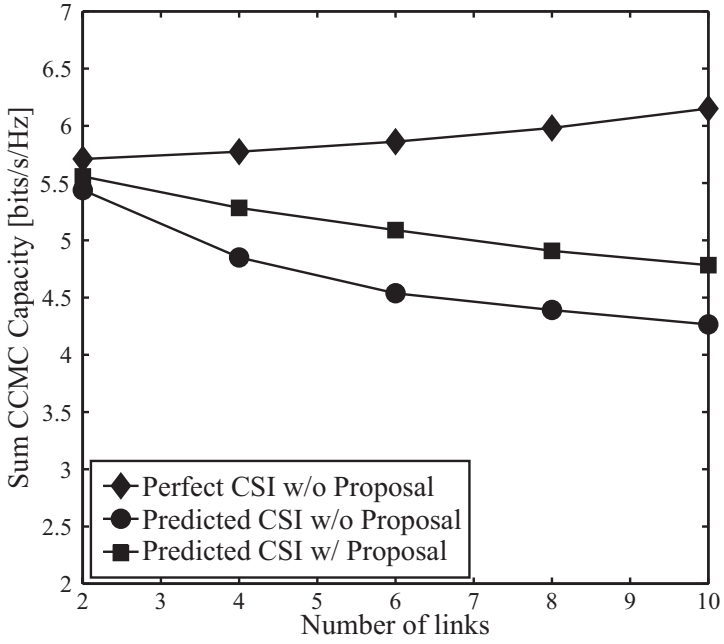

Figure 3.12: Sum CCMC capacity of various BAR control schemes.

- BAR control based on conventional DSC using perfect CSI (Perfect CSI w/o Proposal). Conventional DSC means the DSC that selects all K' subchannels with the highest actual channel gain, i.e., $M = 0$. In this scheme, perfect CSI is used in the subchannel selection process.

- BAR control based on conventional DSC using predicted CSI (Predicted CSI w/o Proposal). This scheme also selects all K' subchannels with the highest predicted channel gain. The predicted CSI is given by channel prediction in Section 3.3.1.

- BAR control based on the proposed subchannel selection using predicted CSI (Predicted CSI w/ Proposal). This scheme selects $(K' - M)$ subchannels having the highest predicted channel gain and selects M subchannels uniformly from low predicted channel gain frequency region. The value of M is optimized by (3.39). The predicted CSI is given by channel prediction in Section 3.3.1.

As shown in the figure, BAR control based on the proposed subchannel selection enhance the spectral efficiency for the network. For instance, when number of links $U = 6$, CCMC capacity enhancement of the proposed subchannel selection from the conventional DSC is 12%. When number of links increases, the CCMC capacity enhancement effect decreases. For example, when $U = 10$, the CCMC capacity enhancement is reduced to 11%. Furthermore, CCMC

capacity of the proposed subchannel selection deteriorates from the conventional DSC using perfect CSI when the number of links U increases. This is because when number of links U increases, the value of K' decreases. In such a case, M increases, i.e., we must allocate more subchannels on low channel gain regions as mentioned in Section 3.4.3.

3.6 Concluding Remarks

In BAR control aided autonomous spectrum sharing, because BAR is set to be smaller when the number of links gets larger, the bandwidth of continuously non-selected subchannels is relatively large. Thus, channel prediction for the entire system band from subchannels sparsely selected by DSC severely deteriorates. As a result the overall spectral efficiency achieved over multiple transmissions decreases.

To deal with this issue, this chapter proposed a subchannel selection which keeps the bandwidth of continuously non-selected subchannels below a theoretically determined threshold while increasing link capacity as high as possible. Numerical results collaborated that BAR control based on the proposed subchannel selection achieves a significantly enhanced spectral efficiency. This result also confirmed the establishment of BAR control technique for autonomous spectrum sharing.

Chapter 4

Band Activity Ratio Control for Broadband AF Relay

4.1 Introduction

In the fixed assigned band scenario, wireless relaying is an efficient solution to guarantee a certain transmission quality under path loss and transmit energy constraint. However, as shown in Section 2.7, spectral efficiency enhancement effect of multi-hop AF relay for broadband transmission degrades compared to DF relay due to the concatenation of CFRs of hops.

In this section, at first, signal spectrum optimization issue for spectral efficiency enhancement of broadband AF relay is clarified. After that, this chapter examines two EA schemes: joint EA and cascaded EA. Next, the effectiveness and the required notification overhead of SP based SM in enhancing the spectral efficiency for cascaded EA is demonstrated. Finally, this chapter proposes spectrum nulling based BAR control as a low overhead alternative for SP based SM.

4.2 Spectrum Optimization Problem

4.2.1 AF Relay with Spectrum Mapping and Energy Allocation

Figure 4.1 shows a configuration of a two-hop broadband AF relay system constituted by one S-node, one R-node, and one D-node. For the sake of simplicity, received signal level of the direct link from the S-node to the D-node is assumed to be negligibly low. Transmitted signals from the S-node and the R-node are completely orthogonalized by transmitting at different time slots. The S-R and R-D links are assumed to be quasi-static frequency selective fading channels,

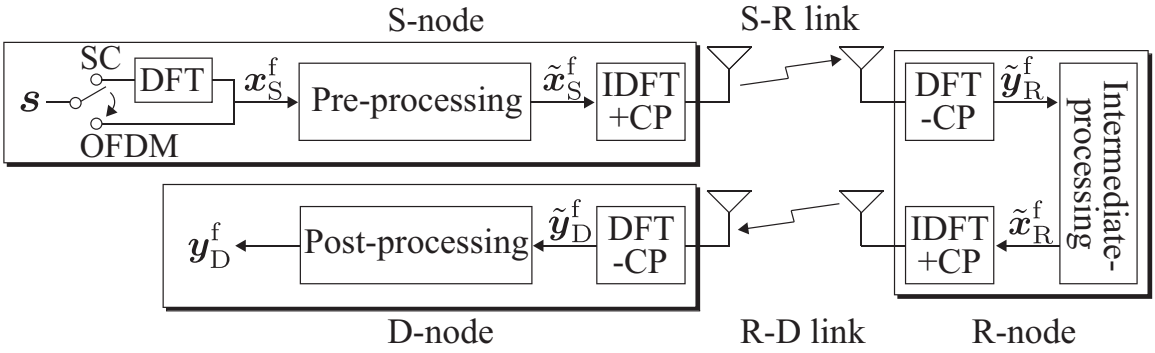

Figure 4.1: Schematic of two-hop AF broadband relaying.

each of which consists of K subchannels due to the broadband signaling.

First of all, a data symbol block $\boldsymbol{s} \in \mathbb{C}^{K' \times 1}$ consisting of K' ($\leq K$) data symbols is generated by the S-node. Average energy of each data symbols is $\mathbb{E}\left\{|s(k')|^2\right\} = E_\mathrm{s}$. In order to enable frequency-domain processing, the spectrum of symbol block is generated by

$$\boldsymbol{x}_\mathrm{S}^\mathrm{f} = \left[x_\mathrm{S}^\mathrm{f}(1), ..., x_\mathrm{S}^\mathrm{f}(k'), ..., x_\mathrm{S}^\mathrm{f}(K')\right]^\mathrm{T} = \begin{cases} \boldsymbol{F}_{K'}\boldsymbol{s} & \text{if SC} \\ \boldsymbol{s} & \text{if OFDM} \end{cases}. \tag{4.1}$$

To improve the spectral efficiency, the S-node carries out a pre-processing on the spectrum $\boldsymbol{x}_\mathrm{S}^\mathrm{f}$. The pre-processing consists of an SM followed by an EA. The details on the SM and EA schemes will be described later. The pre-processing yields a transmitted spectrum denoted by

$$\tilde{\boldsymbol{x}}_\mathrm{S}^\mathrm{f} = \left[\tilde{x}_\mathrm{S}^\mathrm{f}(1), ..., \tilde{x}_\mathrm{S}^\mathrm{f}(k), ..., \tilde{x}_\mathrm{S}^\mathrm{f}(K)\right]^\mathrm{T} = \boldsymbol{M}_\mathrm{S}\boldsymbol{G}_\mathrm{S}\boldsymbol{x}_\mathrm{S}^\mathrm{f}, \tag{4.2}$$

where $\boldsymbol{M}_\mathrm{S} \in \mathbb{R}^{K \times K'}$ and $\boldsymbol{G}_\mathrm{S} \in \mathbb{R}^{K' \times K'}$ denote SM and EA matrices at the S-node, respectively. The transmitted spectrum $\tilde{\boldsymbol{x}}_\mathrm{S}^\mathrm{f}$ is subject to a transmit energy constraint $\mathbb{E}\left\{\frac{1}{K}\sum_{k=1}^{K}\left|\tilde{x}_\mathrm{S}^\mathrm{f}(k)\right|^2\right\} = E_\mathrm{s}$. Note that E_s indicates average transmit energy for each subchannel at the S-node.

After the pre-processing, K point IDFT is applied to $\tilde{\boldsymbol{x}}_\mathrm{S}^\mathrm{f}$ to form a transmitted signal block in the time-domain. For frequency-domain linear processing at the R-node, a CP is appended to the head of the signal block. The CP-appended signal block is then transmitted to the R-node.

At the R-node, CP removal is carried out and K point DFT is applied to generate received spectrum $\tilde{\boldsymbol{y}}_\mathrm{R}^\mathrm{f}$, which is given by

$$\tilde{\boldsymbol{y}}_\mathrm{R}^\mathrm{f} = \left[\tilde{y}_\mathrm{R}^\mathrm{f}(1), ..., \tilde{y}_\mathrm{R}^\mathrm{f}(k), ..., \tilde{y}_\mathrm{R}^\mathrm{f}(K)\right]^\mathrm{T} = \boldsymbol{\Xi}_\mathrm{RS}\tilde{\boldsymbol{x}}_\mathrm{S}^\mathrm{f} + \tilde{\boldsymbol{\eta}}_\mathrm{R}^\mathrm{f}. \tag{4.3}$$

In (4.3), $\boldsymbol{\Xi}_\mathrm{RS} = \mathrm{diag}\left[\xi_\mathrm{RS}(1), ..., \xi_\mathrm{RS}(k), ..., \xi_\mathrm{RS}(K)\right] \in \mathbb{C}^{K \times K}$ indicates the frequency-domain channel matrix of the S-R link, where $\xi_\mathrm{RS}(k)$ is complex-valued CFR of the k-th subchannel.

Furthermore, $\tilde{\boldsymbol{\eta}}_{\mathrm{R}}^{\mathrm{f}} = \left[\tilde{\eta}_{\mathrm{R}}^{\mathrm{f}}(1), ..., \tilde{\eta}_{\mathrm{R}}^{\mathrm{f}}(k), ..., \tilde{\eta}_{\mathrm{R}}^{\mathrm{f}}(K)\right]^{\mathrm{T}}$, where $\tilde{\eta}_{\mathrm{R}}^{\mathrm{f}}(k)$ is a noise spectral component induced at the k-th subchannel in the R-node. We assume that $\tilde{\eta}_{\mathrm{R}}^{\mathrm{f}}(k) \sim \mathcal{CN}(0, N_{\mathrm{R}})$.

Similar to the pre-processing at the S-node, intermediate-processing is carried out to the received spectrum $\tilde{\boldsymbol{y}}_{\mathrm{R}}^{\mathrm{f}}$ at the R-node. The intermediate-processing yields a forward spectrum denoted by

$$\tilde{\boldsymbol{x}}_{\mathrm{R}}^{\mathrm{f}} = \left[\tilde{x}_{\mathrm{R}}^{\mathrm{f}}(1), ..., \tilde{x}_{\mathrm{R}}^{\mathrm{f}}(k), ..., \tilde{x}_{\mathrm{R}}^{\mathrm{f}}(K)\right]^{\mathrm{T}} = \boldsymbol{M}_{\mathrm{R}} \boldsymbol{G}_{\mathrm{R}} \boldsymbol{M}_{\mathrm{S}}^{\mathrm{T}} \tilde{\boldsymbol{y}}_{\mathrm{R}}^{\mathrm{f}}, \tag{4.4}$$

where $\boldsymbol{M}_{\mathrm{R}} \in \mathbb{R}^{K \times K'}$ and $\boldsymbol{G}_{\mathrm{R}} \in \mathbb{R}^{K' \times K'}$ denote SM and EA matrices for the R-D link, respectively. Multiplying $\boldsymbol{M}_{\mathrm{S}}^{\mathrm{T}}$ and $\tilde{\boldsymbol{y}}_{\mathrm{R}}^{\mathrm{f}}$ extracts elements of K' data symbols included in $\tilde{\boldsymbol{y}}_{\mathrm{R}}^{\mathrm{f}}$. Then, the spectrum is shaped by the EA matrix $\boldsymbol{G}_{\mathrm{R}}$. The spectrum is mapped onto K' selected subchannels of the R-D link by the SM matrix $\boldsymbol{M}_{\mathrm{R}}$. The forwarded spectrum $\tilde{\boldsymbol{x}}_{\mathrm{R}}^{\mathrm{f}}$ is subject to a transmit energy constraint $\mathbb{E}\left\{\frac{1}{K}\sum_{k=1}^{K}\left|\tilde{x}_{\mathrm{R}}^{\mathrm{f}}(k)\right|^2\right\} = E_{\mathrm{s}}$. After the intermediate-processing, the R-node performs K point IDFT followed by CP insertion to $\tilde{\boldsymbol{x}}_{\mathrm{R}}^{\mathrm{f}}$ and forwards it to the D-node.

When the signal is received at R-node, carrying out CP removal and K point DFT at the D-node, we have

$$\tilde{\boldsymbol{y}}_{\mathrm{D}}^{\mathrm{f}} = \left[\tilde{y}_{\mathrm{D}}^{\mathrm{f}}(1), ..., \tilde{y}_{\mathrm{D}}^{\mathrm{f}}(k), ..., \tilde{y}_{\mathrm{D}}^{\mathrm{f}}(K)\right]^{\mathrm{T}} = \boldsymbol{\Xi}_{\mathrm{DR}} \tilde{\boldsymbol{x}}_{\mathrm{R}}^{\mathrm{f}} + \tilde{\boldsymbol{\eta}}_{\mathrm{D}}^{\mathrm{f}}. \tag{4.5}$$

In (4.5), $\boldsymbol{\Xi}_{\mathrm{DR}} = \mathrm{diag}\left[\xi_{\mathrm{DR}}(1), ..., \xi_{\mathrm{DR}}(k), ..., \xi_{\mathrm{DR}}(K)\right] \in \mathbb{C}^{K \times K}$ denotes frequency-domain channel matrix of the R-D link, where $\xi_{\mathrm{DR}}(k)$ indicates complex-valued CFR of the R-D link over the k-th subchannel. Furthermore, $\tilde{\boldsymbol{\eta}}_{\mathrm{D}}^{\mathrm{f}} = \left[\tilde{\eta}_{\mathrm{D}}^{\mathrm{f}}(1), ..., \tilde{\eta}_{\mathrm{D}}^{\mathrm{f}}(k), ..., \tilde{\eta}_{\mathrm{D}}^{\mathrm{f}}(K)\right]^{\mathrm{T}}$, where $\tilde{\eta}_{\mathrm{D}}^{\mathrm{f}}(k) \sim \mathcal{CN}(0, N_{\mathrm{D}})$ is spectral component of noise induced at the D-node over the k-th subchannel. After that, at the post-processing, $\tilde{\boldsymbol{y}}_{\mathrm{D}}^{\mathrm{f}}$ is multiplied by $\boldsymbol{M}_{\mathrm{R}}^{\mathrm{T}}$ to form the received data symbol block

$$\boldsymbol{y}_{\mathrm{D}}^{\mathrm{f}} = \left[y_{\mathrm{D}}^{\mathrm{f}}(1), ..., y_{\mathrm{D}}^{\mathrm{f}}(k'), ..., y_{\mathrm{D}}^{\mathrm{f}}(K')\right]^{\mathrm{T}} = \tilde{\boldsymbol{\Xi}}_{\mathrm{DR}} \boldsymbol{G}_{\mathrm{R}} \tilde{\boldsymbol{\Xi}}_{\mathrm{RS}} \boldsymbol{G}_{\mathrm{S}} \boldsymbol{x}_{\mathrm{S}}^{\mathrm{f}} + \tilde{\boldsymbol{\Xi}}_{\mathrm{DR}} \boldsymbol{G}_{\mathrm{R}} \boldsymbol{\eta}_{\mathrm{R}}^{\mathrm{f}} + \boldsymbol{\eta}_{\mathrm{D}}^{\mathrm{f}}, \tag{4.6}$$

where $\tilde{\boldsymbol{\Xi}}_{\mathrm{RS}}$ and $\tilde{\boldsymbol{\Xi}}_{\mathrm{DR}}$ are frequency-domain channel matrix of effective channel for the S-R and R-D links after the applications of SM, which are given by

$$\tilde{\boldsymbol{\Xi}}_{\mathrm{RS}} = \boldsymbol{M}_{\mathrm{S}}^{\mathrm{T}} \boldsymbol{\Xi}_{\mathrm{RS}} \boldsymbol{M}_{\mathrm{S}}, \tag{4.7}$$

$$\tilde{\boldsymbol{\Xi}}_{\mathrm{DR}} = \boldsymbol{M}_{\mathrm{R}}^{\mathrm{T}} \boldsymbol{\Xi}_{\mathrm{DR}} \boldsymbol{M}_{\mathrm{R}}. \tag{4.8}$$

Furthermore, $\boldsymbol{\eta}_{\mathrm{R}}^{\mathrm{f}} = \boldsymbol{M}_{\mathrm{S}}^{\mathrm{T}} \tilde{\boldsymbol{\eta}}_{\mathrm{R}}^{\mathrm{f}}$ and $\boldsymbol{\eta}_{\mathrm{D}}^{\mathrm{f}} = \boldsymbol{M}_{\mathrm{R}}^{\mathrm{T}} \tilde{\boldsymbol{\eta}}_{\mathrm{D}}^{\mathrm{f}}$.

4.2.2 Problem Statement

In this chapter, we assume a CSI availability described in Figure 4.2. As shown in the figure, the S-node captures only the knowledge on $\boldsymbol{\Xi}_{\mathrm{RS}}$ while the R-node captures the knowledge on

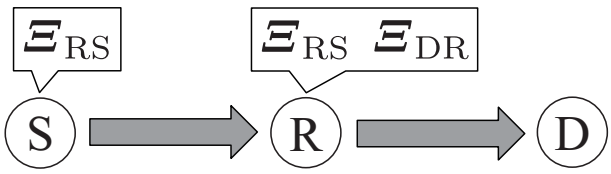

Figure 4.2: Assumption of availability of CSI in the considered two-hop broadband relaying.

both $\boldsymbol{\Xi}_{\mathrm{RS}}$ and $\boldsymbol{\Xi}_{\mathrm{DR}}$. This assumption is reasonable for time division duplex (TDD) systems since in TDD, channel reciprocity holds, i.e., CFR of a link is the same in both forward and reverse directions [57]. We also assume that the D-node does not capture the knowledge on $\boldsymbol{\Xi}_{\mathrm{DR}}$ but only the composite CFR $\tilde{\boldsymbol{\Xi}}_{\mathrm{DR}}\,\boldsymbol{G}_{\mathrm{R}}\,\tilde{\boldsymbol{\Xi}}_{\mathrm{RS}}\,\boldsymbol{G}_{\mathrm{S}}$ in (4.6) which is needed in data detection at the D-node. The acquisition for the composite CFR is as follows. Using matrices $\boldsymbol{M}_{\mathrm{S}}$ and $\boldsymbol{G}_{\mathrm{S}}$, the S-node transmits a reference signal to the R-node. The R-node relays this reference signal to the D-node using $\boldsymbol{M}_{\mathrm{R}}$ and $\boldsymbol{G}_{\mathrm{R}}$. The D-node receives this reference signal and estimates the composite CFR $\boldsymbol{\Xi}_{\mathrm{DR}}$.

The primary issue in this chapter is how to optimize the SM and EA matrices $\boldsymbol{M}_{\mathrm{S}}$, $\boldsymbol{M}_{\mathrm{R}}$, $\boldsymbol{G}_{\mathrm{S}}$ and $\boldsymbol{G}_{\mathrm{R}}$ to maximize the spectral efficiency for the relay system under the CSI availability mentioned above.

4.3 Subchannel Pairing Based Spectrum Mapping

As mentioned in Section 2.7.4, to enhance the end-to-end spectral efficiency for the AF relay, the number of spectral components which experience deep fading throughout the relay transmission should be reduced. To this end, Ref. [41] proposed subchannel pairing (SP) based SM which changes the order of spectral components at the R-node so that every spectral component is transmitted over two subchannels having identical channel gain ranking in the S-R and R-D links. In the SP based SM, spectral components which are transmitted over high gain subchannels in the S-R link are also relayed over those having high channel gain of the R-D links. This results in an improved SNR and the spectral efficiency enhancement comes as a result.

4.3.1 Pre-Processing

Among K subchannels of the S-R link, SM selects K' subchannels having the highest channel gain and maps the K' spectral components onto them *, where K' is determined by the value of BAR. Spectral-null are mapped onto the $(K - K')$ deactivated subchannels. In this stage, our target is to maximize the end-to-end spectral efficiency not by using the whole assigned band but by dynamically activating a number of subchannels in the assigned band. In this case, even if a part of the assigned band is not used by the user, it is still kept null (not reassigned to the other users), because K subchannel band is already assigned to the user, and null subchannel is created because it gives higher throughput than that in the case when all assigned bandwidth is used under the constraint that the assigned power is kept constant.

Let $\psi_{\mathrm{RS}}(k)$ be the channel gain ranking function for the S-R link, indexes of the activated subchannels of the S-R link are determined as $\psi_{\mathrm{RS}}^{-1}(1)$, $\psi_{\mathrm{RS}}^{-1}(2)$, ..., $\psi_{\mathrm{RS}}^{-1}(K')$. For ease of mathematical notations, let $\boldsymbol{o}_{\mathrm{S}} = [o_{\mathrm{S}}(1), ..., o_{\mathrm{S}}(k') ..., o_{\mathrm{S}}(K')]^{\mathrm{T}}$ be the ascending order vector for $\psi_{\mathrm{RS}}^{-1}(1)$, ..., $\psi_{\mathrm{RS}}^{-1}(k')$, ..., $\psi_{\mathrm{RS}}^{-1}(K')$. Then, the SM matrix $\boldsymbol{M}_{\mathrm{S}}$ is defined as follows: the elements at the $o_{\mathrm{S}}(k')$-row and the k'-th column are ones, the others are zeros. Consequently, $\boldsymbol{M}_{\mathrm{S}}^{\mathrm{T}} \boldsymbol{M}_{\mathrm{S}} = \boldsymbol{I}_{K'}$.

On the other hand, the EA matrix is denoted by $\boldsymbol{G}_{\mathrm{S}} = \mathrm{diag}[g_{\mathrm{S}}(1), ..., g_{\mathrm{S}}(k'), ..., g_{\mathrm{S}}(K')]$, where $g_{\mathrm{S}}(k')$ is the gain for the $o_{\mathrm{S}}(k')$-th subchannel. The gain is appropriately defined to maximize the end-to-end spectral efficiency. The optimization of $\boldsymbol{G}_{\mathrm{S}}$ will be discussed later.

4.3.2 Intermediate-Processing

In order to enhance the spectral efficiency, the R-node conducts an SM with SP so that subchannels of the S-R link and the R-D link are coupled according to their channel gain [41]. When $\psi_{\mathrm{DR}}(k)$ is the channel gain ranking function for the R-D link, the k-th subchannel of the S-R link is coupled with the $\psi_{\mathrm{DR}}^{-1}(\psi_{\mathrm{RS}}(k))$-th subchannel of the R-D link. Equivalently, the $o_{\mathrm{S}}(k')$-th element of $\tilde{\boldsymbol{y}}_{\mathrm{R}}^{\mathrm{f}}$ is mapped onto the $\psi_{\mathrm{DR}}^{-1}(\psi_{\mathrm{RS}}(o_{\mathrm{S}}(k')))$-th element of $\tilde{\boldsymbol{x}}_{\mathrm{R}}^{\mathrm{f}}$. Thus, the SM matrix $\boldsymbol{M}_{\mathrm{R}}$ is defined by the following rules: the elements at the $\psi_{\mathrm{DR}}^{-1}(\psi_{\mathrm{RS}}(o_{\mathrm{S}}(k')))$-th row and the k'-th column are ones, the others are zeros.

Figure 4.3 illustrates an example of SM with SP for $K = 4$ and $K' = 3$. The numbers in the circles indicate values of the channel gain ranking functions $\psi_{\mathrm{RS}}(k)$ and $\psi_{\mathrm{DR}}(k)$. As shown in the figure, indexes of $K' = 3$ subchannels with the highest channel gain of the S-R link are $\psi_{\mathrm{RS}}^{-1}(1) = 2$, $\psi_{\mathrm{RS}}^{-1}(2) = 4$, and $\psi_{\mathrm{RS}}^{-1}(3) = 1$. Thus the ascending order vector $\boldsymbol{o}_{\mathrm{S}} = [1, 2, 4]^{\mathrm{T}}$.

*Although according to [41], only the R-node employs SM with SP while the S-node does not employ any SM scheme, in Section 4.3, we assume that the S-node adopts SM with BAR control based on spectrum nulling and the R-node adopts SM with SP for ease of mathematical notations.

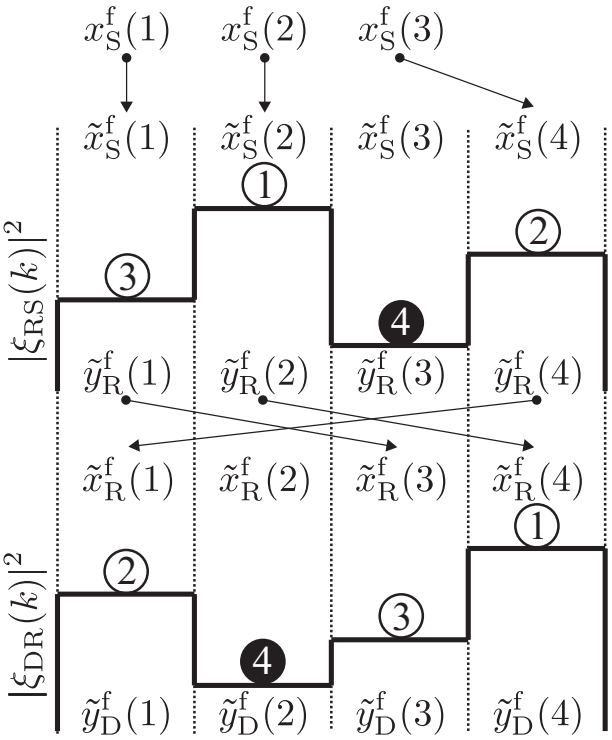

Figure 4.3: An example of SM with SP for $K = 4$ and $K' = 3$.

As a result, SM at the S-node assigns $x_{\mathrm{S}}^{\mathrm{f}}(1)$, $x_{\mathrm{S}}^{\mathrm{f}}(2)$, $x_{\mathrm{S}}^{\mathrm{f}}(3)$ to $\tilde{x}_{\mathrm{S}}^{\mathrm{f}}(1)$, $\tilde{x}_{\mathrm{S}}^{\mathrm{f}}(2)$, $\tilde{x}_{\mathrm{S}}^{\mathrm{f}}(4)$, respectively. After that, SP at the R-node makes pairs of subchannels having the identical values of channel gain ranking to each others. For instance, $\tilde{y}_{\mathrm{R}}^{\mathrm{f}}(1)$, which is transmitted over $\xi_{\mathrm{RS}}(1)$ with channel gain ranking $\psi_{\mathrm{RS}}(1) = 3$, is assigned to $\tilde{x}_{\mathrm{R}}^{\mathrm{f}}(3)$, which is transmitted over $\xi_{\mathrm{DR}}(3)$ with identical channel gain ranking $\psi_{\mathrm{DR}}(3) = \psi_{\mathrm{RS}}(1) = 3$. In this example, SM matrices are expressed as

$$\boldsymbol{M}_{\mathrm{S}} = \begin{bmatrix} 1 & 0 & 0 \\ 0 & 1 & 0 \\ 0 & 0 & 0 \\ 0 & 0 & 1 \end{bmatrix}, \quad \boldsymbol{M}_{\mathrm{R}} = \begin{bmatrix} 0 & 0 & 1 \\ 0 & 0 & 0 \\ 1 & 0 & 0 \\ 0 & 1 & 0 \end{bmatrix}. \tag{4.9}$$

Note that the third subchannel of the S-R link and the second subchannel of the R-D link are deactivated in this example.

On the other hand, the EA matrix is denoted by $\boldsymbol{G}_{\mathrm{R}} = \mathrm{diag}\left[g_{\mathrm{R}}(1), ..., g_{\mathrm{R}}(k'), ..., g_{\mathrm{R}}(K')\right]$, where $g_{\mathrm{R}}(k')$ is the gain for the $o_{\mathrm{R}}(k')$-th subchannel. The gain is appropriately defined to maximize the end-to-end spectral efficiency. The optimization of $\boldsymbol{G}_{\mathrm{R}}$ will be discussed later.

4.3.3 Post-Processing

At the post-processing, $\tilde{\boldsymbol{y}}_{\mathrm{D}}^{\mathrm{f}}$ is multiplied by $\boldsymbol{M}_{\mathrm{R}}^{\mathrm{T}}$ to form the received data symbol block $\boldsymbol{y}_{\mathrm{D}}^{\mathrm{f}}$ given by (4.6). In (4.6)

$$\tilde{\boldsymbol{\Xi}}_{\mathrm{RS}} = \mathrm{diag}\left[\tilde{\xi}_{\mathrm{RS}}(1), ..., \tilde{\xi}_{\mathrm{RS}}(k'), ..., \tilde{\xi}_{\mathrm{RS}}(K')\right], \tag{4.10}$$

$$\tilde{\boldsymbol{\Xi}}_{\mathrm{DR}} = \mathrm{diag}\left[\tilde{\xi}_{\mathrm{DR}}(1), ..., \tilde{\xi}_{\mathrm{DR}}(k'), ..., \tilde{\xi}_{\mathrm{DR}}(K')\right], \tag{4.11}$$

$$\boldsymbol{\eta}_{\mathrm{R}}^{\mathrm{f}} = \left[\eta_{\mathrm{R}}^{\mathrm{f}}(1), ..., \eta_{\mathrm{R}}^{\mathrm{f}}(k'), ..., \eta_{\mathrm{R}}^{\mathrm{f}}(K')\right]^{\mathrm{T}}, \tag{4.12}$$

$$\boldsymbol{\eta}_{\mathrm{D}}^{\mathrm{f}} = \left[\eta_{\mathrm{D}}^{\mathrm{f}}(1), ..., \eta_{\mathrm{D}}^{\mathrm{f}}(k'), ..., \eta_{\mathrm{D}}^{\mathrm{f}}(K')\right]^{\mathrm{T}}, \tag{4.13}$$

where

$$\tilde{\xi}_{\mathrm{RS}}(k') = \xi_{\mathrm{RS}}(o_{\mathrm{S}}(k')), \tag{4.14}$$

$$\tilde{\xi}_{\mathrm{DR}}(k') = \xi_{\mathrm{DR}}\left(\psi_{\mathrm{DR}}^{-1}(\psi_{\mathrm{RS}}(o_{\mathrm{S}}(k')))\right), \tag{4.15}$$

$$\eta_{\mathrm{R}}^{\mathrm{f}}(k') = \tilde{\eta}_{\mathrm{R}}^{\mathrm{f}}(o_{\mathrm{S}}(k')), \tag{4.16}$$

$$\eta_{\mathrm{D}}^{\mathrm{f}}(k') = \tilde{\eta}_{\mathrm{D}}^{\mathrm{f}}\left(\psi_{\mathrm{DR}}^{-1}(\psi_{\mathrm{RS}}(o_{\mathrm{S}}(k')))\right). \tag{4.17}$$

Therefore, (4.6) is rewritten in a scalar form as

$$y_{\mathrm{D}}^{\mathrm{f}}(k') = \tilde{\xi}(k')\, s(k') + \eta(k'), \tag{4.18}$$

where, we have

$$\tilde{\xi}(k') = \tilde{\xi}_{\mathrm{DR}}(k')\, g_{\mathrm{R}}(k')\, \tilde{\xi}_{\mathrm{RS}}(k')\, g_{\mathrm{S}}(k'), \tag{4.19}$$

$$\eta(k') = \tilde{\xi}_{\mathrm{DR}}(k')\, g_{\mathrm{R}}(k')\, \eta_{\mathrm{R}}(k') + \eta_{\mathrm{D}}(k'). \tag{4.20}$$

Recall that $\tilde{\eta}_{\mathrm{R}}(k')$ and $\tilde{\eta}_{\mathrm{D}}(k')$ are zero-mean Gaussian variables with variances N_{R} and N_{D}, respectively. Thus, $\eta_{\mathrm{R}}(k')$ and $\eta_{\mathrm{D}}(k')$ are also zero-mean Gaussian variables with variances N_{R} and N_{D}, respectively. As a result, for the given values of instantaneous channel state $\tilde{\xi}_{\mathrm{DR}}(k')$ and $g_{\mathrm{R}}(k')$, $\eta(k')$ is a zero-mean Gaussian variable with variance given by

$$N_{\eta}(k') = g_{\mathrm{R}}^2(k') \left|\tilde{\xi}_{\mathrm{DR}}(k')\right|^2 g_{\mathrm{S}}^2(k')\, N_{\mathrm{R}} + N_{\mathrm{D}}. \tag{4.21}$$

From (4.2) and (4.4), energy allocated by the S-node and the R-node to the data symbol $s(k')$ are expressed as

$$\omega_{\mathrm{S}}(k') = g_{\mathrm{S}}^2(k')\, E_{\mathrm{s}}, \tag{4.22}$$

$$\omega_{\mathrm{R}}(k') = g_{\mathrm{R}}^2(k') \left[\left|\tilde{\xi}_{\mathrm{RS}}(k')\right|^2 g_{\mathrm{S}}^2(k')\, E_{\mathrm{s}} + N_{\mathrm{R}}\right]. \tag{4.23}$$

Note that, $\omega_{\mathrm{S}}(k')$ and $\omega_{\mathrm{R}}(k')$ are subject to transmit power constraints, which are given by

$$\sum_{k'=1}^{K'} \omega_{\mathrm{S}}(k') = KE_{\mathrm{s}}, \quad \sum_{k'=1}^{K'} \omega_{\mathrm{R}}(k') = KE_{\mathrm{s}}. \tag{4.24}$$

From (4.18), (4.19), (4.21), (4.22), and (4.23), the received SNR for the data symbol $s(k')$ is defined by

$$\gamma_{\mathrm{r}}(k') = \frac{\alpha(k')\,\omega_{\mathrm{S}}(k') \cdot \beta(k')\,\omega_{\mathrm{R}}(k')}{1 + \alpha(k')\,\omega_{\mathrm{S}}(k') + \beta(k')\,\omega_{\mathrm{R}}(k')}, \tag{4.25}$$

where $\alpha(k') = \left|\tilde{\xi}_{\mathrm{RS}}(k')\right|^2 / N_{\mathrm{R}}$, $\beta(k') = \left|\tilde{\xi}_{\mathrm{DR}}(k')\right|^2 / N_{\mathrm{D}}$.

4.4 Optimizations of Energy Allocation

In this section, joint optimization and cascaded optimization for EA matrices $\boldsymbol{G}_{\mathrm{S}}$ and $\boldsymbol{G}_{\mathrm{R}}$ are examined to enhance the end-to-end spectral efficiency. This joint optimization is conducted on the assumption that every transmitter knows CSI for both S-R and R-D links and the transmit power spectrum is controlled jointly, whereas cascaded optimization is conducted on the assumption that the transmit power spectrum for S-node and R-node are independently controlled.

4.4.1 Joint Energy Allocation

From (4.25), the CCMC capacity of (4.18) is given by

$$C_{\mathrm{DRS}}^{\mathrm{AF}} = \frac{1}{2K} \sum_{k'=1}^{K'} \log_2 \left[1 + \frac{\alpha(k')\,\omega_{\mathrm{S}}(k') \cdot \beta(k')\,\omega_{\mathrm{R}}(k')}{1 + \alpha(k')\,\omega_{\mathrm{S}}(k') + \beta(k')\,\omega_{\mathrm{R}}(k')} \right]. \tag{4.26}$$

Note that the coefficient 1/2 indicates that two time slots are occupied by the relaying transmission. The CCMC capacity is maximized by joint optimization of the EA matrices $\boldsymbol{G}_{\mathrm{S}}$ and $\boldsymbol{G}_{\mathrm{R}}$. The maximization of $C_{\mathrm{DRS}}^{\mathrm{AF}}$ in (4.26) is equivalent to the minimization of $-2KC_{\mathrm{DRS}}^{\mathrm{AF}}$. To begin the joint optimization by convex optimization, let us verify the convexity of the objective function, which defined by

$$f_0^*(\boldsymbol{\omega}) = -2KC_{\mathrm{DRS}}^{\mathrm{AF}} = -\sum_{k'=1}^{K'} \log_2 \left[1 + \frac{\alpha(k')\,\omega_{\mathrm{S}}(k') \cdot \beta(k')\,\omega_{\mathrm{R}}(k')}{1 + \alpha(k')\,\omega_{\mathrm{S}}(k') + \beta(k')\,\omega_{\mathrm{R}}(k')} \right], \tag{4.27}$$

where $\boldsymbol{\omega}$ is the joint vector of vector $\boldsymbol{\omega}_{\mathrm{S}} = [\omega_{\mathrm{S}}(1), ..., \omega_{\mathrm{S}}(k'), ..., \omega_{\mathrm{S}}(K')]^{\mathrm{T}}$ and vector $\boldsymbol{\omega}_{\mathrm{R}} = [\omega_{\mathrm{R}}(1), ..., \omega_{\mathrm{R}}(k'), ..., \omega_{\mathrm{R}}(K')]^{\mathrm{T}}$. Vector $\boldsymbol{\omega}$ is expressed by

$$\begin{aligned} \boldsymbol{\omega} &= [\omega(1), ..., \omega(K'), \omega(K'+1), ..., \omega(2K')]^{\mathrm{T}} \\ &= [\omega_{\mathrm{S}}(1), ..., \omega_{\mathrm{S}}(K'), \omega_{\mathrm{R}}(1), ..., \omega_{\mathrm{R}}(K')]^{\mathrm{T}} \qquad (\in \mathbb{R}^{2K' \times 1}). \end{aligned} \tag{4.28}$$

The convexity of a function is verified by its Hessian matrix. The Hessian matrix of function $f_0^*(\boldsymbol{\omega})$ is given by

$$\nabla^2 f_0^*(\boldsymbol{\omega}) = \frac{1}{\log 2} \begin{bmatrix} \theta(1) & \cdots & 0 & \phi(1) & \cdots & 0 \\ \vdots & \ddots & \vdots & \vdots & \ddots & \vdots \\ 0 & \cdots & \theta(K') & 0 & \cdots & \phi(K') \\ \phi(1) & \cdots & 0 & \vartheta(1) & \cdots & 0 \\ \vdots & \ddots & \vdots & \vdots & \ddots & \vdots \\ 0 & \cdots & \phi(K') & 0 & \cdots & \vartheta(K') \end{bmatrix}, \tag{4.29}$$

where

$$\theta(k') = \left[\frac{\alpha(k')}{1+\alpha(k')\omega_{\mathrm{S}}(k')+\beta(k')\omega_{\mathrm{R}}(k')}\right]^2 + \left[\frac{\alpha(k')}{1+\alpha(k')\omega_{\mathrm{S}}(k')}\right]^2, \tag{4.30}$$

$$\vartheta(k') = \left[\frac{\beta(k')}{1+\alpha(k')\omega_{\mathrm{S}}(k')+\beta(k')\omega_{\mathrm{R}}(k')}\right]^2 + \left[\frac{\beta(k')}{1+\beta(k')\omega_{\mathrm{R}}(k')}\right]^2, \tag{4.31}$$

$$\phi(k') = -\frac{\alpha(k')\beta(k')}{\left[1+\alpha(k')\omega_{\mathrm{S}}(k')+\beta(k')\omega_{\mathrm{R}}(k')\right]^2}. \tag{4.32}$$

It is obvious that $\phi(k') < 0$. In such a case, since the condition $\nabla^2 f_0^*(\boldsymbol{\omega}) \succeq \mathbf{0}$ is not satisfied, the function $f_0^*(\boldsymbol{\omega})$ is not convex. Hence, in principle, the global optimization is analytically intractable.

To relax the convexity condition, the following approximation is applied to (4.26) [39] as

$$C_{\mathrm{DRS}}^{\mathrm{AF}} \approx \frac{1}{2K}\sum_{k'=1}^{K'} \log_2\left[1+\frac{\alpha(k')\omega_{\mathrm{S}}(k')\cdot\beta(k')\omega_{\mathrm{R}}(k')}{\alpha(k')\omega_{\mathrm{S}}(k')+\beta(k')\omega_{\mathrm{R}}(k')}\right]. \tag{4.33}$$

In this case, we can obtain an objective function given by

$$f_0(\boldsymbol{\omega}) = -\sum_{k'=1}^{K'} \log_2\left[1+\frac{\alpha(k')\omega_{\mathrm{S}}(k')\cdot\beta(k')\omega_{\mathrm{R}}(k')}{\alpha(k')\omega_{\mathrm{S}}(k')+\beta(k')\omega_{\mathrm{R}}(k')}\right]. \tag{4.34}$$

The Hessian matrix of $f_0(\boldsymbol{\omega})$ also has the same structure as the matrix shown in (4.29) but with

different $\theta(k')$, $\vartheta(k')$ and $\phi(k')$ which are expressed by

$$\theta(k') = \frac{\alpha^2(k')\beta^2(k')\omega_S^2(k')\left[2\Theta(k') + \beta^2(k')\omega_R^2(k')\right]}{\Theta^2(k')\Gamma^2(k')}, \tag{4.35}$$

$$\vartheta(k') = \frac{\alpha^2(k')\beta^2(k')\omega_R^2(k')\left[2\Theta(k') + \alpha^2(k')\omega_S^2(k')\right]}{\Theta^2(k')\Gamma^2(k')}, \tag{4.36}$$

$$\phi(k') = \frac{\alpha(k')\beta(k')}{\Theta(k')} + \frac{\alpha^3(k')\beta^3(k')\omega_S^2(k')\omega_R^2(k')}{\Theta^2(k')\Gamma^2(k')}, \tag{4.37}$$

where

$$\Theta(k') = \alpha(k')\omega_S(k') + \beta(k')\omega_R(k') + \alpha(k')\omega_S(k')\beta(k')\omega_R(k'), \tag{4.38}$$

$$\Gamma(k') = \alpha(k')\omega_S(k') + \beta(k')\omega_R(k'). \tag{4.39}$$

From (4.35), (4.36) and (4.37) it follows that for all $k' \in \{1, 2, ..., K'\}$, $\theta(k') \geq 0$, $\vartheta(k') \geq 0$ and $\phi(k') \geq 0$. Thus, $\nabla^2 f_0(\boldsymbol{\omega}) \geq \mathbf{0}$ and $f_0(\boldsymbol{\omega})$ is jointly convex in $\omega_S(k')$ and $\omega_R(k')$.

Applying Karush-Kuhn-Tucker (KKT) conditions [24] to the optimization problem with the convex object function $f_0(\boldsymbol{\omega})$, we derive the solution to the optimization problem as [39]

$$\omega_S^{\mathrm{JEA}}(k') = \frac{\left[\alpha(k')\beta(k') - \left(\sqrt{\alpha(k')\nu_2} + \sqrt{\beta(k')\nu_1}\right)^2\right]^+}{\left(\sqrt{\alpha(k')\nu_2} + \sqrt{\beta(k')\nu_1}\right)\sqrt{\beta(k')\nu_1}\alpha(k')}, \tag{4.40}$$

$$\omega_R^{\mathrm{JEA}}(k') = \frac{\left[\alpha(k')\beta(k') - \left(\sqrt{\alpha(k')\nu_2} + \sqrt{\beta(k')\nu_1}\right)^2\right]^+}{\left(\sqrt{\alpha(k')\nu_2} + \sqrt{\beta(k')\nu_1}\right)\sqrt{\alpha(k')\nu_2}\beta(k')}, \tag{4.41}$$

where ν_1 and ν_2 are the Lagrange multipliers, and $[x]^+ = \max\{0, x\}$. Substituting (4.40) and (4.41) into (4.24), we obtain two equations related to ν_1 and ν_2. Since it is infeasible to analytically solve these simultaneous equations, the values of ν_1 and ν_2 are obtained by numerical analysis based on Newton-Raphson method [58] in this dissertation. Note here that the joint energy allocation (JEA) is near-global optimal in terms of CCMC capacity due to the high approximation shown in (4.33).

In order to carry out JEA, both the S-node and R-node need to determine the EA matrices $\boldsymbol{G}_S$ and $\boldsymbol{G}_R$ whose elements are given by (4.40) and (4.41), respectively. Because in the considered relay system, only the R-node is capable of capturing CSI of both the S-R and R-D links, and only the R-node is able to calculate the JEA matrices $\boldsymbol{G}_S$ and $\boldsymbol{G}_R$. Hence, the R-node needs to notify the matrix $\boldsymbol{G}_S$ to the S-node so that the S-node can carry out its EA. It is obvious that this notification is too heavy since the elements of the matrix $\boldsymbol{G}_S$ take continuous real values. Therefore, a cascaded energy allocation (CEA) scheme in which the S-node determines $\boldsymbol{G}_S$

using only knowledge on $\boldsymbol{\Xi}_{\mathrm{RS}}$, and the R-node calculates $\boldsymbol{G}_{\mathrm{R}}$ using knowledge on both $\boldsymbol{\Xi}_{\mathrm{RS}}$ and $\boldsymbol{\Xi}_{\mathrm{DR}}$ is more practical. This cascaded EA will be discussed in the next section.

4.4.2 Cascaded Energy Allocation

Recalling (4.26), it can be rewritten as

$$C_{\mathrm{DRS}}^{\mathrm{AF}} = C_1 + C_2, \tag{4.42}$$

where

$$C_1 = \frac{1}{2K}\sum_{k'=1}^{K'} \log_2\left[1+\alpha\left(k'\right)\omega_{\mathrm{S}}\left(k'\right)\right], \tag{4.43}$$

$$C_2 = \frac{1}{2K}\sum_{k'=1}^{K'} \log_2\left[\frac{1+\beta\left(k'\right)\omega_{\mathrm{R}}\left(k'\right)}{1+\alpha\left(k'\right)\omega_{\mathrm{S}}\left(k'\right)+\beta\left(k'\right)\omega_{\mathrm{R}}\left(k'\right)}\right]. \tag{4.44}$$

Thus, the S-node maximizes C_1 using only knowledge on $\boldsymbol{\Xi}_{\mathrm{RS}}$, as well as the R-node maximizes C_2 using knowledge on both $\boldsymbol{\Xi}_{\mathrm{RS}}$ and $\boldsymbol{\Xi}_{\mathrm{DR}}$.

To apply convex optimization to the two optimization problems, let us verify the convexity of C_1 and C_2. In this case, the two separate objective functions are

$$f_{0,\mathrm{S}}\left(\boldsymbol{\omega}_{\mathrm{S}}\right) = -\sum_{k'=1}^{K'} \log_2\left[1+\alpha\left(k'\right)\omega_{\mathrm{S}}\left(k'\right)\right], \tag{4.45}$$

$$f_{0,\mathrm{R}}\left(\boldsymbol{\omega}_{\mathrm{R}}\right) = -\sum_{k'=1}^{K'} \log_2\left[\frac{1+\beta\left(k'\right)\omega_{\mathrm{R}}\left(k'\right)}{1+\alpha\left(k'\right)\omega_{\mathrm{S}}\left(k'\right)+\beta\left(k'\right)\omega_{\mathrm{R}}\left(k'\right)}\right], \tag{4.46}$$

where $\boldsymbol{\omega}_{\mathrm{S}} = \left[\omega_{\mathrm{S}}\left(1\right),...,\omega_{\mathrm{S}}\left(k'\right),...,\omega_{\mathrm{S}}\left(K'\right)\right]^{\mathrm{T}}$ and $\boldsymbol{\omega}_{\mathrm{R}} = \left[\omega_{\mathrm{R}}\left(1\right),...,\omega_{\mathrm{R}}\left(k'\right),...,\omega_{\mathrm{R}}\left(K'\right)\right]^{\mathrm{T}}$. The Hessian matrices of the objective functions given in (4.45) and (4.46) are

$$\nabla^2 f_{0,\mathrm{S}}\left(\boldsymbol{\omega}_{\mathrm{S}}\right) = \frac{1}{\log 2}\mathrm{diag}\left[\theta_{\mathrm{S}}\left(1\right),...,\theta_{\mathrm{S}}\left(k'\right),...,\theta_{\mathrm{S}}\left(K'\right)\right], \tag{4.47}$$

$$\nabla^2 f_{0,\mathrm{R}}\left(\boldsymbol{\omega}_{\mathrm{R}}\right) = \frac{1}{\log 2}\mathrm{diag}\left[\theta_{\mathrm{R}}\left(1\right),...,\theta_{\mathrm{R}}\left(k'\right),...,\theta_{\mathrm{R}}\left(K'\right)\right], \tag{4.48}$$

where

$$\theta_{\mathrm{S}}\left(k'\right) = \left[\frac{\alpha\left(k'\right)}{1+\alpha\left(k'\right)\omega_{\mathrm{S}}\left(k'\right)}\right]^2, \tag{4.49}$$

$$\theta_{\mathrm{R}}\left(k'\right) = \left[\frac{\beta\left(k'\right)}{1+\beta\left(k'\right)\omega_{\mathrm{R}}\left(k'\right)}\right]^2 - \left[\frac{\beta\left(k'\right)}{1+\alpha\left(k'\right)\omega_{\mathrm{S}}\left(k'\right)+\beta\left(k'\right)\omega_{\mathrm{R}}\left(k'\right)}\right]^2. \tag{4.50}$$

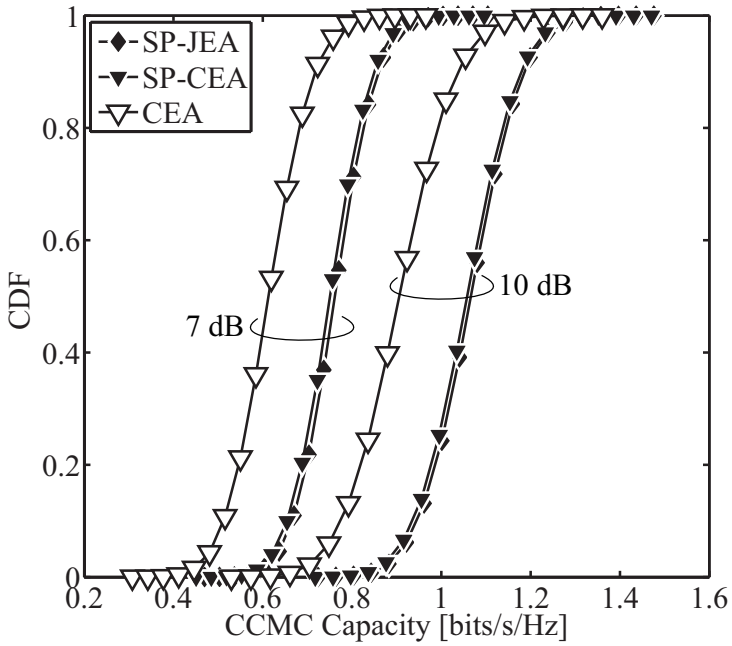

Figure 4.4: Effectiveness of SP-based SM in CCCM capacity enhancement of CEA.

Since $\theta_{\mathrm{S}}(k') > 0$ and $\theta_{\mathrm{R}}(k') > 0$ for all $k' \in \{1, 2, ..., K'\}$, $f_{0,\mathrm{S}}(\boldsymbol{\omega}_{\mathrm{S}})$ and $f_{0,\mathrm{R}}(\boldsymbol{\omega}_{\mathrm{R}})$ are convex in $\omega_{\mathrm{S}}(k')$ and $\omega_{\mathrm{R}}(k')$, respectively.

Using KKT conditions, we derive solutions to these separate optimization problems as

$$\omega_{\mathrm{S}}^{\mathrm{CEA}}(k') = \left[\frac{1}{\nu_1} - \frac{1}{\alpha(k')}\right]^{+}, \tag{4.51}$$

$$\omega_{\mathrm{R}}^{\mathrm{CEA}}(k') = \frac{1}{\beta(k')}\left[\frac{\alpha(k')\,\omega_{\mathrm{S}}(k')}{2}\left(\sqrt{1+\frac{4\beta(k')}{\nu_2\alpha(k')\,\omega_{\mathrm{S}}(k')}}-1\right)-1\right]^{+}. \tag{4.52}$$

Equation (4.51) indicates that the S-node calculates $\omega_{\mathrm{S}}(k')$ by applying water-filling theorem [6] according to knowledge on $\boldsymbol{\Xi}_{\mathrm{RS}}$. Meanwhile, (4.52) implies that the R-node is able to calculate $\omega_{\mathrm{R}}(k')$ by using knowledge on $\boldsymbol{\Xi}_{\mathrm{RS}}$ and $\boldsymbol{\Xi}_{\mathrm{DR}}$ together with $\omega_{\mathrm{S}}(k')$ calculated by (4.51).

4.5 Effectiveness of Subchannel Pairing

4.5.1 CCMC Capacity Performance

Figure 4.4 shows CDFs of the CCMC capacities for AF relay systems with three schemes: CEA, SP combined with CEA (SP-CEA), and SP combined with JEA (SP-JEA). In this evaluation, positions of the three nodes are fixed and the distance from the S-node to the R-node

is equal to that from the R-node to the D-node. The S-R and R-D links are assumed to be frequency selective fading channels with equal gain 16 path Rayleigh fading models. The number of subchannels of the assigned band is $K = 256$ points and all of them are activated for transmissions, i.e., $K' = 256$. The variances of noises induced at the R-node and the D-node are assumed to be $N_{\mathrm{R}} = N_{\mathrm{D}} = N_0$. Since at this stage, we focus on the impact of independent frequency-variances of the S-R and R-D links, path loss and shadowing are omitted to avoid divergence of discussions. This means the energy gain of the two links are normalized as $\Psi_{\mathrm{RS}} = \Psi_{\mathrm{DR}} = 1$. As a result, the transmit SNR for the two links are the same as SNR $= E_{\mathrm{s}}/N_0$. In this evaluation, transmit SNR is set to 10 dB.

Figure 4.4 confirms that SP significantly improves CCMC capacity performance of CEA. To be specific, when only CEA is employed and SP is not employed, 50% value of CCMC degrades by 19.8% compared to that of SP-JEA. Note that, from the information theoretic perspective, SP-JEA is near-global optimal to maximize CCMC capacity [59]. However, when CEA is combined with SP in SP-CEA, CCMC capacity is very tight to that of SP-JEA.

4.5.2 Issues of Notification and Discrete Modulation

It is verified in Sections 4.5.1 that SP-CEA almost achieves the same CCMC capacity performance with the near-global optimal SP-JEA. However, in practical systems, this method have two drawbacks:

1. Overhead caused by notification of SM and EA matrices for SP-CEA is too large.
2. In broadband systems with discrete modulation scheme, DCMC capacity should be considered rather than CCMC capacity.

Thus, the rest of this chapter proposes a novel technique to solve these drawbacks.

Issue of Notification

Figure 4.5 specifies the required notification under the assumption given in Section 4.2.2. The figures 4.5(a) and 4.5(b) imply that when SP-CEA rather than SP-JEA is employed, the notification of continuous values of $\boldsymbol{G}_{\mathrm{S}}$ is exempted as mentioned in Section 4.4.2. Hence, the required notification in SP-CEA is only $\boldsymbol{M}_{\mathrm{R}}$ to the D-node. However, note that to carry out the post-processing, the D-node needs knowledge on positions of ones in the $\psi_{\mathrm{DR}}^{-1}(1)$-th, ..., $\psi_{\mathrm{DR}}^{-1}(k')$-th, ..., $\psi_{\mathrm{DR}}^{-1}(K')$-th rows of the SM matrix $\boldsymbol{M}_{\mathrm{R}}$ as shown in (4.9), which requires a $K \log_2 K$ bit notification from the R-node to the D-node.

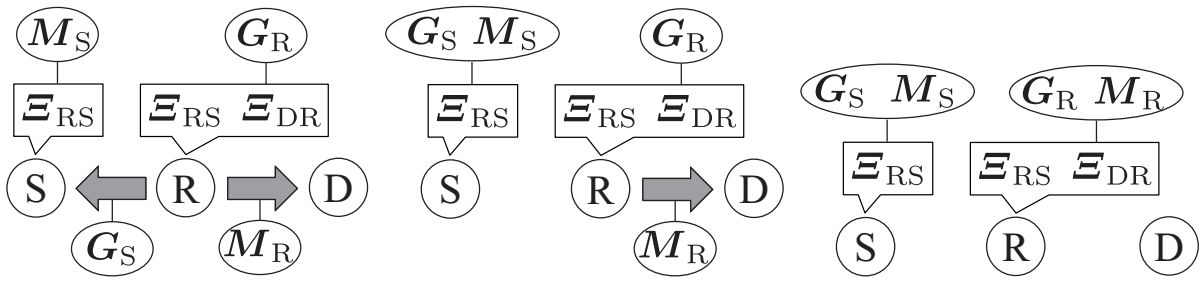

(a) SP-JEA (b) SP-CEA (c) ABC-CEA

Figure 4.5: Notification of SM and EA matrices for relay schemes

A main challenge of the following sections is to reduce the amount of such notification while maintaining almost the same performance with that of SP-CEA or SP-JEA strategies. A simple approach to the challenge is an adaptive BAR control (ABC) accompanied with CEA (ABC-CEA). In ABC-CEA, as depicted in Figure 4.5(c), the $K \log_2 K$ bit notification is not required since SP is not applied. In such a case, spectral components transmitted over high gain subchannels of the S-R link may be relayed over low gain subchannels of the R-D link, and vice versa. Because the composite channel gain of the relay system is given by the multiplication of channel gains of all the links, spectral components transmitted over low gain subchannels in a link would be received with low energy at the D-node. Therefore, the proposed ABC-CEA may suffer from a capacity loss compared to SP-CEA. To reduce the loss, BAR is adaptively controlled according to SNR of the two links, or according to both SNR and CSI $\boldsymbol{\Xi}_{RS}$ and $\boldsymbol{\Xi}_{DR}$. When BAR is sufficiently reduced, spectral components will be transmitted over higher gain subchannels in both the S-R and R-D links. This phenomenon reduces the number of spectral components transmitted over low composite channel gain. Thus, we can expect that ABC-CEA achieves almost the same spectral efficiency with SP-CEA. More importantly, we can expect a significant reduction in notification overhead when ABC is employed instead of SP. According to conditions for application of BAR control in Section 2.5.2, when BAR is applied, only the status of selected/non-selected of each subchannels of the S-R and R-D links needs to be passed from the R-node to the S-node and D-node, respectively. Fortunately, because the S-node captures CSI of the S-R link and the D-node captures CSI of the R-D link, only the number of selected subchannels in each link needs to be notified. As a result, the ABC-CEA based on both SNR and CSI requires only a $\log_2 K$ bit notification while the SNR based ABC-CEA causes a negligibly small notification overhead.

Issue of discrete modulation

In order to realize CCMC capacity, the modulation symbols $s(k')$ must be drawn from a continuous input set, whose elements obey a Gaussian process [6]. However, since such an ideal modulation scheme is not applicable due to complexity of the demodulation, practical systems employ discrete modulation schemes instead. It is also reported in [60] that DCMC capacity is obtained by EA on the basis of mercury/water-filling principle. Thus, DCMC instead of CCMC is used in the following sections to validate the considered schemes.

4.6 Spectrum Nulling Based Adaptive BAR Control

4.6.1 Spectrum Mapping with Spectrum Nulling

In SM with ABC, the SM matrix at the S-node $\boldsymbol{M}_{\mathrm{S}}$ is identical to that in Section 4.3.1, but the SM matrix at the R-node $\boldsymbol{M}_{\mathrm{R}}$ is different from that in Section 4.3.2. Let the ascending order vector for $\psi_{\mathrm{DR}}^{-1}(1)$, ..., $\psi_{\mathrm{DR}}^{-1}(k')$, ..., $\psi_{\mathrm{DR}}^{-1}(K')$ be $\boldsymbol{o}_{\mathrm{R}} = [o_{\mathrm{R}}(1), ..., o_{\mathrm{R}}(k'), ..., o_{\mathrm{R}}(K')]^{\mathrm{T}}$. Recall that $\psi_{\mathrm{DR}}(k)$ is the channel gain ranking function for the R-D link. The SM matrix at the R-node $\boldsymbol{M}_{\mathrm{R}}$ is defined as follows: the elements at the $o_{\mathrm{R}}(k')$-th row and the k'-th column are ones, the others are zeros. As a consequence, in SM with ABC, $\tilde{\xi}_{\mathrm{DR}}(k') = \xi_{\mathrm{DR}}(o_{\mathrm{R}}(k'))$.

Figure 4.6 illustrates an example of SM with ABC for $K' = 3$ and $K = 4$. In this example, indexes of $K' = 3$ subchannels with the highest channel gain of the S-R link are $\psi_{\mathrm{RS}}^{-1}(1) = 2$, $\psi_{\mathrm{RS}}^{-1}(2) = 4$, and $\psi_{\mathrm{RS}}^{-1}(3) = 1$. Thus, $\boldsymbol{o}_{\mathrm{S}} = [1, 2, 4]^{\mathrm{T}}$. Similarly, $\boldsymbol{o}_{\mathrm{R}} = [1, 3, 4]^{\mathrm{T}}$. As shown in the figure, SM at the S-node assigns $x_{\mathrm{S}}^{\mathrm{f}}(1)$, $x_{\mathrm{S}}^{\mathrm{f}}(2)$, $x_{\mathrm{S}}^{\mathrm{f}}(3)$ to $\tilde{x}_{\mathrm{S}}^{\mathrm{f}}(1)$, $\tilde{x}_{\mathrm{S}}^{\mathrm{f}}(2)$, $\tilde{x}_{\mathrm{S}}^{\mathrm{f}}(4)$, respectively. After that, SM at the R-node assigns $\tilde{y}_{\mathrm{R}}^{\mathrm{f}}(1)$, $\tilde{y}_{\mathrm{R}}^{\mathrm{f}}(2)$, $\tilde{y}_{\mathrm{R}}^{\mathrm{f}}(4)$ to $\tilde{x}_{\mathrm{R}}^{\mathrm{f}}(1)$, $\tilde{x}_{\mathrm{R}}^{\mathrm{f}}(3)$, $\tilde{x}_{\mathrm{R}}^{\mathrm{f}}(4)$, respectively. Therefore, SM matrices are expressed as

$$\boldsymbol{M}_{\mathrm{S}} = \begin{bmatrix} 1 & 0 & 0 \\ 0 & 1 & 0 \\ 0 & 0 & 0 \\ 0 & 0 & 1 \end{bmatrix}, \quad \boldsymbol{M}_{\mathrm{R}} = \begin{bmatrix} 1 & 0 & 0 \\ 0 & 0 & 0 \\ 0 & 1 & 0 \\ 0 & 0 & 1 \end{bmatrix}. \tag{4.53}$$

Note that the third subchannel of the S-R link and the second subchannel of the R-D link are deactivated, and the order of $s(1)$, $s(2)$ and $s(3)$ is maintained through the S-R and R-D links.

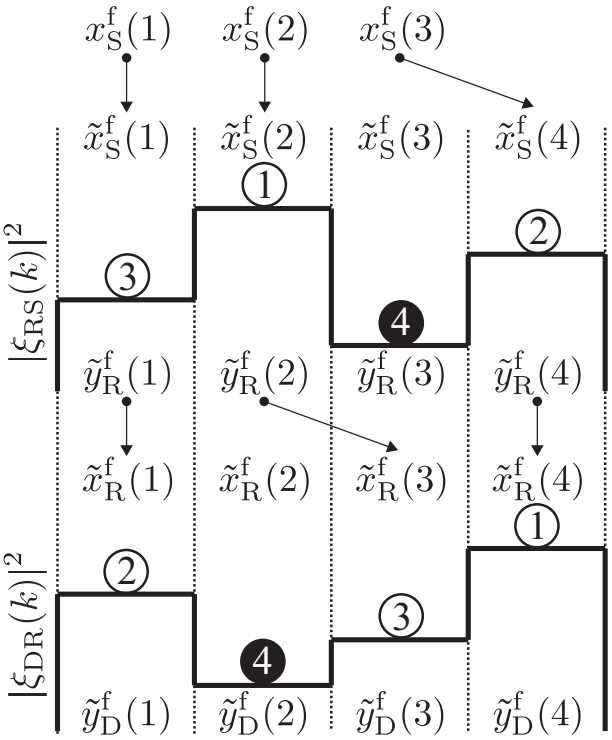

Figure 4.6: An example of SM with ABC for $K = 4$ and $K' = 3$.

4.6.2 Necessity of BAR Control

We investigate CCMC capacity and DCMC capacity achieved by three schemes: SP-JEA, SP-CEA and ABC-CEA for various values of BAR = K'/K. In this evaluation, positions of the three nodes are fixed and the distance from the S-node to the R-node is equal to that from the R-node to the D-node. The S-R and R-D links are assumed to be frequency selective fading channels with 16 path equal gain Rayleigh fading models. The number of subchannels of the assigned band is $K = 256$ points and the number of activated subchannels K' is varied so that BAR takes values from 0 to 1. The variances of AWGNs induced at the R-node and the D-node are assumed to be $N_{\mathrm{R}} = N_{\mathrm{D}} = N_0$. The impact of path loss and shadowing are omitted to avoid divergence of discussions. As a result, the transmit SNR for the two links are the same as transmit SNR = E_{s}/N_0. In this analysis, transmit SNR is set to 7 dB or 10 dB.

Assuming all data symbols $s(k')$'s are drawn from one constellation set $\mathcal{S}$ containing Q constellation points $\left\{\mathcal{S}_1, ..., \mathcal{S}_q, ..., \mathcal{S}_Q\right\}$, applying (2.89) in Section 2.4.3, we calculate DCMC capacity for the relay system by

$$D_{\mathcal{S}} = \frac{K'}{2K}\log_2 Q - \frac{1}{2KQ}\sum_{k'=1}^{K'}\sum_{q=1}^{Q}\int_{-\infty}^{\infty} p\left(y_{\mathrm{D}}^{\mathrm{f}}(k')\,|\mathcal{S}_q\right)\log_2\left[\sum_{j=1}^{Q}\frac{p\left(y_{\mathrm{D}}^{\mathrm{f}}(k')\,|\mathcal{S}_j\right)}{p\left(y_{\mathrm{D}}^{\mathrm{f}}(k')\,|\mathcal{S}_q\right)}\right] dy_{\mathrm{D}}^{\mathrm{f}}(k')\,. \quad (4.54)$$

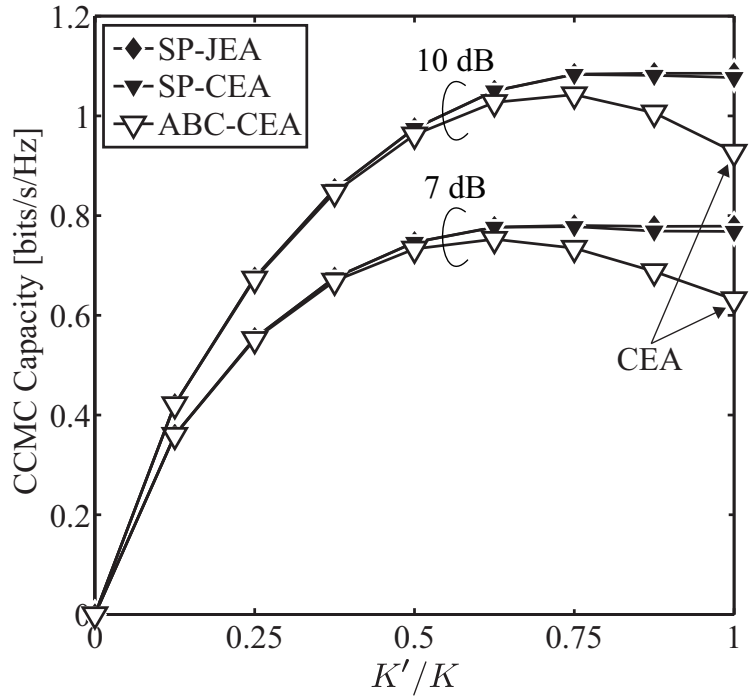

(a) CCMC Capacity

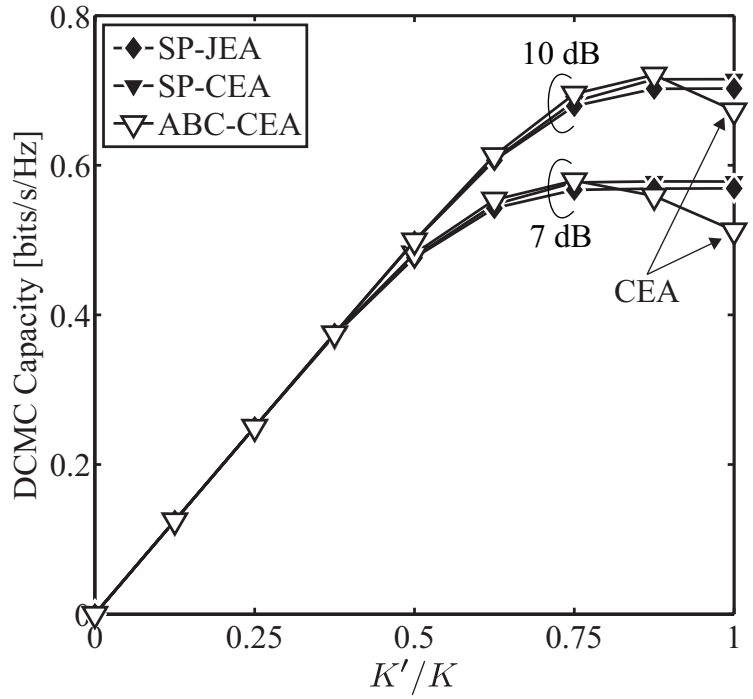

(b) DCMC Capacity

Figure 4.7: Spectral efficiency for various values of BAR K'/K.

Based on the signal model given by (4.18), the conditional PDF $p\left(y_{\mathrm{D}}^{\mathrm{f}}(k')\,|\mathcal{S}_q\right)$ is given by

$$p\left(y_{\mathrm{D}}^{\mathrm{f}}(k')\,|\mathcal{S}_q\right) = \frac{1}{\pi N_\eta(k')}\exp\left(-\frac{\left|y_{\mathrm{D}}^{\mathrm{f}}(k') - \tilde{\xi}(k')\,\mathcal{S}_q\right|^2}{N_\eta(k')}\right). \tag{4.55}$$

Assuming discrete modulation scheme used by the S-node is QPSK, we approximate the DCMC capacity in (4.54) as below to relax computational complexity [49].

$$D_S \approx \frac{1}{2K}\sum_{k'=1}^{K'}\left\{\log_2\left[1+\gamma_{\mathrm{r}}(k')\right] - \frac{1}{2}\log_2\left[1+\frac{\gamma_{\mathrm{r}}^2(k')}{16}\right]\right\}, \tag{4.56}$$

where $\gamma_{\mathrm{r}}(k')$ is defined in (4.25).

Figures 4.7(a) and 4.7(b) respectively characterize CCMC capacity and DCMC capacity averaged over 50000 channel realizations for each of $\boldsymbol{\Xi}_{\mathrm{RS}}$ and $\boldsymbol{\Xi}_{\mathrm{DR}}$. As shown in these figures when BAR $K'/K = 1$, ABC-CEA corresponds to CEA since ABC is actually not applied. These figures indicate that when BAR $K'/K = 1$, SP-CEA and SP-JEA significantly improve CCMC and DCMC capacities compared to CEA. This fact implies that SP makes significant contributions to the spectral efficiency enhancement because when SP is applied in SP-CEA and SP-JEA, spectral components transmitted over high gain subchannels in the S-R link are also relayed over high gain subchannels in the R-D link as illustrated in Figure 4.3.

Figures 4.7(a) and 4.7(b) also show that there is an optimal value of BAR = K'/K (< 1) for ABC-CEA in both CCMC and DCMC cases. The reason is as follows. When BAR is equal to 1, the assigned band is fully used, i.e., subchannels with low channel gain of the S-R and R-D links might be activated for transmissions. In such a case, it is highly possible for some spectral components which are transmitted over high gain subchannels in the S-R link, are then relayed over low gain subchannels in the R-D link, and vice versa. This phenomenon causes extremely low composite channel gains and reduces the spectral efficiency. On the other hand, when BAR is reduced from 1, it becomes less probable for low gain subchannels to be used for transmission, thereby the probability of occurrence of low composite channel gain is reduced. As a result, when BAR is reduced, the capacity is increased. However, when BAR becomes too small, the capacity is also reduced because transmit bandwidth becomes too narrow. Therefore, there is an optimal value of BAR that maximizes the capacity. This means BAR should be appropriately controlled to improve the capacity.

4.6.3 Adaptive BAR Control

Hereafter, instead of CCMC capacity, DCMC capacity is used for BAR control and performance evaluations because it is efficient in characterizing the mutual information of discrete

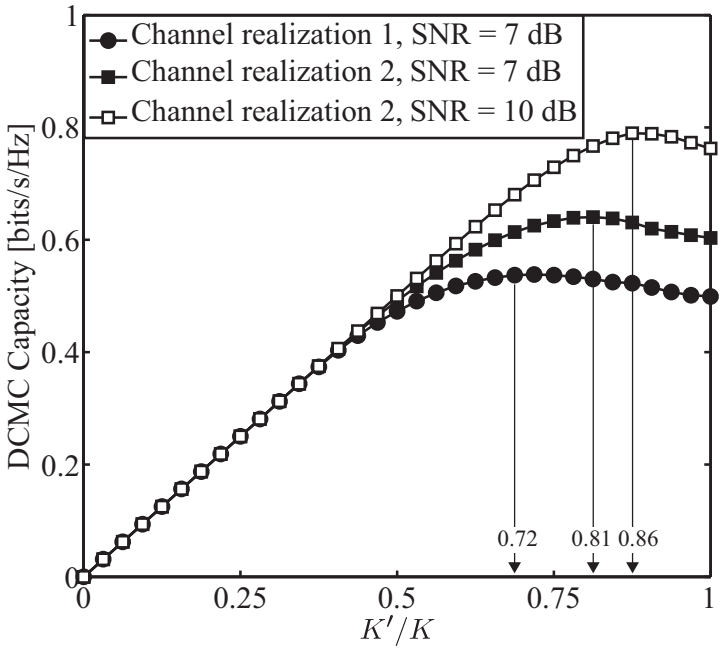

Figure 4.8: DCMC capacity of ABC-CEA for two channel realizations when BAR K'/K varies.

modulations which are adopted in practical systems. As shown in Figure 4.7(b), BAR can be controlled according to value of SNR to maximize the average DCMC capacity. In this SNR based ABC-CEA, the optimal value of BAR is calculated using computer simulations and notified to all the nodes prior to the transmissions. Thus notification overhead caused by this scheme is negligibly small. For further performance enhancement, BAR can be controlled according to both SNR and instantaneous CSI $\boldsymbol{\Xi}_{\mathrm{RS}}$ and $\boldsymbol{\Xi}_{\mathrm{DR}}$ to maximize instantaneous DCMC capacity.

Figure 4.8 characterizes optimal values of BAR to attain the maximum DCMC capacity under two randomly generated channel realizations at transmit SNR = 7 dB and SNR = 10 dB. The figure suggests that BAR needs to be adaptively determined for each channel realization and value of SNR. Since the R-node is able to capture knowledge on both $\boldsymbol{\Xi}_{\mathrm{RS}}$ and $\boldsymbol{\Xi}_{\mathrm{DR}}$, optimization of BAR is conducted at the R-node in an exhaustive search manner. This ABC-CEA based on both SNR and CSI is described as follows.

1. For each $K' \in \{1, ..., K\}$, select K' subchannels having the highest channel gain in each link to define SM matrices $\boldsymbol{M}_{\mathrm{S}}$ and $\boldsymbol{M}_{\mathrm{R}}$.

2. Compute $\alpha(k')$ and $\beta(k')$. Then, compute energy allocated to each data symbol by (4.51) and (4.52).

3. Compute DCMC capacity $D_{\mathcal{S}}(K')$ by (4.54) or (4.56).

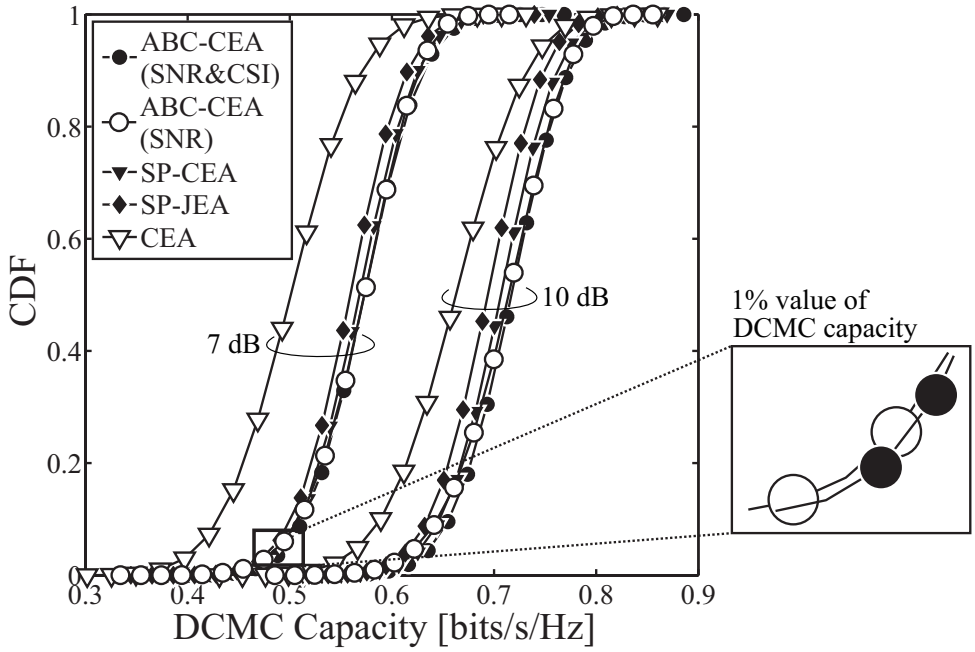

Figure 4.9: DCMC capacity performance in balanced SNR.

4. After completing the calculation of $D_{\mathcal{S}}(K')$ for all $K' \in \{1, ..., K\}$, search for $K'_{\text{opt}} = \arg \max_{K' \in \{1,...,K\}} D_{\mathcal{S}}(K')$.

After that the R-node notifies the optimal value K'_{opt} to the S-node and the D-node. Since $K'_{\text{opt}} \in \{1, 2, ..., K\}$, the amount of this information data is $\log_2 K$ bits.

4.7 Effectiveness of Spectrum Nulling Based Adaptive BAR Control

4.7.1 DCMC Capacity Performance

Figure 4.9 shows CDFs of DCMC capacity for SP-JEA, SP-CEA, CEA, SNR based ABC-CEA, and ABC-CEA based on SNR and CSI. Note that, in the cases of SP-JEA, SP-CEA, and CEA, BAR K'/K is not controlled, i.e., $K' = K = 256$. On the other hand, in the cases of ABC-CEA, K'/K is controlled by using the procedure explained in Section 4.6.3. Recall that, in SNR based ABC-CEA, the optimal value of BAR is determined to maximize average DCMC capacity using computer simulations and notified to all the nodes prior to the transmissions. Meanwhile, in ABC-CEA based on SNR and CSI, BAR is controlled according to both SNR and

instantaneous CSI to maximize instantaneous DCMC capacity. Thus, we can expect that SNR based ABC-CEA drastically reduces notification overhead while ABC-CEA based on SNR and CSI further enhances the spectral efficiency.

Figure 4.9 confirms that the two ABC-CEA schemes significantly increase DCMC capacity compared to ABC. Specifically, the 50% values of DCMC capacity of the two ABC-CEA schemes are the same value. This value is enhanced by 14.5% at SNR = 7 dB, and 8.2% at SNR = 10 dB compared to that of CEA. Furthermore, the 1% value of DCMC capacity of the ABC-CEA based on both SNR and CSI scheme slightly improves from that of the SNR based ABC-CEA scheme. This improvement is due to the fact that ABC-CEA based on SNR and CSI maximizes instantaneous DCMC capacity according to each instantaneous CSI and SNR while SNR based ABC-CEA maximizes average DCMC capacity according to SNR. As mentioned in the discussion of Figure 4.7, ABC is effective in DCMC capacity enhancement and is able to achieve almost the same or slightly better performances than SP. Moreover, by employing ABC instead of SP, the required notification information is the number of selected subchannels in each links. Thus, we can reduce the amount of notification data from $K \log_2 K = 2048$ bits to $\log_2 K = 8$ bits in ABC-CEA based on SNR and CSI, and to negligibly small in SNR based ABC-CEA. The reason that the proposed ABC-CEA schemes slightly outperform SP-CEA and SP-JEA is that a CCMC capacity maximization policy based scheme suffers from degradation in DCMC capacity. SP-JEA suffers from the most degradation since it is near-global optimal in terms of CCMC capacity. SP-CEA slightly outperforms SP-JEA since SP-CEA is only local optimal scheme. The two ABC-CEA schemes slightly outperform SP-CEA since SP-CEA is local optimal in terms of CCMC capacity while in the two ABC-CEA schemes, BAR is determined to enhance DCMC capacity.

4.7.2 Frame Error Rate Performance in Balanced SNR

FER performances are evaluated to verify effectiveness of the proposed ABC-CEA schemes for the relay system described in Section 4.6.2 with all simulation parameters shown in Table 4.1. In this evaluation, OFDM is employed as broadband transmission scheme for the relay system. The BAR $K'/K = 1$ for the cases of CEA, SP-JEA and SP-CEA, whereas it is adaptively controlled for the cases of two ABC-CEA schemes. As the number of data symbols transmitted in each OFDM symbols K' varies when two ABC-CEA schemes are applied, we employ a rate-1/3 turbo encoder with circular buffer rate matching (CBRM) [61] to keep the transmission rate to be 1 bits/s/Hz. At the S-node, a frame of 2048 information bits is encoded by the turbo encoder which comprises two component convolutional encoders (constraint length = 4, rate =

Table 4.1: Simulation parameters for FER evaluation.

Transmission	OFDM
Modulation	QPSK
Channel encoder	Rate-1/3 Turbo encoder with circular buffer rate matching (Component encoder: constraint length = 4, rate = 1/2)
Channel decoder	Turbo decoder Max-Log-Map with Jacobian logarithm (Number of iterations = 8)
Frame length	2048 bits
Number of blocks/frame	8
Number of subchannels	$K = 256$
Channel model	16 path equal gain Rayleigh fading
Channel estimation	perfect
Noise variance estimation	perfect

1/2). After that, CBRM is applied to generate a $16 \times K'$ bit-length codeword. The codeword is then fed to a QPSK modulator to generate a sequence of $8 \times K'$ data symbols. The data symbol sequence is then divided into 8 blocks, each consists of K' data symbols. One block forms an OFDM symbol which is transmitted over an assigned band with $K = 256$ subchannels. We assume that channel state of all links are constant during the transmission of one frame, which spans over 8 OFDM symbols. We also assume that the D-node is able to perfectly estimate the effective CFR $\tilde{\xi}(k')$ in (4.19) and variance of the noise term $\eta(k')$ in (4.20).

FER performances of CEA, SP-CEA, SP-JEA, SNR based ABC-CEA, and ABC-CEA based on SNR and CSI are shown in Figure 4.10. FER performances of the two ABC-CEA schemes are improved significantly from that of CEA. The performance of ABC-CEA based on SNR and CSI slightly surpasses those of those of SP-CEA and SP-JEA. Specifically, transmit SNR gain of this ABC-CEA scheme compared to CEA, SP-JEA and SP-CEA at FER = 10^{-3} are 1.6 dB, 0.3 dB, and 0.1 dB, respectively. This result collaborates that ABC-CEA based on SNR and CSI is an efficient approach to improve reliability for the relay system with an 8 bit notification. Meanwhile, performance of SNR based ABC-CEA scheme, which causes a negligibly small overhead is almost the same with that of SP-JEA and SP-CEA. The gap between FER performances of the two ABC-CEA schemes reflects the gap in 1% values of their DCMC capacities.

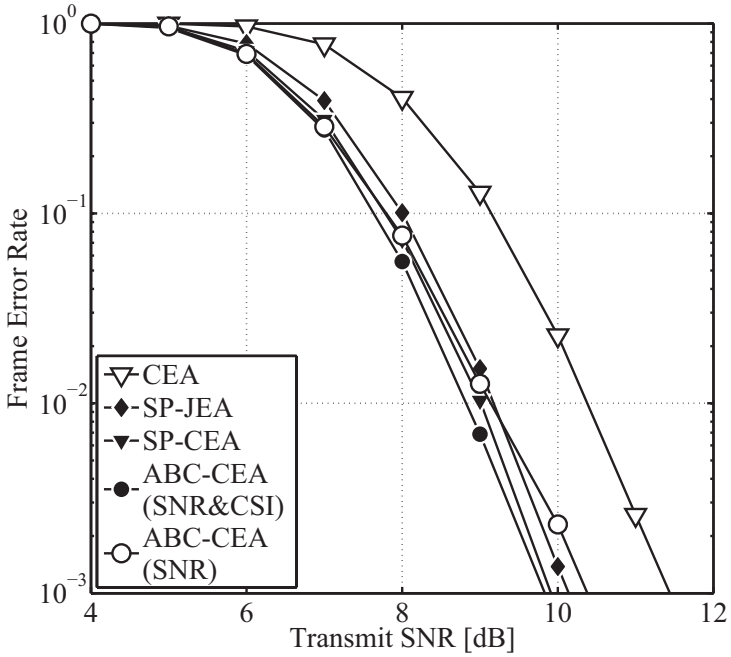

Figure 4.10: Frame error rate performance in balanced SNR.

4.7.3 Frame Error Rate Performance in Imbalanced SNR

We evaluate FER performance in the case where there is an imbalance between average SNRs of the S-R and R-D links. In this evaluation, the positions of the S-node and the D-node are fixed while the R-node is on the line between the S-node and the D-node. Let d_{RS} and d_{DS} be the distance from the S-node to the R-node and that from the S-node to the D-node, respectively. We assume here that path loss exponent is $\mu = 3.5$ while shadowing is not considered for the sake of simplicity. Under this constraint, when the R-node is right in the middle of the S-node and the D-node, i.e., $d_{\mathrm{RS}}/d_{\mathrm{DS}} = 0.5$, average SNRs of the S-R and R-D links are an identical value. This value is chosen as the reference SNR, which is denoted by $\mathrm{SNR}_{\mathrm{ref}}$ and set to 10 dB. Therefore, SNRs of the S-R and R-D links for an arbitrary position of the R-node are determined by

$$\mathrm{SNR}_{\mathrm{RS}} = (2d_{\mathrm{RS}}/d_{\mathrm{DS}})^{-\mu}\,\mathrm{SNR}_{\mathrm{ref}}, \tag{4.57}$$

$$\mathrm{SNR}_{\mathrm{DR}} = (2\,(1 - d_{\mathrm{RS}}/d_{\mathrm{DS}}))^{-\mu}\,\mathrm{SNR}_{\mathrm{ref}}. \tag{4.58}$$

Figure 4.11 verifies the characteristics of FER performances as functions of the relative distance $d_{\mathrm{RS}}/d_{\mathrm{DS}}$. When $0.1 \leq d_{\mathrm{RS}}/d_{\mathrm{DS}} \leq 0.3$, transmission distance of the R-D link is far longer than that of the S-R link. Consequently, average SNR of the R-D link becomes extremely low and severely degrades the overall FER performances of the relay system. Similarly, when

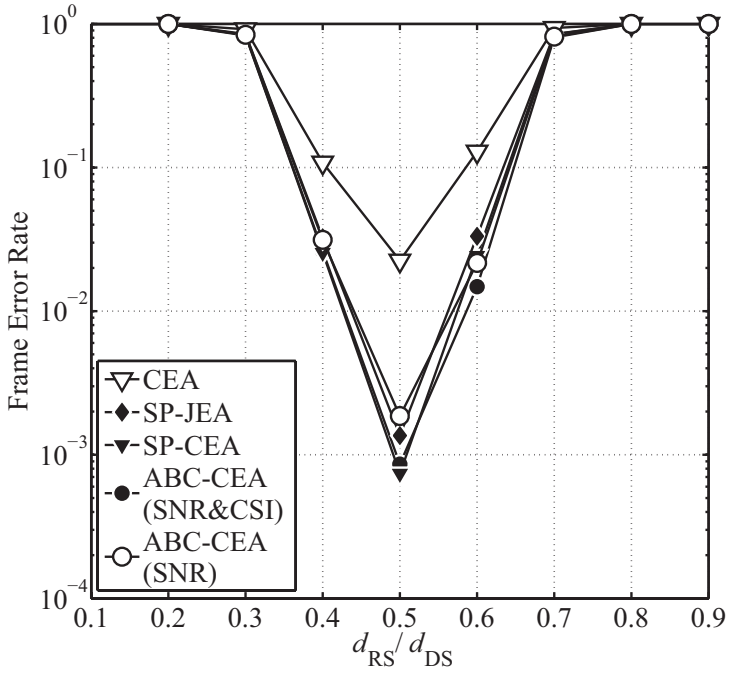

Figure 4.11: Frame error rate as a function of d_{RS}/d_{DS} when SNR_{ref} = 10 dB.

$0.7 \leq d_{RS}/d_{DS} \leq 0.9$, transmission distance of the S-R link is far longer than that of the R-D link. Thus, average SNR of the S-R link becomes extremely low and severely degrades the overall FER performances. Therefore, when d_{RS}/d_{DS} is in the range between 0.1 and 0.3 or between 0.7 and 0.9, the relay link does not effectively work and shows almost disconnected situations.

When d_{RS}/d_{DS} is in the range between 0.3 and 0.7, advantages of relay link can be obtained. This range can be considered as the effective region of d_{RS}/d_{DS} for the relay system. In this range, FER performance of ABC-CEA based on SNR and CSI is almost the same as that of SP-JEA and SP-CEA when $d_{RS}/d_{DS} = 0.3$ or 0.4. ABC-CEA based on SNR and CSI slightly outperforms the two SP employed schemes when $d_{RS}/d_{DS} = 0.5$ or 0.6. These results confirm that the proposed ABC-CEA based on SNR and CSI gives almost the same or better FER performance than the conventional SP schemes in the effective region of d_{RS}/d_{DS}.

When we compare the FER performance of SNR based ABC-CEA, although the performance is slightly worse than that of the ABC-CEA based on both SNR and CSI, it is almost the same as that of SP-CEA except the case when $d_{RS}/d_{DS} = 0.5$. However, the degradation at $d_{RS}/d_{DS} = 0.5$ can be considered to be acceptable considering reduction of the signal processing burden in the BAR control. With these results, we can conclude that the FER performances of the proposed ABC-CEA schemes are almost acceptable for any value of d_{RS}/d_{DS} in the range between 0.1

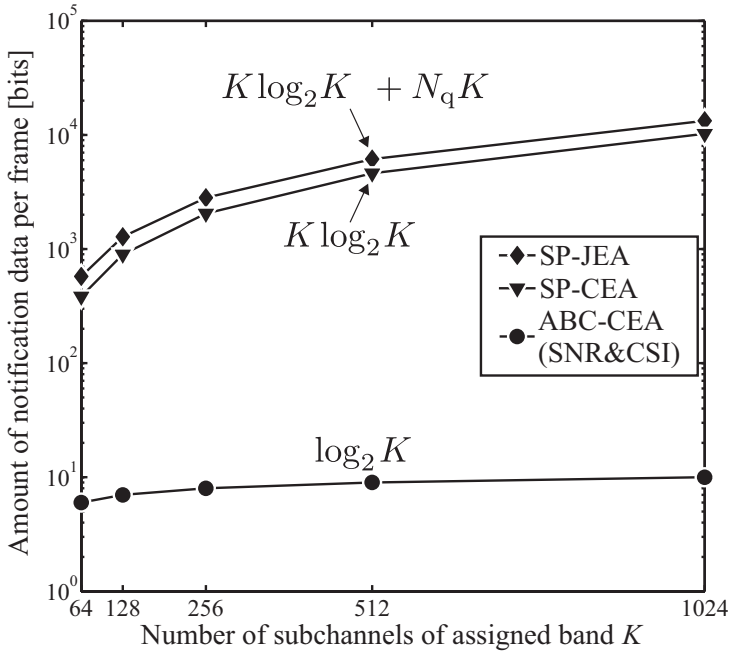

Figure 4.12: Amount of notification data.

and 0.9.

4.7.4 Notification Overhead

As CEA and the SNR based ABC-CEA scheme require solely negligibly small notification overheads, we compare the amount of notification data required by the three schemes: SP-CEA, SP-JEA and the ABC-CEA based on both SNR and CSI. When BAR is optimized according to both SNR and CSI, ABC alone requires a $\log_2 K$ bit notification of the optimal value K'_{opt} as mentioned in Section 4.6.3. SP alone requires a $K\log_2 K$ bit notification of SP based SM matrix $\boldsymbol{M}_{\text{R}}$ in (4.9). JEA requires a $N_{\text{q}}K$ bit notification of the real-valued EA matrix $\boldsymbol{G}_{\text{S}}$ in (4.40), where N_{q} is the quantization bit rate for each real-valued diagonal element of the matrix $\boldsymbol{G}_{\text{S}}$. The amount of notification data required by the three schemes are summarized in Figure 4.12 for the case of $N_{\text{q}} = 3$. When $K = 256$, the amounts of notification data per frame for SP-JEA, SP-CEA and the ABC-CEA scheme are 2816 bits, 2048 bits and 8 bits, respectively. This means the ABC-CEA scheme reduces the amount of notification data by 99.6% from SP-CEA and 99.7% from SP-JEA at $K = 256$. It is inefficient to apply SP-JEA and SP-CEA to practical systems since their notification overheads are as large as 11 and 8 OFDM symbols, respectively. On the contrary, the ABC-CEA based on both SNR and CSI can be applied to practical systems

because it costs a notification overhead of only $1/32$ OFDM symbols. Furthermore, it is obvious that the SNR based ABC-CEA is also applicable since it costs a negligibly small overhead.

4.8 Concluding Remarks

At first, this chapter proposed SP combined with CEA (SP-CEA) in order to enhance the end-to-end spectral efficiency for broadband AF relay. SP changes the order of spectral components at the relay node so that each spectral component is transmitted over subchannels having identical channel gain ranking in each hop throughout the relay transmission. Meanwhile, CEA conducts EAs at the source and the relay node in serial based on convex optimization. CCMC capacity and FER performance evaluation verified that SP-CEA achieves almost the same performances with those of the near-global optimal SP-JEA scheme.

After that, in order to reduce overhead caused by notification of spectral component order in SP, this chapter proposed two ABC schemes based on spectrum nulling so that all spectral components are consistently transmitted over relatively high gain subchannels of all links of the relay system. Numerical analyses confirmed that with reasonable notification overheads, when CEA is applied, the proposed ABC schemes can achieve almost the same or slightly enhanced DCMC capacity and FER performances compared to those of SP.

Chapter 5

Conclusions

This dissertation is a summary of the study on BAR control for broadband wireless transmissions in multiple link networks which is conducted by the author during his work toward the Ph.D. degree at the Department of Information and Communications Technology, Graduate School of Engineering, Osaka University, Japan. The main results and conclusions obtained in this research are highlighted below.

In the autonomous spectrum sharing employing DSC, each link dynamically selects a certain amount of higher gain subchannels from the common system band. In such a scenario, without a centralized spectrum management, we can enhance the spectral efficiency with a reasonable overhead by selecting a relatively small BAR, basically from around 0.5 to close to 0 depending on the number of links.

To realize the DSC, CSI for the entire system band, including the non-selected subchannels, is predicted from the selected subchannels for each user. Because BAR is relatively small, the bandwidth of continuously non-selected subchannels tends to be relatively large. As a consequence, reliability of the predicted CSI deteriorates, resulting in a degradation in the spectral efficiency. To improve the spectral efficiency, instead of selecting all subchannels with higher gain, we should select higher gain subchannels while keeping the bandwidth of continuously non-selected subchannels lower than a threshold to guarantee the CSI reliability. By doing so, we can enhance the spectral efficiency by 12% for a network with 6 links and 11% for a network with 10 links.

In a two-hop broadband AF relay, the end-to-end channel gain is the multiplication of the channel gains of the source-to-relay and relay-to-destination links. In order to improve the end-to-end spectral efficiency, spectral components transmitted via subchannels with higher gains in the first link should be relayed over subchannels with higher gains in the second link. The adaptive BAR control, which is proposed in this dissertation is a solution to realize this idea with a reasonable overhead. The proposed adaptive BAR control deactivates an appropriate

number of low gain subchannels of each link so that all spectral components are consistently transmitted over relatively high gain subchannels of the two links. The proposed BAR control achieves almost the same performance with that of a near-global optimal scheme while reducing the required notification overhead by more than 99.6%.

It is confirmed by the arguments above that by appropriately controlling the utilization of higher gain subchannels, which dominates the spectral efficiency, we can significantly enhance the spectral efficiency with a reasonable notification overhead.

In the future, the number of wireless terminals is predicted to explosively increase. In such a case, the transmit power optimization, which maximizes the spectral efficiency, faces two challenging problems. The first problem is the increase in computational complexity to optimize the signal spectrum according to characteristics of all links in the network. The second problem is the drastically increased notification overhead to realize the optimized transmit spectrum. It is obvious that even if the transmit spectrum is optimized, throughput of the whole network can not be significantly improved since it is overwhelmed by the extremely heavy notification overhead. Thus, rather than chasing the transmit spectrum optimization, enhancing the spectral efficiency with a reasonable notification overhead becomes more crucial. In such a circumstance, the knowledge of enhancing spectral efficiency with a reasonable notification overhead by appropriately controlling the utilization of higher gain subchannels, which is obtained by conducting this research, may become a hint for solving the problem.

Bibliography

[1] P. K. Bondyopadhyay, "Sir. J. C. Bose diode detector received Marconi's first transatlantic wireless signal of December 1901 (the "Italian Navy Coherer" Scandal Revisited)," *Proceedings of the IEEE*, pp.259–285, Jan. 1998.

[2] "Cisco visual networking index: Global mobile data traffic forecast update, 2013–2018," *Technical Report of Cisco Systems, Inc.*, Feb. 2014.

[3] R. G. Gallager, "Claude E. Shannon: A retrospective on his life, work, and impact," *IEEE Transactions on Information Theory*, vol.47, no.7, pp.2681–2695, Nov. 2001.

[4] P. K. Bondyopadhyay, "In the beginning," *Proceedings of the IEEE*, vol.86, no.1, pp.63–77, Jan. 1998.

[5] C. E. Shannon, "A mathematical theory of communication," *Bell System Technical Journal*, vol.27, June 1948.

[6] T. M. Cover and J. A. Thomas, *Elements of Information Theory*, 2nd ed., John Wiley & Sons, 2006.

[7] M. G. D. Benedetto and B. R. Bojcic, "Ultra wide band wireless communications: A tutorial," *Journal of Communications and Networks*, vol.5, no.4, pp.290–302, Dec. 2003.

[8] A. F. Molisch, "Ultrawideband propagation channels-theory, measurement, and modeling," *IEEE Transactions on Vehicular Technology*, vol.54, no.5, pp.1528–1545, Sept. 2005.

[9] Z. Pi and F. Khan, "An introduction to millimeter-wave mobile broadband systems," *IEEE Communications Magazine*, vol.49, no.6, pp.101–107, June 2011.

[10] N. Guo, R. C. Qiu, S. S. Mo, and K. Takahashi, "60 GHz millimeter wave radio; principle, technology and new results," *EURASIP Journal on Wireless Communications and Networking*, vol.2007, pp.48–58, Jan. 2007.

[11] S. K. Young and C. Chong, "An overview of multigigabit wireless through milimeter wave technology: potentials and technical challenges," *EURASIP Journal on Wireless Communications and Networking*, vol.2007, pp.58–68, Jan. 2007.

[12] M. Peter, W. Keusgen, and J. Luo, "A survey on 60 GHz broadband communication: Capability, applications and system design," *European Microwave Intergrated Circuit Conference 2008*, Amsterdam, Netherlands, Oct. 2008.

[13] J. G. Proakis, *Digital Communications*, 4th ed., McGraw-Hill Series in Electrical and Computer Engineering, Aug. 2001.

[14] T. S. Rappaport, *Wireless Communications: Principles and Practice*, 2nd ed., Prentice Hall, New Jersey, 2002.

[15] S. B. Weinstein and P. W. Ebert, "Data transmission by frequency-division multiplexing using the discrete Fourier transform," *IEEE Transactions on Communication Technology*, vol.19, no.5, pp.628–634, Oct. 1971.

[16] J. A. C. Bingham, "Multicarrier modulation for data transmission: An idea whose time has come," *IEEE Communications Magazine*, vol.28, no.5, pp.5–14, May 1990.

[17] S. Haykin, *Adaptive Filter Theory*, 2nd ed., Prentice Hall, New Jersey, 1991.

[18] Z. Wang, X. Ma, and G. B. Giannakis, "OFDM or single-carrier block transmissions?," *IEEE Transactions on Communications*, vol.52, no.3, pp.380–394, Mar. 2004.

[19] J. Tubbax, B. Come, L. V. Perre, and L. Deneire, "OFDM versus single carrier with cyclic prefix: a system-based comparision," *Proceedings of IEEE Vehicular Technology Conference (VTC)-Fall 2001*, Atlantic City, NJ, USA, pp.1115–1119, Oct. 2001.

[20] D. Falconer, S. L. Ariyavisitakul, A. Benyamin-Seeyar, and B. Eidson, "Frequency domain equalization for single-carrier broadband wireless systems," *IEEE Communications Magazine*, vol.40, no.4, pp.58–66, Apr. 2002.

[21] R. Koetter, A. C. Singer and M. Tüchler, "Turbo equalization," *IEEE Signal Processing Magazine*, vol.21, no.1, pp.67–80, Jan. 2004.

[22] P. A. Bello, "Characterization of randomly time-variant linear channels," *IEEE Transactions on Communication Systems*, vol.CS-11, pp.360–393, 1963.

[23] M. C. Jeruchim, P. Balaban, and K. S. Shanmugan, *Simulation of Communication Systems*, 2nd ed., Springer, Oct. 2000.

[24] S. Boyd and L. Vandengerghe, *Convex Optimization*, Cambridge University Press, New York, 2004.

[25] M. Nekovee, "Danamic spectrum access with cognitive radios: Future architectures and research challenges," *Proceedings of International Conference on Cognitive Radio Oriented Wireless Networks (CROWNCOM) 2006*, Mykonos Island, Greece, June 2006.

[26] S. Sampei, S. Miyamoto, and S. Ibi, "Spectrum loading type dynamic spectrum allocation technique for cognitive radio systems," *Proceedings of CROWNCOM 2007*, Orlando, FL, USA, pp.535–539, Aug. 2007.

[27] S. Sampei and S. Ibi, "Enabling technologies and strategies for radio resource management in decentralized heterogeneous wireless networks," *Proceedings of International Symposium on Personal Indoor and Mobile Radio Communications (PIMRC) 2008*, Cannes, France, pp.1–5, Sept. 2008.

[28] S. Sampei and S. Ibi, "Dynamic spectrum control that bridges dynamic spectrum access and adaptive transmit/receive control in cognitive radio systems," *Proceedings of International Symposium on Wireless Personal Multimedia Communications (WPMC) 2009*, Sendai, Japan, Sept. 2009.

[29] M. K. Ozdemir and H. Arslan, "Channel estimation for wireless OFDM systems," *IEEE Communications Surveys & Tutorials*, vol.9, no.2, pp.18–48, July 2007.

[30] Q. T. Duong, S. Ibi, and S. Sampei, "Dynamic spectrum control aided spectrum sharing with nonuniform sampling-based channel sounding," *IEICE Transactions on Communications*, vol.E96-B, no.12, pp.3172–3180, Dec. 2013.

[31] Q. T. Duong, S. Ibi, and S. Sampei, "A study on channel prediction for dynamic spectrum control aided spectrum sharing," *Proceedings of WPMC 2012*, Taipei, Taiwan, Sept. 2012.

[32] P. Fertl and G. Matz, "Channel estimation in wireless OFDM systems with irregular pilot distribution," *IEEE Transactions on Signal Processing*, vol.58, no.6, pp.3180–3194, June 2010.

[33] R. Negi and J. Cioffi, "Pilot tone selection for channel estimation in a mobile OFDM system," *IEEE Transactions on Consumer Electronics*, vol.44, no.3, pp.1122–1128, Aug. 1998.

[34] K. Gröchenig and T. Strohmer, "Numerical and theoretical aspects of non-uniform sampling of band-limited images," *Nonuniform Sampling: Theory and Practice*, ed. F. Marvasti, pp.283–324, Kluwer, NewYork, 2001.

[35] Q. T. Duong, S. Ibi, and S. Sampei, "A study on band activity ratio control aided autonomous spectrum sharing under predicted CSI," *Proceedings of IEICE Spring Conference 2013*, B-5-130, Mar. 2014 (in Japanese).

[36] J. N. Laneman and G. W. Wornell, "Energy-efficient antenna sharing and relaying for wireless networks," *Proceedings of IEEE Wireless Communications and Networking Conference (WCNC) 2000*, Chicago, IL, USA, vol.1, pp.7–12, Sept. 2000.

[37] A. Sendonaris, E. Erkip, and B. Aazhang, "User cooperation diversity part i and part ii," *IEEE Transactions on Communications*, vol.51, no.11, pp.1927–1948, Nov. 2003.

[38] Q. T. Duong, S. Ibi, and S. Sampei, "Adaptive band activity ratio control with cascaded energy allocation for amplify-and-forward ofdm relay systems," accepted for publication in *IEICE Transactions on Communications*, vol.E97-B, no.11, Nov. 2014.

[39] Q. T. Duong, S. Ibi, and S. Sampei, "Spectrum shaping combined with spectrum mapping for two-hop amplify-and-forward relay links," *Proceedings of WPMC 2009*, Sendai, Japan, Sept. 2009.

[40] Q. T. Duong, S. Ibi, and S. Sampei, "A study on spectrum shaping for two-hop transmissions with spectrum re-mapping at relay node," *Proceedings of IEICE Spring Conference 2008*, B-5-87, Mar. 2009 (in Japanese).

[41] M. Herdin, "A chunk based ofdm amplify-and-forward relaying scheme for 4G mobile radio systems," *Proceedings of IEEE International Conference on Communications (ICC) 2006*, Istanbul, Turkey, pp.4507–4512, June 2006.

[42] Q. T. Duong, S. Ibi, and S. Sampei, "A study on spectrum mapping for amplify-and-forward relay links under frequency selective fading channels," *Technical Report of IEICE*, RCS2011-92, July 2011.

[43] W. C. Jakes, *Microwave Mobile Communications*, John Wiley & Sons, 1974.

[44] B. Sklar, *Digital Communications: Fundamentals and Applications*, Prentice Hall, New Jersey, 1988.

[45] A. F. Molisch, *Wireless Communications*, IEEE Press - Wiley, 2005.

[46] B. Glance and L. J. Greenstein, "Frequency-selective fading effects in digital modile radio with diversity combining," *IEEE Transactions on Communications*, vol.31, no.9, pp.1085–1094, Sept. 1983.

[47] B. Shim and N. Shanghag, "Complexity analysis of multicarrier and single carrier systems for very high-speed digital subscriber line," *IEEE Transactions on Signal Processing*, vol.51, no.1, pp.282–292, Jan. 2003.

[48] L. Hanzo, S. X. Ng, T. Keller, and W. Webb, *Quadrature Amplitude Modulation*, Wiley, Chichester, UK, 2004.

[49] L. Xu, J. Zhu, and L. Qiu, "Adaptive modulation and space-time coding scheme based on constellation-constrained capacity," *Proceedings of VTC-Fall 2010*, Ottawa, Canada, pp.1–5, Sept. 2010.

[50] A. Lozano, A. M. Tulino, and S. Verdú, "Mercury/waterfilling: optimum power allocation with arbitrary input constellations," *Proceedings of IEEE International Symposium on Information Theory (ISIT) 2005*, Adelaide, Australia, pp.1773–1777, Sept. 2005.

[51] K. Yokomakura, S. Toh, Y. Hamaguchi, M. Kubota, S. Ibi, and S. Sampei, "A spectrum-overlapped resource management in dynamic spectrum control technique," *Proceedings of PIMRC 2008*, Cannes, France, pp.1–5, Sept. 2008.

[52] T. Aoki, S. Ibi, and S. Sampei, "Enhancement of throughput efficiency using adaptive bandwidth control for autonomous distributed networks in multiuser environments," *Prooceedings of PIMRC 2010*, Istanbul, Turkey, pp.1004–1009, Sept. 2010.

[53] T. Aoki, S. Ibi, and S. Sampei, "Adaptive bandwidth control for dynamic spectrum control aided spectrum sharing in private wireless networks," *IEICE Transactions on Communications*, vol.E95-B, no.4, pp.1093–1099, Apr. 2012.

[54] A. Okada, S. Ibi, and S. Sampei, "Spectrum shaping technique combined with SC/MMSE turbo equalizer for high spectral efficient broadband wireless access systems," *Proceedings of International Conference on Signal Processing and Communication Systems (ICSPCS) 2007*, Gold Coast, Australia, Dec. 2007.

[55] A. Ben-Israel and T. N. E. Greville, *Generalized Inverses: Theory and applications*, 2nd ed., Springer, New York, 2003.

[56] U. Grenander and G. Szegö, *Toeplitz Forms and Their Applications*, Chelsea, New York, 1984.

[57] G. Barriac and U. Madhow, "Space-time communication for OFDM with implicit channel feedback," *IEEE Transactions on Information Theory*, vol.50, no.12, pp.3111–3129, Dec. 2004.

[58] W. H. Press, S. A. Teukolsky, W. T. Vetterling, and B. P. Flannery, *Numerical Recipes: The Art of Scientific Computing*, 3rd ed., Cambridge University Press, New York, Sept. 2007.

[59] Y. Li, W. Wang, J. Kong, and M. Peng, "Subcarrier pairing for amplify-and-forward and decode-and-forward OFDM relay links," *IEEE Communications Letters*, vol.4, no.13, pp.209–211, Apr. 2009.

[60] A. Lozano, A. M. Tulino, and S. Verdú, "Optimum power allocation for parallel Gaussian channels with arbitrary input distributions," *IEEE Transactions on Information Theory*, vol.52, no.7, pp.3033–3051, July 2006.

[61] J. F. Cheng, A. Nimbalker, Y. Blankenship, B. Classon, and T. K. Blankenship, "Analysis of circular buffer rate matching for LTE turbo code," *Proceedings of VTC-Fall 2008*, Calgary, Canada, pp.1–5, Sept. 2008.

List of Publications by the Author

A Transactions

[A1] Q. T. Duong, S. Ibi, and S. Sampei, "Dynamic spectrum control aided spectrum sharing with nonuniform sampling-based channel sounding," *IEICE Transactions on Communications*, vol.E96-B, no.12, pp.3172–3180, Dec. 2013.

[A2] Q. T. Duong, S. Ibi, and S. Sampei, "Adaptive band activity ratio control with cascaded energy allocation for amplify-and-forward OFDM relay systems," accepted for publication in *IEICE Transactions on Communications*, vol.E97-B, no.11, Nov. 2014. (to be published)

B International Conferences

[B1] Q. T. Duong, S. Ibi, and S. Sampei, "Spectrum shaping combined with spectrum mapping for two-hop amplify-and-forward relay links" *Proceedings of WPMC 2009*, Sendai, Japan, Sept. 2009.

[B2] Q. T. Duong, S. Ibi, and S. Sampei, "A study on channel prediction for dynamic spectrum control aided spectrum sharing, " *Proceedings of WPMC 2012*, Taipei, Taiwan, Sept. 2012.

C Technical Report of IEICE

[C1] Q. T. Duong, S. Ibi, and S. Sampei, "A study on spectrum mapping for amplify-and-forward relay links under frequency selective fading channels, " *Technical Report of IEICE*, RCS2011-92, July 2011.

D Domestic Conferences in Japan

[D1] Q. T. Duong, S. Ibi, and S. Sampei, “A study on spectrum shaping for two-hop transmissions with spectrum re-mapping at relay node, ” *Proceedings of IEICE Spring Conference 2008*, B-5-87, Mar. 2009 (in Japanese).

[D2] Q. T. Duong, S. Ibi, and S. Sampei, “A study on band activity ratio control aided autonomous spectrum sharing under predicted CSI,” *Proceedings of IEICE Spring Conference 2013*, B-5-130, Mar. 2014 (in Japanese).